INTERPLAY BETWEEN STRESS GRANULES, CELLULAR STRESS RESPONSE, AND COXSACKIEVIRUS B3 INFECTION

by

Gabriel Fung

B.Sc., The University of British Columbia, 2011

A THESIS SUBMITTED IN PARTIAL FULFILLMENT OF

THE REQUIREMENTS FOR THE DEGREE OF

DOCTOR OF PHILOSOPHY

in

THE FACULTY OF GRADUATE AND POSTDOCTORAL STUDIES

(Pathology and Laboratory Medicine)

THE UNIVERSITY OF BRITISH COLUMBIA

(Vancouver)

July 2016

Abstract

Viral infection affects a multitude of cellular processes to facilitate successful replication. Such responses include the formation of stress granules (SGs) and the activation of autophagy. SGs are stalled translational complexes and function to restore cellular homeostasis after stress. Autophagy is a cellular process that recycles misfolded proteins and damaged organelles and plays an important role in various stress responses. We previously demonstrated that infection with Coxsackievirus B3 (CVB3), a common human pathogen for viral myocarditis, disrupts the autophagic process to support effective viral replication. However, the interplay between CVB3 and SGs, and the ability of SGs to regulate autophagy have not been investigated. Here we showed that SGs are formed early and actively disassembled late during CVB3 infection due to viral protease $3C^{pro}$-mediated cleavage of Ras-GAP SH3 domain binding protein 1 (G3BP1), a key nucleating protein of SGs. Overexpression of G3BP1 inhibits CVB3 replication, indicating an anti-viral function of SGs. We further demonstrated that the C-terminal product of G3BP1 has a toxic gain-of-function that further inhibits SG formation. We also examined the interaction between CVB3 and the transactive response DNA-binding protein-43 (TDP-43), an RNA binding protein that mislocates to SGs under cellular stress. We found that TDP-43 is translocated from the nucleus to SGs upon infection through the activity of viral protease $2A^{pro}$, followed by cleavage by protease $3C^{pro}$. The C-terminal product of TDP-43 is quickly degraded by the proteasome, whereas the N-terminal truncate acts as a dominant-negative mutant that inhibits the function of native TDP-43 in alternative RNA splicing. Knockdown of TDP-43 results in an increase in viral titres, suggesting a protective role for TDP-43 in CVB3 infection. Lastly, we explored the possible role of G3BP1-SGs in regulating autophagy. We showed that G3BP1 inhibits autophagic flux, likely by binding to cytoplasmic signal transducer and activator

of transcription 3 (STAT3). Taken together, our results reveal that the host SGs and associated proteins, including G3BP1 and TDP-43, are utilized and modified during CVB3 infection to promote efficient viral replication and induce viral pathogenesis. Moreover, we propose a novel mechanism by which G3BP1 binds cytoplasmic STAT3 to inhibit autophagy.

Preface

The content of the dissertation is derived from three original research papers and two review articles. **Chapter 1** includes modified review topics and tables from two review articles [Fung G., Luo H., Qiu Y., Yang D., McManus B. (2016) Myocarditis. *Circ Res*. 118:496-514. Doi: 10.1161/CIRCRESAHA.115.306573] and [Onomoto K., Yoneyama M., Fung G., Kato H., Fujita T. (2014) Antiviral innate immunity and stress granule responses. *Trends Immunol*. 35(9):420-8. Doi: 10.1016/j.it.2014.07.006]. **Chapter 3** is based on a modified portion of the original research article [Fung G., Ng CS., Zhang J., Shi J., Wong J., Piesik P., Han L., Chu F., Jagdeo J., Jan E., Fujita T., Luo H. (2013) Production of a dominant-negative fragment due to G3BP1 cleavage contributes to the disruption of mitochondria-associated protective stress granules during CVB3 infection. *PLoS ONE*. 8(11):e79546]. **Chapter 4** is based on a modified portion of the original research article [Fung G., Shi J., Deng H., Hou J., Wang C., Hong A., Zhang J., Jia W., Luo H. (2015) Cytoplasmic translocation, aggregation, and cleavage of TDP-43 by enteroviral proteases modulate viral pathogenesis. *Cell Death Differ*. 22:2087-2097. Doi:10.1038/cdd.2015.58]. **Chapter 5** is based on a manuscript that is currently in preparation and tentatively titled "G3BP1 negatively regulates autophagy potentially via direct recruitment of STAT3". The reuse and reprint of all published work is with permission from all journals referenced. During my PhD study, I also conducted additional projects and experiments with collaborating laboratories, resulting in contributions to 11 other co-author peer-reviewed articles. All CVB3 studies were approved by The University of British Columbia Research Ethics Board (Biosafety #B14-0190 and Animal #A13-0237).

Molecular tools that were generously provided from researchers outside of our laboratory were acknowledged appropriately. I completed, or actively contributed to, all data analyses that are presented in this dissertation.

Table of Contents

List of Tables

List of Figures

List of Abbreviations

ALS: Amyotrophic Lateral Sclerosis

AV: Adenovirus

BAF: Bafilomycin A1

BSA: Bovine Serum Albumin

CAR: Coxsackievirus and Adenovirus Receptor

CD: Cluster of Differentiation

cDNA: Complementary DNA

CFTR: Cystic Fibrosis Transmembrane Conductance Regulator

CMV: Cytomegalovirus

CP: Cleavage Product

CVB3: Coxsackievirus Type B3

CXCL: C-X-C Motif Chemokine Ligand

DAF: Decay Accelerating Factor

DAPI: 4’ 6-diamino-2-phenylindole

DCM: Dilated Cardiomyopathy

DMEM: Dulbecco’s Modified Eagle’s Medium

DMSO: Dimethyl Sulfoxide

dsRNA: Double-stranded RNA

DTT: Diothiothreotol

EBV: Epstein-Barr Virus

EF: Ejection Fraction

eIF: Eukaryotic Initiation Factor

EMB: Endomyocardial Biopsy

EMCV: Encephalomyocarditis Virus

ER: Endoplasmic Reticulum

EV: Enterovirus

FBS: Fetal Bovine Serum

Fc: Fragment Crystallization

FTLD: Frontotemporal Lobar Degeneration

G3BP1: Ras-GAP SH3 Domain Binding Protein-1

GAPDH: Glyceraldehyde 3-Phosphate Dehydrogenase

GCN2: General Control Non-depressible-2

GFP: Green Fluorescence Protein

HA: Hemagglutinin

HBSS: Hank's Balanced Salt Solution

HCV: Hepatitis C Virus

HEK: Human Embryonic Kidney

HF: Heart Failure

HHV: Human Herpes Virus

HIV: Human Immunodeficiency Virus

hnRNP: Heterogeneous Ribonucleoproteins

HRI: Heme-Regulated Inhibitor

HRV: Human Rhinovirus

IAV: Influenza A Virus

IEM: Immuno-Electron Microscopy

IFN: Interferon

IKK: Inhibitor of Nuclear Factor Kappa-B Kinase

IL: Interleukin

IP: Immunoprecipitation

IRES: Internal Ribosomal Entry Site

IVIG: Intravenous Immune Globulin

L: Leucine

LC3: Light Chain 3

LVAD: Left Ventricular Assist Device

MAVS: Mitochondrial Anti-Viral Signaling

MDA5: Melanoma Differentiation-Associated Protein 5

Met: Methionine

MHC: Major Histocompatibility Complex

miRNA: Micro Ribonucleic Acid

MOI: Multiplicity of Infection

mTOR: Mammalian Target of Rapamycin

NES: Nuclear Export Signal

NK: Natural Killer

NLS: Nuclear Localization Signal

Nrf2: Nuclear Factor Erythroid 2-related Factor

NSAID: Nonsteroidal Anti-Inflammatory Drug

NTF2: Nuclear Transport Factor 2

NYHA: New York Heart Association

ORF: Open Reading Frame

PFU.: Plaque-Forming Units

PABP: Poly-A Binding Protein

PAMP: Pathogen Associated Molecular Pattern

PBS: Phosphate-Buffered Saline

PCR: Polymerase Chain Reaction

PERK: PKR-like Endoplasmic Reticulum Kinase

PKR: Protein Kinase R

PolyI:C: Polyinosinic:polycytidylic

PRR: Pathogen Recognition Receptor

PV: Poliovirus

PV: Processing Body

PVB19: Parvovirus B19

Q: Glutamine

RANTES: Regulated on Activation Normal T Cell Expressed and Secreted

RIG-I: Retinoic Acid-inducible Gene-1

RIPA: Radio-Immunoprecipitation Assay

RLR: RIG-I-like Receptors

RNAi: RNA-interference

ROCM: Recent Onset Non-ischemic Cardiomyopathy

ROS: Reactive Oxygen Species

RRM: RNA Recognition Motif

SDS-PAGE: Sodium Dodecyl Sulfate-Polyacrylamide Gel Electrophoresis

SG: Stress Granule

SILAC: Stable Isotope Labeling by Amino Acids in Cell Culture

siRNA: Small Interfering RNA

SRF: Serum Response Factor

ssRNA: Single-Stranded RNA

STAT3: Signal Transducer of Activation 3

TAILS: Terminal Amine Isotopic Labeling of Substrates

TAK1: Transforming Growth Factor Beta-Activated Kinase 1

TBS-T: Tris-Buffered Saline – Tween

TDP-43: Transactive Response DNA Binding Protein-43

TEM: Transmission Electron Microscopy

TIA1: T Cell Restricted Intracellular Antigen-1

TIAR: TIA-Related Protein

TIMP-1: Tissue Inhibitor of Metalloproteinase 1

TNF: Tumor Necrosis Factor

TRIF: Toll/Interleukin-1 Receptor Domain-containing Adaptor Inducing Interferon-Beta

tRNA: Transfer-RNA

UTR: Untranslated Region

VCP: Valosin Containing Protein

Z-VAD-FMK: Z-Valine-Alanine-Aspartate-Fluoromethylketone

Acknowledgements

I would like to give special thanks to my research supervisor, Dr. Honglin Luo. With no doubt, Dr. Luo has been an excellent supervisor not only by providing constructive criticism, words of encouragement and career advice, but also by always being easy to reach at any time of the day. Her guidance and advice has really set an example for me and my fellow laboratory members for our future academic careers.

I would also like to give a special thanks to all the fellow researchers I have met at the Centre for Heart Lung Innovation, including those that directly worked with me; Jingchun Zhang, Dr. Jerry Wong, Dr. Junyan Shi, Dr. Haoyu Deng, Ye Qiu, Paulina Piesik, Andy Hong and Lillian Han. In addition, I thank my committee members Dr. Eric Jan, Dr. DeCheng Yang, Dr. Janet Chantler, and Dr. Sharon Gorski for their unselfish commitments to participate actively in guiding my research progress. I attribute much of my academic success to the guidance of Dr. Honglin Luo and my graduate committee.

Last but not least, I send a special thanks to my friends who have supported me throughout my studies: Hugo Mak, Ives Leung, Brian Choi, Mable Chan, and my dearest Cindy Cheong. Their encouragement, inspiration and support have built a strong base for me to grow, learn and to approach challenges. Special thanks are owed to my parents, whose have supported me throughout my years of education, both morally and financially.

Chapter 1: Introduction

1.1 Myocarditis

1.1.1 Definition and diagnosis

In 1749, inflammation of the heart and the difficulty in discerning such was described by a physician, Jean Baptiste Senac in Versailles, France, in his work entitled "Traité des maladies du Coeur" (Treatise on disease of the Heart). The term "myocarditis" was ultimately coined by Joseph Freidrich Sobernheim in 1837; however the use of this term included other cardiomyopathies that were previously undocumented including ischemic heart disease and hypertensive heart disease. It wasn't until the 1980's that the World Health Organization and the International Society and Federation of Cardiology attempted to differentiate between myocarditis and other cardiomyopathies [1]. Generally, myocarditis is identified as an inflammatory disease of the heart muscle cells and is pathologically identified by conventional histology and immunohistochemical techniques as an infiltration of lymphocytes to the myocardium. Myocarditis can be acute, subacute, or chronic and may involve either focal or diffuse areas of the myocardium. A recent update to the definition of myocarditis has been discussed by Caforio et al.[2] in defining myocarditis, using immunohistochemical data, as individuals that exhibit $\geq$ 14 lymphocytes/mm^2 including up to 4 monocytes/mm^2 with the presence of CD3-positive T-lymphocytes $\geq$ 7 cells/mm^2. This definition utilizes immunohistochemical data that requires endomyocardial biopsy collection and thus is limited to a relatively smaller cohort of patients or post-mortem autopsy samples. Moreover, while this definition of myocarditis has been quite widely accepted [2, 3, 4], it lacks information on the complexity of cellular infiltrates such as macrophage subtypes (classical/intermediate/non-classical), effector (Th1/Th2/Th17) and regulatory (FoxP3+/CD4+) T-lymphocyte subtypes, and

thus fails to differentiate a pro-fibrotic response from a healing inflammatory response. Future transcriptome-based analysis of biopsies may further our definition of myocarditis [5].

Patients of suspected myocarditis are clinically evaluated to distinguish fulminant lymphocytic myocarditis from acute lymphocytic myocarditis. In the case of fulminant myocarditis, patients exhibit New York Heart Association (NYHA) class IV symptoms, such as flu-like symptoms with left ventricle systolic dysfunction and cardiogenic shock [6]. Other characteristics include leukocytosis, eosinophilia (including rare cases of eosinophilic myocarditis), elevated erythrocyte sedimentation rate, and increased levels of cardiac troponin or the creatine kinase biomarker. Fulminant myocarditis may possess multiple foci of active myocarditis that typically can resolve within 6 months. Less frequently, giant cell myocarditis has been associated with fulminant acute myocarditis. In contrast, non-fulminant myocarditis may be acute or chronic myocarditis that often progresses in an insidious manner. While both acute and chronic myocarditis can be inferred upon echocardiography as heart failure with left ventricle dysfunction, acute myocarditis may lead to complete resolution or stable dilated cardiomyopathy, whereas chronic active myocarditis is defined as ongoing myocarditis with visible fibrosis and giant cells. Development of new molecular techniques such as miRNA profiling, nested polymerase chain reaction (PCR) and *in situ* hybridization have improved accuracy of diagnosis and prognostic value of endomyocardial biopsy samples significantly, allowing for improved definitions of the various types of myocarditis, including less prevalent subtypes of myocarditis such as eosinophilic and giant cell myocarditis [7].

1.1.2 Epidemiology

Myocarditis can be caused by a broad range of infectious agents, including viruses, bacteria, Chlamydia, rickettsia, fungi, and protozoa, as well as non-infectious triggers, such as

toxins and hypersensitive reactions [8]. Among these triggers, viral infection has been documented to constitute the most prevalent cause of myocarditis, particularly in children [8]. A wide spectrum of viral genomes in the endomyocardial specimens of patients with clinically suspected myocarditis or dilated cardiomyopathy has been identified by polymerase chain reaction and virus-specific *in situ* hybridization, which includes Enterovirus (EV), Parvovirus B19 (PVB19), Adenovirus (AV), Influenza A virus (IAV), Human Herpes virus (HHV), Epstein-Barr virus (EBV), Cytomegalovirus (CMV), Hepatitis C virus (HCV), and Human Immunodeficiency Virus (HIV) [9] (**Table 1**).

Between 1980 and 1990, virus-induced myocarditis was most associated with EV and AV infections [10]. As molecular technologies continued to improve, viral-induced myocarditis epidemiology in certain geographical locations shifted predominantly towards PVB19 and HHV6 infections [11, 12]. However, the geographical distribution of cardiotropic viral infections that induce cardiomyopathy is still in debate [13]. In a study performed by Andreoletti et al. [14], active Coxsackievirus type B (CVB) genomes and viral capsid proteins, VP1, were observed in immunostained post-mortem endomyocardial tissue of patients who died suddenly in the context of acute myocardial infarction in France. Furthermore, Ali Yilmaz et al.[13] showed that endomyocardial biopsies performed in Germany consistently, and almost exclusively, tested positive for PVB19 or HHV6, and that positive detection of EV genomes were rare. These discrepancies are speculated to be either derived from technical issues involving unspecific cross-reactivity of antibodies with necrotic or apoptotic human cardiomyocytes, or on the possibility that cardiotropic viruses exist along the French-German border. In fact, the waves of outbreaks in human viral diseases documented over the years by agencies like the Centers for Disease Control in the USA would suggest a variable series of outbreaks, from time to time, and

from region to region. Co-infections by various cardiotropic viruses have also become an attractive hypothesis for the confusing epidemiological variability. In 2006, HCV was detected in 4.4% of Japanese patients with myocardial manifestations by using antibodies specific for HCV epitopes in frozen blood samples [15]. In 2010, H1N1 IAV was demonstrated in 4 of 80 children confirmed as IAV-related myocarditis [16]. These studies raise a striking concern over studies investigating the epidemiology of viral myocarditis.

Table 1. Studies investigating viral prevalence in myocarditis patients

Study	Year	PVB %	EV %	AV %	HSV %	EBV %	CMV %	HHV %	Notes
Kandolf et al. [17]	1991	ND	**24.2**	ND	ND	ND	ND	ND	23/95 (24.2%) in suspected myocarditis patients, 10/33 (30.3%) in patients with DCM using PCR
Griffin et al. [18]	1995	ND	**21**	**31**	**3.4**	ND	**3.4**	ND	58 cases of fixed and frozen myocardial autopsy samples for PCR
Bowles et al. [19]	2003	<1	**14**	**23**	<1	<1	**3**	ND	PCR using EMB samples from 624 patients with myocarditis
Kuhl et al. [20]	2005	**36.6**	**32.6**	**8.1**	ND	ND	ND	**10.5**	12% dual infection in acute myocarditis, generally PVB + HHV in 172 patients using PCR
Caforio et al. [21]	2007	**3.0**	**12.5**	**5.0**	ND	**4.0**	**2.5**	ND	174 confirmed viral myocarditis patients
Breinholt et al. [11]	2010	**82.6**	ND	**1**	ND	**19.8**	**2.5**	ND	PCR using EMB samples of 99 children (3 weeks to 18 years of age)
Gaaloul et al. [22]	2014	ND	**28**	ND	ND	ND	ND	ND	Evaluated CVB genomes in hospitalized patients with inflammatory heart diseases. 1 case of CVB1, 27 of CVB3
Cooper and Knowlton [23]	2015	**11-56**	**15-30**	**2-23**	ND	ND	ND	ND	Discussed in Braunwald's Heart disease Textbook, 10th ed.

PVB = Parvovirus B; EV = Enterovirus; AV = Adenovirus; HSV = Herpes simplex virus; EBV = Epstein-Barr Virus; CMV = Cytomegalovirus; HHV = Human herpes virus; DCM = Dilated Cardiomyopathy; EMB = Endomyocardial biopsy; PCR = Polymerase chain reaction; CVB = Coxsackievirus B; ND = Not Determined

1.1.3 Viral myocarditis is a tri-phasic disease

The use of mouse model systems has proven useful in understanding the pathogenesis of DCM in viral myocarditis as mouse models closely represent human cases of virus-induced myocarditis. Three distinct immuno-virological and pathological phases of disease has been characterized in mouse models (**Figure 1**).

In mice, the first stage of viral myocarditis, the acute phase, encompasses day 0 to 4 days post infection. The **acute phase** is characterized by viremia, cardiomyocyte damage by viral assault, focal microcalcification, and high viral titre in cardiomyocytes. Viral entry at day 1 introduces a set of pathogen associated molecular patterns, such as foreign single-stranded RNA (ssRNA) and double-stranded RNA (dsRNA), that trigger various innate immune responses of cardiomyocytes and fibroblasts, leading to macrophage activation, release of interleukin-1α (IL-1α), IL-1β, IL-2, IL-6, IL-18, tumor necrosis factor-α (TNFα), TNFβ, IFNα, IFNβ and IFNγ by day 3-4 post infection [24]. The release of inflammatory cytokines and chemokines leads to the **subacute phase** from day 5 to approximately day 15 post infection. The subacute phase is characterized by the presence of viral release in the interstitium, recruitment of natural killer (NK) cells and macrophages to sites of injury, major infiltration of antigen-specific T lymphocytes, increase in major histocompatibility complex-I surface proteins and adhesion molecules, and the influx of neutralizing antibodies [25, 26, 27]. As a consequence, total viral titres begin to decline, leading to the chronic phase of myocarditis spanning days 15 post infection and beyond. The **chronic phase** of myocarditis is characterized by immuno-competency and viral clearance from peripheral tissues [28]. However, viral RNA and viral protein may persist in heart, spleen and lymph nodes [29, 30]. Myocardial fibrosis, calcification, ventricular dilation and cardiac hypertrophy become evident as the inflammatory response subsides [31, 32]. Sustained expression of

various cytokines have also been reported during the chronic stage of viral myocarditis, suggesting that the pathological progression of viral myocarditis to DCM is mainly due to the damaging effect of persistent infiltration and secretion of cytokines in the myocardium [33]. Ultimately, heart failure is an end-stage consequence and currently can only be treated with heart transplantation.

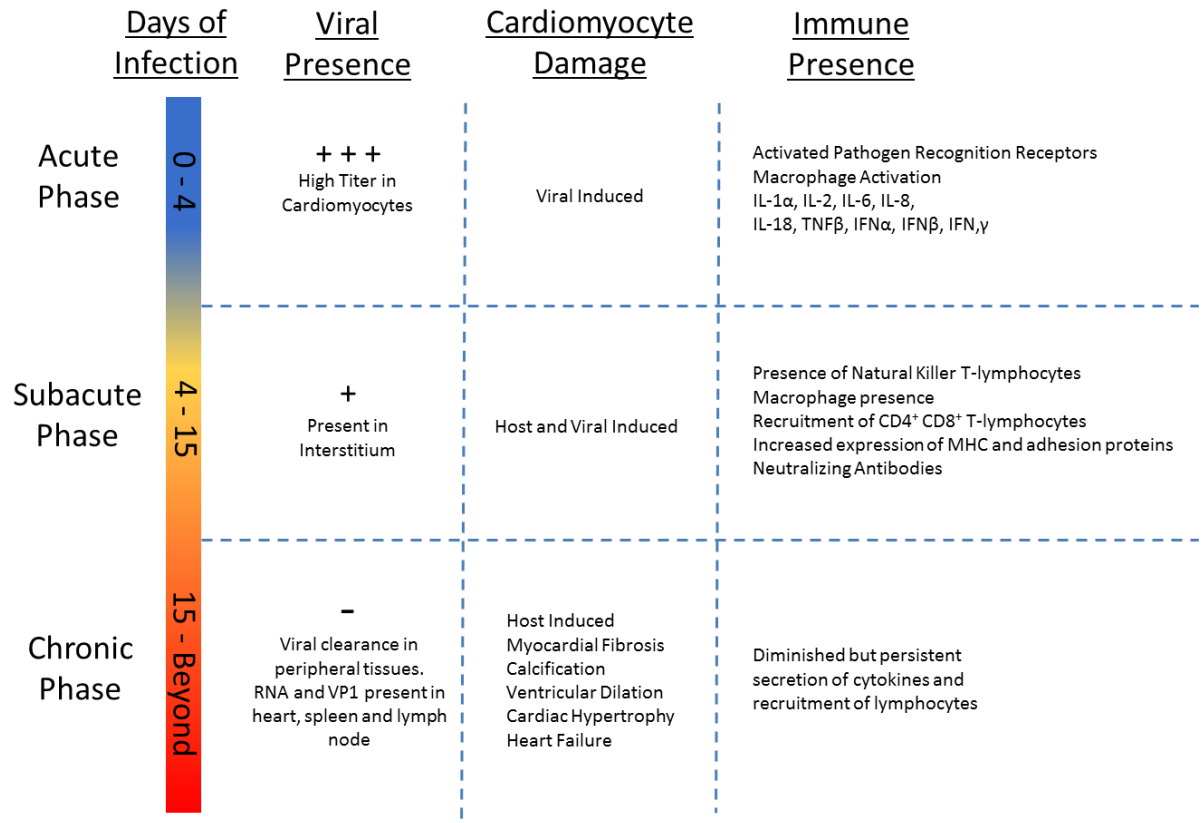

Figure 1. Viral myocarditis is a tri-phasic disease

Acute phase: Day 0-4, is characterized by viremia, virus-induced cardiomyocyte damage, and low activation of pathogen recognition receptors and macrophages. Subacute phase: Day 4-15, is characterized by low viral load, host- and viral-induced cardiomyocyte damage, increased expression of MHC and adhesion proteins, and presence of natural killer T-lymphocytes, macrophages, $CD4^+$ $CD8^+$ T-lymphocytes and neutralizing antibodies. Chronic phase: Day 15 –

beyond, is characterized by viral clearance, host-induced myocardial damage and fibrosis, and a diminished, but persistent, secretion of cytokines and recruitment of lymphocytes. RNA and VP1 may still be detected in infected tissues of the heart, spleen and lymph nodes.

1.1.4 Treatment

Treatment for viral myocarditis is currently aimed mostly at symptoms and signs of heart dysfunction. Patients presenting symptoms of end-stage DCM typically have rather unfortunate outcomes, with a five-year survival in biopsy-proven myocarditis/DCM to be approximately 50%. Currently, patients may either be given supportive therapy for left ventricular dysfunction or a heart transplantation, which in itself significantly lowers quality of living.

Mechanical circulatory supports for heart function aids in the recovery of myocarditis. Although such supports cannot cure myocarditis itself, the devices allow avoidance of fatality and increase the survival longevity of patients, especially in those with cardiogenic shock. A myocarditis and acute cardiomyopathy 2 (IMAC2) study showed that myocarditis was the strongest predictor of bridge to recovery in recent onset non-ischemic cardiomyopathy (ROCM) patients requiring the support of left ventricular assist devices (LVADs). Furthermore, female sex was associated with even greater likelihood of BTR in myocarditis patients on LVAD support [34]. As for fulminant myocarditis, a ventricular assist device is associated with complete recovery of myocardial function [35]. Moreover, external pulsatile mechanical ventricular assistance also improves survival in patients with acute myocarditis [36]. If myocarditis leads to end-stage heart failure, cardiac transplantation is the ultimate measure that should be considered [37].

Specific anti-viral drugs for viral myocarditis have also been developed and evaluated in animal models and in clinical trials. These drugs include Isoxazoles (WIN54954) and Pleconaril (VP63843) [38, 39]. Isoxazoles block viral enterovirus uncoating and have been shown to have beneficial effects, while Pleconaril experimentally binds a hydrophobic pocket in viral capsid protein 1 (VP1) in order to block viral attachment and entry [38, 39, 40]. Previously, Pleconaril failed to secure the approval of the Food and Drug Administration because Pleconaril introduced Cytochrome P450 3A (CYP3A) activity and potentially interfered with oral contraceptives [41]. Research involving the efficacy of Pleconaril remains to be ongoing for the treatment of viral-myocarditis. An exhaustive list of animal studies or clinical trials of anti-viral treatments to viral myocarditis is provided (**Table 2**). Insofar, no anti-viral agents are currently available for clinical treatment of myocarditis due to challenges such as drug efficacy and delivery. Furthermore, attempts to design a fully effective vaccine for enterovirus infections have not been completely successful, likely due to the high fidelity of viral RNA-dependent RNA-polymerases leading to increased rates of adaptive mutations.

Taken together, different strategies for the therapy of myocarditis have been introduced, but most are still yet to be verified in the research laboratory and are far from clinical application. As well, most clinical assessments performed regarding myocarditis treatment are still related to symptoms and depend much on the clinical presentation. Development of new monitoring and therapeutic techniques, such as molecular diagnoses, nucleic acid-based anti-viral drug development and targeted drug delivery will greatly enhance the therapy for myocarditis in the future.

Table 2. Studies of anti-viral and immunomodulatory treatments for myocarditis

Research Phase	Compound	Model	Results	Ref.
Clinical trials	IFN-β	CVB3 confirmed patients	Total viral clearance, improved LV function	[42]
	Pleconaril	Enterovirus infected human neonates	Full recovery	[43]
	Yiqi Yangxin/Sheng song yangxin	General viral induced myocarditis in humans	Increase heart function	[44]
	Azathioprine & Prednisone	Viral & non-viral myocarditis patients	Increase LVEF	[45]
	IVIG	Children with fulminant myocarditis	Increase LV function	[46]
	Eplerenone	Chronic HF patients, murine myocarditis	Decrease hospitalization, mast cell-derived proteinases & cardiac fibrosis	[47]
Animal models	IFN-β	CVB3 infected mice	Reduced cardiac viral load	[48]
	IFN-α	CVB3 infected mice	Prevent myocardial injury, reduce inflammation	[48]
	Ganciclovir	CMV-induced myocarditis in mice	Reduced myocarditis severity	[49]
	Cidofovir	CMV-induced myocarditis in mice	Reduced myocarditis severity	[49]
	WIN 54954	HRV-14 infected mice	Inhibition of viral replication, decrease overall mortality	[50]
	Astragaloside IV	CVB3 infected mice	Upregulate IFN-γ, reduce mononuclear infiltration and fibrosis in the myocardium, increase survival rate	[51, 52]
	Sophoridine	CVB3 infected mice	Attenuates myocardial fibrosis, induce IL-10, IFN-γ, decrease TNF-α	[53]
	Phyllaemblicin B	CVB3 infected mice	Alleviate pathological damage in the myocardium	[54]
	Amlodipine	Viral-induced HF in mice	Decrease overexpression of nitric oxide	[55]
	General antisense oligodeoxynucleotides	Cultured mammalian cells, mouse myocarditis models	Attenuate viral replication	[56]
	NSAID	Viral infected mice	Increase myocardium inflammation and mortality	[57, 58]
	siRNA for TIMP-1	CVB3 infected mice	Reduce CVB3-induced myocarditis	[59]
	Captopril	CVB3 infected mice	Ameliorate inflammation, necrosis and myocarditis	[60, 61]
	Losartan	Mice with viral and autoimmune myocarditis	Ameliorate inflammation, necrosis and fibrosis	[62, 63]
	Carvedilol	Mice with experimental autoimmune myocarditis	Suppress LV fractional shortening, heart rates, LV wall thickening, and myocarditis, decrease heart rate, decrease inflammatory cytokine expression	[64]
	Peptide-conjugated morpholino oligomers	CVB3 infected mice and mammalian cells	Decrease viral titre and cardiac tissue damage	65
	Emodin	CVB3 infected mice and mammalian cells	Inhibit viral protein synthesis, enhance survival	66
***In-vitro* studies**	Isatin derivative 45	CVB3 infected cultured mammalian cells	Activates ER stress-mediated responses, inhibit viral replication	[67]
	CAR-Fc, DAF-Fc	Cultured Mammalian cells	Attenuate viral replication	[68, 69, 70, 71]

IFN = Interferon; CVB3 = Coxsackievirus B3; LV = Left ventricle; CMV = Cytomegalovirus; HRV = Human Rhinovirus; IL = Interleukin; TNF = Tumor necrosis factor; CAR = Coxsackievirus and adenovirus receptor; Fc = Fragment crystallization; DAF = Decay accelerating factor; EF = Ejection fraction; NSAID = Nonsteroidal anti-inflammatory drug; IVIG = Intravenous immune globulin; siRNA = small interfering RNA; TIMP-1 = Tissue inhibitor of metalloproteinase 1; HF = Heart failure

1.2 Coxsackievirus

1.2.1 History and classification

In an attempt to search for a "parapoliomyelitis virus" during the 1940's, when epidemics of paralytic poliomyelitis in the United States of America was present, Dr. Gilbert Dalldorf isolated viruses from two children exhibiting poliomyelitis-like symptoms [72]. These isolated viruses constituted a new group of enteroviruses called coxsackie, in recognition of a small village located on the Hudson River, south of Albany, in which the two children were residents [73]. These coxsackieviruses were unique in a way that they could not be neutralized by antisera against poliovirus, and that coxsackievirus had the ability to grow in mice, while poliovirus have not been demonstrated to grow in mice [73]. However, further serologic tests for specific neutralizing antibodies against Coxackieviruses in 8477 patients showed significantly altered titers in 0.9% of patients suspected to have heart disease, of which 12% were cases of definite myopericarditis [74]. In addition, 41% of 1980 cases of suspected myalgic encephalomyelitis yielded seropositive results for coxsackieviruses [74]. These studies formed the initial correlations between various forms of heart failure and coxsackievirus type B serotypes.

During the characterization of these coxsackieviruses in mouse models, Dalldorf and his colleagues noticed that a subset of the coxsackieviruses induce skeletal muscle destruction and ultimately fatal paralysis of infected newborn mice [75]. This outcome was distinct from other isolates of coxsackievirus, and thus resulted in two classifications of coxsackieviruses, type A

and type B. Type A refers to strains that cause general myositis and now include 23 different serotypes, whereas type B includes 6 different serotypes causing infection in many different organs of newborn mouse, leading to a more slower, spastic paralytic death (5-7 days) with destruction of pancreatic acinar cells, cardiomyocytes, hepatocytes, lesions in the central nervous system, adrenal tissue, and focal myositis. Of the type B serotypes, coxsackievirus type B (CVB) 1, 3 and 5 resulted in viral myocarditis, with CVB3 being the most prominent type of virally-induced cardiomyopathy [75, 76]. Soon after the discovery of coxsackie serotypes, researchers began avoiding the investigation of these viruses due to dismal outcomes in infected patients [10]. Furthermore, funds to study these viruses decreased significantly once a vaccine for polioviruses had been discovered [77, 78]. However, these vaccines were not entirely effective for coxsackievirus serotypes, thus coxsackievirus infections remain a globally spread virus in the 21st century [10].

1.2.2 Properties

CVB3 is a non-enveloped, single-stranded, positive-sensed RNA virus. The viral genome is ~7,400 bases in length and comprises of a single open reading frame (ORF) encoding 11 viral proteins, flanked on both 5' and 3' ends by untranslated regions (UTRs). The 5'UTR contains ~800 bases that is spontaneously folded into conserved secondary structures comprising an internal ribosomal entry site (IRES) that directs viral genome translation initiation in a cap-independent manner [79, 80, 81]. While eukaryotic messenger-RNA (mRNA) contains a 5'-7-methylguanosine triphosphate cap, CVB3 5'-UTR contains a small viral polypeptide, VPg (also known as the non-structural protein 3B), that similarly blocks from endonuclease activity and serves to prime the viral RNA-dependent RNA-polymerase 3D for viral replication [80, 81, 82]. Furthermore, the 3'-UTR of CVB3 is poly-adenylated, similarly to eukaryotic mRNA [80].

The translation of the viral transcript produces a single polypeptide that codes for 4 structural proteins (VP1, VP2, VP3 and VP4), two viral proteases (2A and 3C), an RNA-dependent-RNA-polymerase (3D), a small peptide for RNA synthesis initiation (3B, or VPg), an ATPase (2C), and two host membrane modifiers (2B and 2A) (**Figure 2**). The process of generating individual viral proteins requires the formation of three functional intermediates; 2BC, 3AB and 3CD [83]. Ultimately, viral proteins and transcripts are packaged into a tight icosahedral capsid ~30nm in diameter composed of the 4 structural proteins [80, 84].

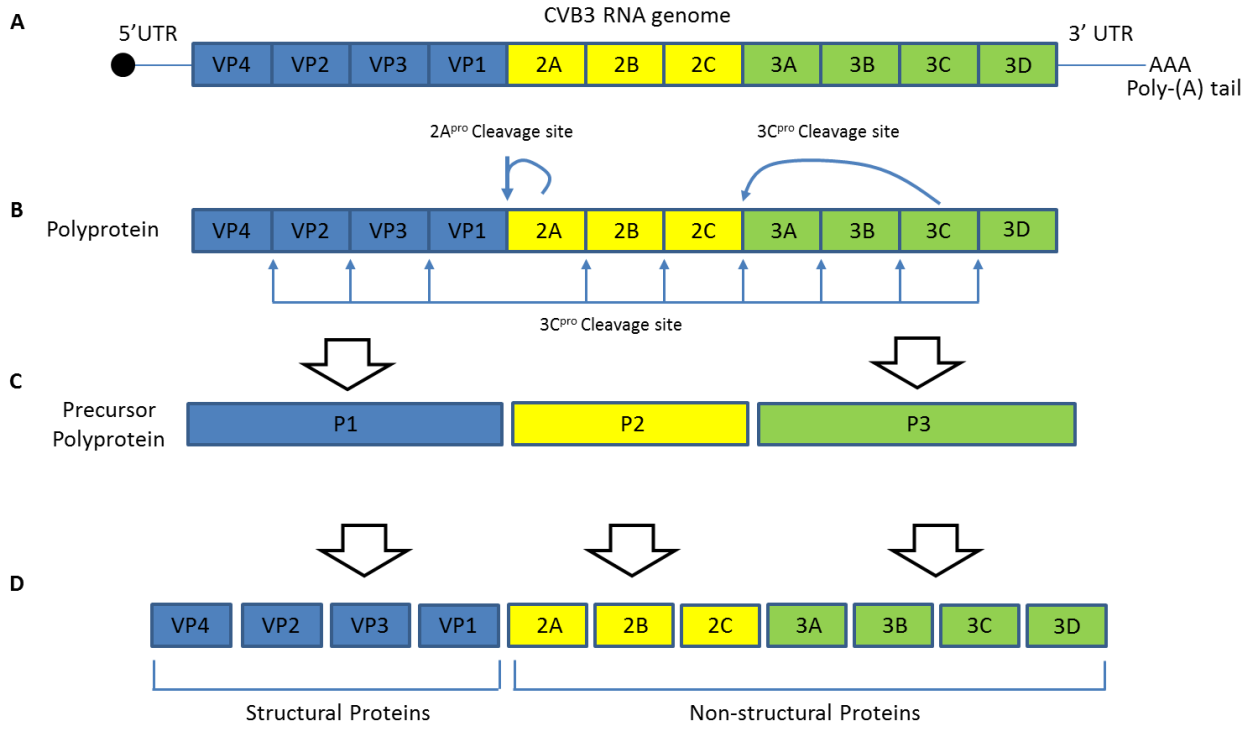

Figure 2. CVB3 genome schematic and post-translational cleavage of CVB3 polyprotein by virus-encoded $2A^{pro}$ and $3C^{pro}$

A) Virus single-stranded RNA genome is represented with a poly-adenylated (A) tail, 5'- and 3'-untranslated region (UTR), and viral genes labeled in the open reading frame. B) Translated Polyprotein is shown including the encoded cleavage site for viral polyprotein maturation. C) Viral polyprotein is cleaved between VP1-2A by $2A^{pro}$ to generate P1 and P2 precursor polyproteins, while $3C^{pro}$ cleaves between 2C-3A to generate the P2 and P3 precursor

polyproteins. D) Precursor polyproteins are further processed by $3C^{pro}$-induced cleavage to generate the individual viral proteins.

1.2.3 Proteolytic cleavage of host proteins by viral proteases

Virally encoded protease 2A and 3C are responsible for proper splicing and maturation of the viral polyprotein. However, it is well established that viral protease 2A and 3C also play a critical role in the molecular pathogenesis of virus-induced cardiomyopathy by targeting key host proteins to promote viral replication (**Table 3**). For example, 2A partly inhibits host cap-dependent protein translation during CVB3 infection by directly cleaving eukaryotic initiation factor (eIF) 4GI and 4GII [85]. In addition, 2A also selectively targets serum response factor (SRF) leading to the dysregulation of critical cardiac regulatory factors, including those involved in the contractile apparatus of cardiomyocytes [86]. Furthermore, 2A cleaves cardiac cytoskeletal proteins such as dystrophin, resulting in compromised cytoskeletal integrity contributing to DCM [87]. On the other hand, viral protease 3C has been shown to cleave mitochondrial anti-viral signaling protein (MAVS), Toll/Interleukin-1 receptor domain-containing adaptor inducing interferon-beta (TRIF), and melanoma differentiation-associated protein 5 (MDA5) as a strategy to evade host anti-viral responses [88, 89]. A large list of proteins has been demonstrated to be targeted by viral protease 2A and/or 3C, however an updated analysis of CVB3 protease targets is long overdue [90]. Recently, Jagdeo et al.[91] used terminal amine isotopic labeling of substrates (TAILS), a large scale screen for identifying novel targets of proteinases, to determine substrate proteins of poliovirus proteases. The other attempt to solve the targeting specificity of picornavirus proteases utilized a surface exposure prediction algorithm that was made publically available for researchers to identify potential cleavage sites of proteins of interest (www.cbs.dtu.dk/services/NetPicoRNA/) [90]. However, this software remains inaccurate and is

based on outdated algorithms of general picornavirus proteases, rather than specific strains. Thus researchers can easily miss true protein targets, while observing large lists of potential cleavage sites of false positives. A demand remains to be filled by novel screening methods to identify target proteins under CVB3 infection. Understanding the full spectrum of target proteins may shed light on the importance of specific cellular stress responses that contribute to DCM.

Table 3. Enteroviral proteinase targets

	Proteinase	Virus	Gene Symbol	Full Gene Name	Ref.
Cellular Defense	**2A**	PV, EV71	MDA5	Melanoma Differentiation-Associated protein 5	88, 92
	2A, 3C	CVB3, HRV, EV71, PV	MAVS	Mitochondrial antiviral signaling	89, 92, 93
	3C	CVB3, PV, EV71	RIG-I	Retinoic acid-inducible gene 1	88, 94
	2A, 3C	EV71	NLRP3	NACHT, LRR and PYD domains-containing protein 3	95
	3C	EV71, CVB3	TRIF	TIR domain-containing adaptor inducing beta interferon	96
RNA/Protein Dynamics	**2A**	PV	DCP1a	mRNA decapping enzyme 1A	97
	3C	PV	La/SSB	Lupas autoantigen/Sjogren syndrome antigen B	98
	2A	CVB3	p62/SQSTM1	Sequestosome 1	99
	2A, 3C	CVB3	NBR1	Neighbour of BRCA1 gene 1	100
	3C	CVB3	RIP3	Receptor interacting protein kinase-3	101
Cellular Integrity	**2A**	CVB3	Dysferlin	Dysferlin	102
	2A	CVB3	Dystrophin	Dystrophin	87
	2A	HRV	Cytokeratin 8	Cytokeratin 8	103
	3C	PV	MAP-4	Microtubule-associated protein 4	104
Transcription	**3C**	PV	Oct-1	Octomer binding transcription factor	105
	2A	PV	TBP	TATA-binding protein	106
	3C	PV	TFIIIC	Transcription factor for polymerase III A	107
	3C	PV	CREB	cAMP response element-binding protein	107
	2A	CVB3	SRF	Serum response factor	86
	3C	CVB3	AUF1	(AU)-rich element RNA binding factor 1	108
	3C	PV	PTB	Polypyrimidine tract-binding protein	109
	3C	PV	hnRNP M	Heterogenous nuclear ribonucleoprotein M	68
	2A	PV	Gemin3	Gemin3	110
	3C	CVB3	TDP-43	Transactive response DNA-binding protein-43	111
Translation	**2A**	CVB3, PV, EV71, RV	eIF4GI, -II	Eukaryotic initiation factor 4GI, -II	112, 113
	2A, 3C	CVB3, PV	PABP	Poly-A binding protein	114
	2A	CVB3	DAP5	Death-associated protein 5	115
	3C	CVB3, PV, HRV	eIF5B	Eukaryotic initiation factor 5B	197
	3C	PV	PCBP	Poly(rC)-binding protein	116
	3C	PV, HRV	p65-RelA	Nuclear factor (NF)-κ-B p65 subunit	117
Other	**3C**	CVB3	IKBα	Inhibitor of κBα	118
	2A, 3C	CVB3	GAB1	Growth factor receptor bound 2-associated binding protein 1	93, 119
	2A	HRV	Nup	Nucleoporin	120
	3C	PV, CVB3, EMCV	G3BP1	Ras-GTPase Activating Protein SH3 binding protein 1	97, 121, 122

CVB3 = Coxsackievirus B3; PV = Poliovirus; EMCV = Encephalomyocarditis virus; EV = Enterovirus; HRV = Human Rhinovirus

1.3 Stress granules

1.3.1 Definition and composition of stress granules

Cells respond to various insults including heat, oxidative stress, nutrient starvation, proteotoxic stress, and viral infection by forming cytoplasmic nucleoprotein aggregates termed stress granules (SGs) [123, 124, 125, 126]. Multiple RNA-binding proteins localize to SGs, and some have been used as markers for these cytoplasmic bodies. Although the formation of SGs in live cells can be detected by monitoring a plethora of proteins documented to localize to SGs using fluorescence-tagged protein markers, biochemical isolation of SGs is notoriously challenging due to its non-membranous property and the overall heterogeneity during cellular stress. However, a recent breakthrough by Jain et al.[127] has shown that SGs are composed of stable protein cores that contain a large set of RNA-binding proteins, poly-adenylated mRNA, stalled translation initiation factors, heat shock proteins, DEAD-box proteins, DNA/RNA helicases, and many other proteins previously not demonstrated to localize to SGs, some of which remain to be verified.

SG formation has been interpreted as a response that prevents the generation of abnormal proteins by transient stalling of translation in times of cellular stress. Stalled transcripts undergo translation upon recovery from stress, or alternatively they are degraded in another granular compartment termed the processing body (P body) [128, 129]. However the mechanism underlying the proposed exchange of mRNA and proteins is unclear. SG proteins, as defined by studies using proteins characteristic to SGs as markers [130], are either diffusely distributed in the cytoplasm or localized in the nucleus in normal conditions, followed by aggregation in the

cytoplasm during cellular stress [123, 131]. Currently, the list of proteins with demonstrated SG localization during cellular stress is growing rapidly (**Table 4**).

Table 4. Protein components of stress granules

Gene symbol	Full Gene Name	Functions	Ref.
Xrn1	5'-3' Exoribonuclease 1	5'-3' exonuclease	132, 133
APOBEC3G	Apolipoprotein B mRNA-editing enzyme, catalytic polypeptide-like 3G	Anti-viral activity	134, 135
TTP	Tristetraprolin	ARE-mediated mRNA decay	132
BRF1	Butyrate response factor 1	ARE-mediated mRNA decay	132
Caprin-1	Cell Cycle Associate protein 1	Cell growth, SG assembly	136, 137
ZBP1	Z-DNA-binding protein 1	DNA sensor, translational regulator	138, 139
G3BP1	Ras-GTPase-activating protein SH3-domain-binding protein	Endonuclease, Ras signaling, SG assembly	140
phospho-eIF2α	eukaryotic translation initiation factor 2A	Initiation factor	132, 141
eIF4G	eukaryotic translation initiation factor 4G	Initiation factor	123
HuR/ELAVL1	Hu antigen R/ELAV-like RNA-binding protein 1	mRNA stability, translation regulator	123, 142
PABP1	PolyA binding protein 1	mRNA stability, translation regulator	131
eIF3	eukaryotic translation initiation factor 3	Multisubunit initiation factor	123
RAP55/LSM14A	RNA-associated protein 55	PB assembly, antiviral activity	138, 143
CPEB	Cytoplasmic polyadenylation element binding protein	Polyadenylation, translation regulator	144
DDX3	DEAD box helicase 3	Polyadenylation, translation regulator	145, 146
40S	Eukaryotic small ribosomal subunit	Ribosome	123
ADAR	Adenosine deaminase, RNA-specific	RNA editing, RNA stability	147
DDX6/RCK	DEAD box helicase 6	RNA helicase, antiviral activity, PB assembly	144, 148
RHAU/DHX36	RNA helicase associated with AU-rich element/DEAH box protein 36	RNA helicase, SG assembly, antiviral activity	149, 150
SMN	Survival of motor neuron	RNA metabolism, SG assembly	151, 152
Ago2	Argonaute RISC catalytic component 2	RNA silencing, Processing body assembly	153, 154
STAU1	Staufen dsRNA binding protein 1	RNA transport, SG assembly	155
FAST	Fas-activated Ser/Thr kinase	Splicing regulator	132
TDP-43	Transactive response DNA binding protein-43	Splicing regulator	156
OGFOD1	2-Oxoglutarate and iron-dependent oxygenase domain containing 1	Translation regulator	157
TIAR	TIA-1-related protein	Translation regulator	131
Pum1	Pumilio RNA-binding family member 1	Translation regulator, cell growth	158
HDAC6	Histone deacetylase 6	Translation regulator, SG assembly	159
Pum2	Pumilio RNA-binding family member 2	Translation regulator, SG assembly	160
TIA1	T cell restricted intracellular antigen-1	Translation regulator, SG assembly	131, 161

1.3.2 Stress granule activation and formation

A common event downstream of cellular stress conditions is phosphorylation of eIF2α at serine 51, which is considered to be an initial trigger for SG formation. Four kinases are responsible for eIF2α phosphorylation under different cellular stresses; these include heme-regulated inhibitor (HRI) in response to heat shock, oxidative and osmotic stress, protein kinase R (PKR) in response to foreign dsRNA including viral RNA, PKR-like endoplasmic reticulum kinase (PERK) in response to ER stress and hypoxia, and general control non-derepressible-2 (GCN-2) in response to nutrient deprivation [162, 163, 164, 165, 166, 167, 168, 169, 170, 171, 172] (**Figure 4**). The mechanisms that connect eIF2α phosphorylation to SG formation remain to be elucidated.

Some proteins have been shown to be crucial for the formation or stability of SGs. These include Ras-GAP SH3 domain binding protein-1 (G3BP1), a phosphorylation-dependent endonuclease [140, 173], and T cell restricted intracellular antigen-1 (TIA1) and TIA-related protein (TIAR) that are collectively termed TIA1/TIAR [131, 161]. Of these, G3BP1 has been the most widely studied and commonly used as a molecular marker of SGs. Removal of these regulators by genomic deletion or RNA-interference (RNAi) blocks SG formation by sodium arsenite [140]. However, due to analytical constraints, the molecular machinery underlying the formation of SGs remains unclear.

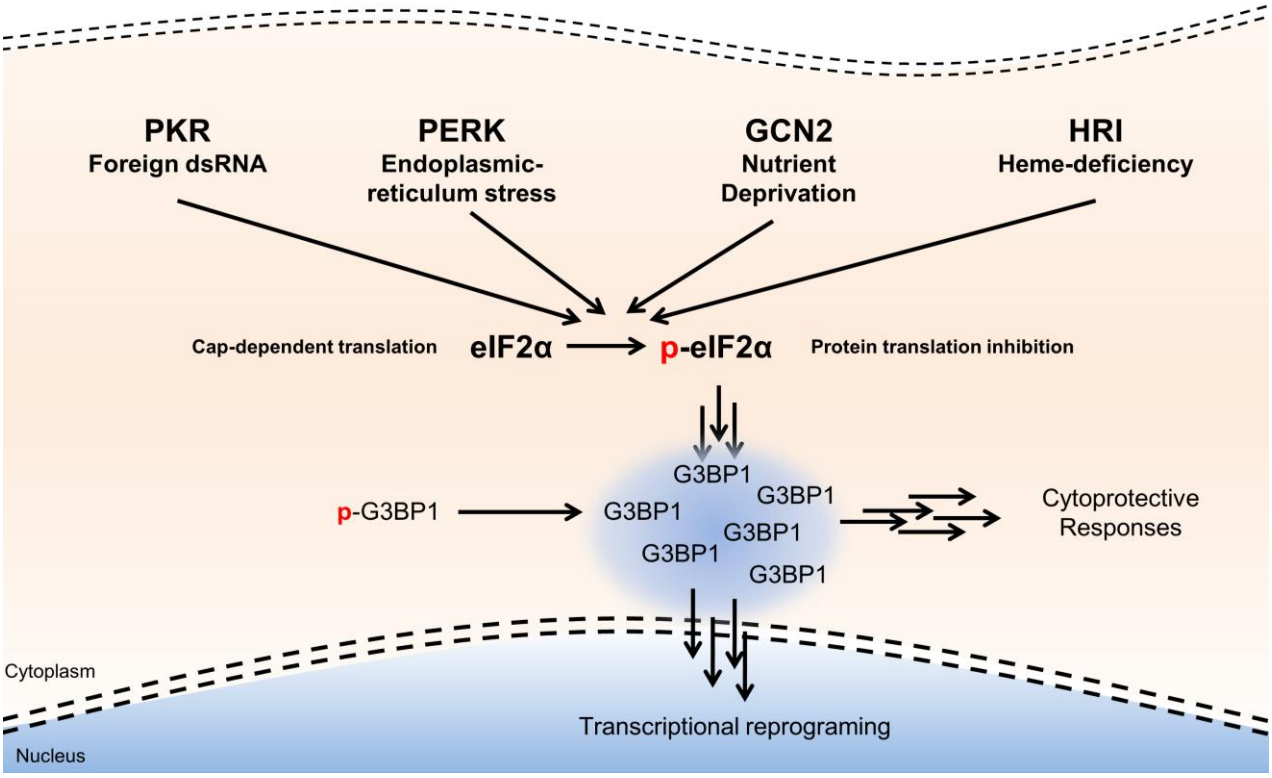

Figure 3. Protein translation inhibition and stress granule formation during cellular stress

eIF2α phosphorylation occurs via 4 kinases: Protein kinase R (PKR), in response to foreign dsRNA, Protein kinase RNA-like endoplasmic reticulum kinase (PERK), in response to ER-stress, general control non-derepressible-2 (GCN-2), in response to nutrient deprivation, and heme-regulated inhibitor (HRI) in response to heme deficiency in erythroid cells. Phosphorylation of eIF2α results in protein translation inhibition by depleting cellular concentrations of eIF2-GTP-met-tRNA$_i$, ultimately leading to G3BP1 aggregation and SG formation. SG formation plays a cytoprotective role against cellular stress and has been implicated in translational reprogramming, antiviral responses and even cancer metastasis.

G3BP1 contains an internal RRM (RNA recognition motif) domain for protein-RNA interaction, as well as an NTF2 (nuclear transport factor 2)-like domain for protein-protein interaction [140]. G3BP1 mutants lacking the NTF2-like domain fail to form G3BP1-SGs, suggesting that the role of the NTF2-like domain to undergo intra- and inter-molecular interactions is critical to SG formation. In addition, homogeneously diffuse cytoplasmic G3BP1 contains a constitutively phosphorylated serine residue at position 149 at resting states [140]. During cellular stress, S149 is dephosphorylated, inducing a conformational change that permits protein aggregation in a fashion similar to that of prion aggregation [79, 174]. A constitutively phosphorylated mutant form of G3BP1 (S149E) acts as a dominant inhibitor against SG formation [140]. Disrupted G3BP1 aggregation results in the failure to successfully mount downstream responses such as innate immune activation [174]. Therefore, G3BP1 plays particularly significant roles in SG formation and function, and is indispensable during cellular stress.

SGs were initially hypothesized to function in translational repression [175], however it appears that SG are not required for global translation repression [176]. Therefore, SGs are currently hypothesized to reprogram mRNA transcription and protein translation during cellular stress. Furthermore, cells demonstrating impaired SG formation fail to sequester apoptotic regulatory proteins, suggesting a vital role of SGs in the regulation of apoptosis [177]. However, detrimental SGs hypothesized to possess a toxic gain-of-function have been implicated in neurodegenerative diseases [178]. It is also speculated that aberrant sequestration of RNA-binding proteins to SGs results in a nuclear loss-of-function contributing to disease pathogenesis [178]. Lastly, SGs sequester many cancer-associated RNA-binding proteins and have been demonstrated to be co-opted to support oncogenesis and metastasis [179]. The overall significance

and function of SGs are likely underscored, as SGs are highly dynamic and heterogeneous cellular components that remain poorly understood.

1.3.3 Role of stress granules in viral infection

In the case of viral infection, an increasing amount of literature have demonstrated a key role for SGs in anti-viral defense mechanisms, where anti-viral factors such as retinoic acid-inducible gene-1 (RIG-I)-like receptors (RLRs) utilize SGs for aggregation and localization to mitochondrial surfaces for signal amplification, ultimately inducing activation of interferon-stimulated genes [149, 180, 181, 182, 183]. Failure to induce SG activation during infection results in attenuated anti-viral immune activation of IL1-α, IL1-β, IL-6, IFN-α, IFN-β and CXCL-10 [184]. The disruption of SG formation and function is therefore vital for host survivability during pathogen invasion. Many pathogens have developed mechanisms to evade anti-viral SG responses by preventing SG assembly, or actively targeting key nucleating proteins to disassemble SGs using viral proteases [181, 184, 185]. Currently, multiple mechanisms by which viral pathogens may inhibit SG formation and function have been documented. These include a multitude of mechanisms that inhibit eIF2α phosphorylation (Sendai virus [186, 187], Measles virus [188], Influenza virus [182, 189, 190], Junin virus [191]), caprin 1 blockage (Japanese Encephalitis Virus [136]), and active disassembly of transient SGs (Poliovirus [173, 192], Encephalomyocarditis virus [122], Sindbis virus [122, 166], Reovirus [193, 194]). In contrast, there have been a few cases of viral pathogens that usurp SG factors to benefit viral replication. West Nile virus and Dengue virus have previously been shown to recruit TIA1/TIAR to replication complexes to facilitate viral replication [195, 196]. Taken together, while some invading viral pathogens disrupt SG formation and function in order to block the activation of innate immune responses, other pathogens have

developed mechanisms to utilize SG and their respective components to benefit viral replication, contributing to detrimental outcomes related to viral pathogenesis.

1.3.4 Transactive response DNA binding protein-43 and stress granules

Transactive response DNA-binding protein-43 (TDP-43) is a heterogeneous ribonucleoprotein (hnRNP) that plays a critical role in RNA processing through interacting with ribonucleoprotein complexes in the nucleus to regulate transcription and pre-RNA maturation of selected RNA [197, 198]. It has been demonstrated that during cellular stress and under diseased states TDP-43 translocates from the nucleus to the cytoplasm [199]. Among the many SG-associated proteins already mentioned, TDP-43 localization to SGs has been strongly associated with cytotoxic affects and the progression of diseases, such as amyotrophic lateral sclerosis (ALS) and frontotemporal lobar degeneration (FTLD) [200]. However, the interaction between viral infection and TDP-43 remains largely unknown.

1.4 Autophagy

1.4.1 Autophagy activation and function

Autophagy is cellular self-digestion, a catabolic process that frees up vital nutrients and recycles organelles through lysosome-mediated degradation. Autophagy is capable of both bulk degradation and selective degradation of polyubiquitinated protein aggregates including SGs [201, 202]. Autophagy is required for the baseline function of cells and plays a key role in the maintenance of cellular homeostasis. Basal levels of autophagy are necessary to promote the turnover of misfolded proteins and damaged mitochondria [203, 204]. If basal autophagy is inhibited, unresolved toxic protein aggregates and malfunctioning mitochondria accumulate within the cells, contributing to cell stress and consequently resulting in severe pathologies [205]. Autophagy

can also determine whether a cell subjected to chronic stress either continues to survive or commits to programmed cell death, or apoptosis. When promoting survival, autophagy targets proteins for turnover and spares the mitochondria [206]. However, under prolonged stress, autophagy can co-operate with apoptosis to promote cell death [207, 208]. Therefore, in addition to maintaining cellular homeostasis, autophagy is a general stress-coping mechanism.

Autophagy is activated by multiple pathways depending on the context of multiple stress responses. These pathways include the class III phosphatidylinositol-3-kinase Vps34, ATG1 (regulated via the mammalian target of rapamycin [mTOR] pathway), and ATG8/LC3-I lipidation. Yeast and mammalian models that harbor a nonphosphorylatable mutant of eIF2α at residue S51 fail to successfully mount an autophagic response under nutrient deprivation, suggesting that eIF2α and its respective kinases may play a critical role in regulating autophagy activation. Furthermore, signal transducer of activation 3 (STAT3) represses autophagy via direct binding with PKR, thus inhibiting PKR kinase activity on eIF2α S51 [209]. STAT3 knockout mice and cell cultures treated with STAT3 inhibitors exhibit elevated levels of autophagy via activation of PKR and subsequent phosphorylation of eIF2α [209]. The cellular adaptation of post-translational regulatory mechanisms to mount immediate autophagic responses suggests that autophagy plays a multifaceted role in cell survival.

Autophagy, while primarily being known as a starvation response mechanism, plays important roles in numerous forms of cellular functions. During starvation, the mTOR pathway senses amino acid and ATP levels, inducing autophagy when these components are low [210]. Moreover, following detection of pathogens using pathogen recognition receptors (PRRs), autophagy is induced for the targeted clearance of certain bacteria and viruses [211, 212]. When a cell experiences stress as a result of DNA damage, the activation and nuclear localization of tumor

suppressor p53 induces autophagy to promote cell survival during growth arrest [213]. Similarly, autophagy induced by PERK signaling reinforces cell survival during oxygen deprivation or hypoxia [214]. Hypoxia and DNA damages are often associated with oxidative stress, a condition characterized by the production of toxic reactive-oxygen species (ROS). On its own, the autophagic adaptor, p62, combats oxidative stress by activating nuclear factor erythroid 2-related factor (Nrf2), a transcription factor that induces expression of anti-oxidant proteins [215]. The ROS generated by oxidative stress are associated with increased autophagy. Taken together, autophagy plays a crucial role in maintaining normal cellular function during physiological challenge.

1.4.2 Autophagy and stress granules

SG degradation has been shown to occur via autophagy in a process referred to as granulophagy [163]. The targeting of SGs to the autophagic pathway depends on the function of valosin containing protein (VCP). Failure of autophagy to recruit SGs has been associated with pathological mutations of VCP [202]. Other studies have demonstrated a vital link between autophagic activity and SG formation and degradation [216]. Moreover, dysregulation and aberrant accumulation of SGs are speculated to be a contributing factor to downstream cytotoxic effects [217]. Thus, formation and degradation of SGs may be a fine balance, where initial SG formation may play a cytoprotective role in the face of environmental challenge; however, persistent formation or the dysregulate clearance of SGs may result in a toxic gain-of-function, contributing to disease progression. Therefore, regulation of SG formation and degradation by autophagy is critical to cell viability. On the other hand, the reciprocal role that SGs may play in regulating autophagy remains to be investigated and may contribute significantly to the understanding of diseases development.

1.5 Rationale, hypothesis and specific aims

SGs formation and function are associated with vital cytoprotective roles during cellular stress. In response to viral infection, SGs have been shown to play both anti-viral [97, 184] and pro-viral functions [195, 196]. On the one hand, cells exposed to certain viral infections have been demonstrated to induce SG accumulation, leading to activation of innate immune responses [122, 149, 181, 182]. On the other hand, some viruses can adapt mechanisms to usurp the components of SGs for the advantage of their viral replication [195, 196]. However, the effect of CVB3 infection on SG formation/function and the role of SGs in CVB3 infection are largely unclear. Understanding the host-pathogen interaction between CVB3 and cellular SG may shed valuable insight on virus-induced cardiomyopathy.

As an important protein in regulating RNA processing, the function of TDP-43 in viral infection, in particular, CVB3 infection, has not been previously studied. In addition, translocation of TDP-43 from the nucleus to cytoplasmic SGs has been strongly associated with cell death and disease progression [218]. However, its role in CVB3-induced pathogenesis has not yet been studied.

Finally, degradation of SGs has been shown to be, in part, due to autophagy [163]. Given that cellular stress responses such as autophagy and SGs share common activation pathways, and are likely interconnected in function and activation, we speculate that SGs may also play a role in the regulation of autophagy. However, no studies have been previously reported in this regard.

My hypotheses in this dissertation are: **(1) CVB3 infection dysregulates the formation and function of stress granules by targeting G3BP1 and TDP-43 to promote viral replication and contribute to viral pathogenesis; and (2) G3BP1, as a key component of SGs, plays an important role in the regulation of autophagy**.

To address these hypotheses, my specific aims are:

1) To determine the interplay between CVB3 infection and the formation and significance of SGs (**Chapter 3**).

   I examined the impact of CVB3 infection on SG dynamics (assembly and disassembly) and explored the possible mechanisms involved. I also assessed the effects of modulating critical SG components on viral replication.

2) To determine the interaction between CVB3 infection and the DNA/RNA binding protein TDP-43 (**Chapter 4**).

   I examined the effect of CVB3 infection on TDP-43 localization and protein expression, and investigated the mechanisms by which CVB3 dysregulates TDP-43. I also determined the significance of TDP-43 in regulation of CVB3 infection.

3) To elucidate the role of G3BP1-SGs in regulating autophagy (**Chapter 5**).

   I examined the effects of overexpression and knockdown of G3BP1 on p62 degradation and LC3-I/LC3-II conversion in response to starvation. I also assessed the influences of overexpression and knockdown of G3BP1 on autophagic flux (fusion of autophagosomes with lysosomes and autophagic degradation activity). Furthermore, I used a quantitative proteomics approach to identify G3BP1 binding partners and explored the potential mechanism by which G3BP1 regulates autophagy.

Chapter 2: Materials and Methods

2.1 Cell culture, animal protocol, and viral infection

HeLa and HEK293 cells (American Type Culture Collection) were grown in Dulbecco's modified Eagle's medium (DMEM, Thermo Cat. #SH30243.01) supplemented with 10% heat-inactivated newborn fetal bovine serum (FBS, Life Technologies Cat. #12483-020).

Isolation and culture of primary neonatal mouse cardiomyocytes were performed as described previously [219]. Briefly, neonatal cardiomyocytes were obtained by enzymatic dissociation of cardiac ventricles from 1-2 day old A/J mouse neonates. Non-myocytes were removed via two rounds of pre-plating on culture dishes and cytosine 1-β-D-arabinofuranoside (Sigma-Aldrich, #C1768) was added to inhibit the growth of contaminating non-myocytes. The enriched cardiomyocytes were cultured in DMEM with 10% FBS and 10% horse serum.

CVB3 viral infections were performed by incubating HeLa and HEK293 cells with CVB3 (Kandolf strain) at multiplicities of infection (MOI) of 10, unless otherwise indicated, for 1 hour in serum free DMEM. After 1 hour, the medium containing virus was then replaced with 10% FBS supplemented DMEM for the remaining time points indicated. Sham infected cells were treated with equal volumes of phosphate-buffered saline (PBS).

For experiments involving Z-VAD-FMK, a broad caspase inhibitor, when virus-containing medium was replaced after 1 hour post-infection, 10% FBS supplemented medium was treated with 50 μM Z-VAD-FMK (BD Biosciences Cat. #550377). For experiment involving MG132 or Bafilomycin A1 (BAF), when FBS-containing medium was replaced after 6 hours transfection, 10% FBS supplemented medium was treated with titrating concentrations of MG132 (Sigma-Aldrich, Cat. #C2211) as indicated or 20 nM BAF for 16 hours.

CVB3 infection of A/J mice, ~5 weeks of age was performed via intraperitoneal injection with 10^5 plaque-forming units (p.f.u.) of CVB3 or sham infected with PBS. After 9 days, mice hearts were harvested for protein analysis. These studies were performed in strict accordance with the recommendation in the Guide for the Care and Use of Laboratory Animals of the Canadian Council on Animal Care and were approved by the Animal Care Committee at the University of British Columbia.

2.2 Plasmids, siRNA and transfections

Plasmid encoding GFP-G3BP1 was a generous gift from Dr. Jamal T. at the Institut de Génétique Moléculaire de Montpellier, France. Plasmids of the viral protease 2A driven by the IRES promoter were designed by cloning the open reading frame (ORF) of 2A into the BamHI and SalI sites of the pIRES vector, while 3C-ORF was cloned into the XbaI and SalI restriction sites. N-terminus of G3BP1 (amino acid 1-325) and C-terminus of G3BP1 (amino acid 326-466) were cloned into the p3×FLAG-CMV vector. The HA-tagged TDP-43 construct was used as the template to generate the HA-TDP-43-N_{1-327} and HA-TDP-43-$C_{328-414}$ constructs. The HA-TDP-43^{Q327L}-GFP mutant was established to replace the 327 glutamine (Q) of wild-type TDP-43 at amino acid 327 with leucine (L). The small interfering RNAs (siRNAs) against human G3BP1 (siG3BP1) and human TDP43 (siTDP43) was purchased from Santa Cruz and Dharmacon (#L-012394), respectively. Transient transfection was conducted using Lipofectamine 2000 (Invitrogen, #11668019) and Oligofectamine (Invitrogen, #12252-011) according to manufacturer's protocol. Cells were grown at a confluence of ~90% were transiently transfected with plasmids using Lipofectamine 2000 for 24 hrs. siRNA transfections were performed on HeLa cells at 30-50% confluence using Oligofectamine (Life Technologies) for 48 hrs.

2.3 Western blot analysis

Cells were harvested with lysis buffer (250mM NaCl, pH 7.2, 50mM Tris-HCl, 0.1% NP-40, 2mM EDTA, and 10% glycerol). Equal amounts of proteins were loaded for sodium dodecyl sulfate-polyacrylamide gel electrophoresis (SDS-PAGE). The membranes were blocked for 1 hr with 5% non-fat dry milk solution containing 0.1% tween-20. The blots were incubated in 1 hr of primary antibody diluted in 2.5% non-fat dry milk solution containing 0.1% tween-20, washed 3 × with TBS-T, followed by another 1 hr incubation in secondary antibody. Immunoreactive bands were visualized by enhanced chemiluminescence.

2.4 Plaque assay

CVB3 replication was determined by measuring the virus titer in the cell supernatant using an agar overlay [220]. Supernatant of CVB3-infected cells was serially diluted by 10 fold and overlaid on a 90-95% confluent monolayer of HeLa cells for 1 hr. After PBS wash, cells were overlaid with complete medium containing 0.75% agar and incubated at 37°C for 72 hrs. Carnoy's fixative (75% ethanol-25% acetic acid) and 1% crystal violet were used for fixation and staining, respectively. Plaques were quantitated and viral titers were calculated based on PFU per milliliter.

2.5 Real-time quantitative reverse-transcription polymerase chain reaction (RT-PCR)

Total RNA was isolated using the RNeasy Mini kit (Qiagen). Equal concentrations of RNA were used for cDNA synthesis using SuperScript III First-Strand Synthesis SuperMix (Life Technologies). Primers previously designed to target the 5' UTR of CVB3 were optimized for SYBR Green quantitative PCR [221]. The 25μl per reaction mix consisted of 1nL cDNA template, 500nM forward and reverse primers, and 1× Quantities SYBR Green PCR Master Mix (Qiagen). The PCR program, run on a Via 7 Real-Time PCR System (Applied Bios stems), included a 15

min polymerase activation step at 95°C, and 40 cycles of 94°C/15s, 53°C/30s, and 72°C/30s where endpoint fluorescence was recorded. A terminal dissociation curve was included to assess primer specificity and dimmer formation. Triplicate samples were run with a 10× serial dilution of sample cDNA as a standard for determining PCR efficiency.

2.6 Indirect immunocytochemical microscopy

Indirect immunofluorescence assay was performed firstly by fixing in 4% paraformaldehyde for either 16 hrs at 4°C, or 30 minutes at room temperature. Following permeabilization, coverslides were incubated in blocking solution (5% normal goat serum, 2.5% bovine serum albumin in PBS) for 1 hr. Coverslides were then incubated in primary antibody for either 1hr at room temperature, or 16 hrs at 4°C, followed by three consecutive PBS washes for 5 mins each. After washing, the cells were incubated with the secondary antibody for 1 hr at room temperature. Coverslides were again washed three times in PBS as previously mentioned. Cell nuclei were counterstained with 4', 6-diamidino-2-phenylindole (DAPI) and mounted onto glass slides. Images were captured under a Leica SP2 AOBS confocal microscope. The quantification of SG formation was performed by counting the number of cells expressing 3 or more punctates and dividing by the number of cells expressing the corresponding fluorophore, where each image should consist of 20 or more cells. Quantification of images for TDP-43 cytoplasmic translocation was performed by counting at least 10 images where each image contained five or more cells. Values were presented as % of cells expressing cytoplasmic TDP-43. TDP-43 and dsRNA localization was evaluated using Pearson's correlation algorithm as described. In order to quantify red and yellow LC3 puncta, at least 10 images were quantified to count red and yellow aggregates using Volocity software version 5.2.1 and expressed as # of puncta per cell.

2.7 Transmission electron microscopy

To visualize ultrastructural changes during CVB3 infection, HeLa cells infected with CVB3 for 3 hrs were fixed in 2.5% glutaraldehyde (Polysciences Inc.) in PBS, pH 7.2, for 10 mins at room temperature. Cells were then post-fixed in 1% Osmium tetroxide (Polysciences Inc.), 1% potassium ferrocyanide, 100mM sodium cacodylate buffer, pH 7.4, for 1 hr at room temperature. We then proceeded to rinse several rounds in deionized water, and dehydrate in a series of acetone washes. Cells were then embedded in Eponate 12 resin (Ted Pella Inc.), sectioned at a thickness of 60nm, and viewed on a Tecnai 12 transmission electronic microscope (FEI Inc.).

2.8 Immunoelectron microscopy

For immuno-labelling of G3BP1, rabbit anti-G3BP1 polyclonal antibody (Cat.ab39533, Abcam) was diluted at 1:60. F(ab') 2 fragment of ultra-small goat-anti-rabbit IgG was diluted at 1:50. Following steps were performed using a Pelco Biowave Microwave. Free aldehydes were blocked using 50mM glycine, blocked in 5% goat serum containing 0.18% cold water fish skin gelatin, washed in acetylated-BSA (BSA-c) and incubated with primary antibody. Controls were incubated in normal goat serum diluted at 1:60. Sections were washed, and incubated in secondary antibody, sequentially washed in BSA-c, PBS, 2% glutaraldehyde, distilled water, and Silver R-Gent SE-EM. Finally, sections were stained in 2% uranyl acetate, lead citrate, air dried and analyzed on a Tecnai 12 electron microscope.

2.9 Viral protease purification

CVB3 $2A^{pro}$ was purified from pET-C×2A expressed in BL21 bacterial cells by ion exchange chromatography and size exclusion chromatography. CVB3 $3C^{pro}$ was cloned into a pET29b plasmid containing a His-tag and expressed in BL21 bacterial cells for 4 hrs at 30°C.

Bacterial cells were lysed by sonication in 50mM NaCl, 50mM Tris pH 8, 5mM imidazole, 5mM β-mercaptoethanol, 5% glycerol, then purified by Ni-nitrilotriacetic acid chelating resin affinity chromatography.

2.10 *In vitro* cleavage assay

Cleavage reactions were performed in 20mM HEPES (pH 7.4), 150mM KOAc and 1mM DTT. Each sample comprised of HeLa lysates with purified CVB3 $2A^{pro}$ or $2A^{pro}$ catalytically inactive mutant at 5ng/µl or CVB3 $3C^{pro}$ at 100ng/µl. Reaction mixtures were incubated at 37°C for the amount of time as indicated and the reaction was stopped by the addition of SDS-PAGE sample buffer. Cleavage activity was assessed by western blotting as mentioned above.

2.11 *In situ* hybridization

HeLa cells on coverslips were fixed in 4% paraformaldehyde for 30 mins at room temperature were incubated in hybridization buffer (2× SSC [1× SSC is 0.15 M NaCl plus 0.015 M sodium citrate], 20% formamide, 0.2% bovine serum albumin (BSA), 1 µg/µl *Saccharomyces cerevisiae* tRNA) for 15 mins at 37°C. HeLa cells were then hybridized with 1mg/ml DNA probes, oligo(dT) conjugated to Cy-3, or antisense CVB3 conjugated to Cy-5 overnight at 46°C in hybridization buffer (IDT). Cells were then washed with 2× SSC with 20% formamide twice for 5 mins each at 37°C, 2× SSC twice for 5 min each at 37°C, and 1× SSC once for 5 min. Where further immunostaining was required, cells were co-stained by indirect immunofluorescence protocol as mentioned above. The antisense CVB3 RNA probe sequence was AAGCCAATCTAAATTATTTCAAATT conjugated to Cy-5 (Sigma).

2.12 Splicing assay

TDP-43 functional activity was evaluated through amplifying the cystic fibrosis transmembrane conductance regulator (CFTR) splicing. HeLa cells were co-transfected with

TG(15)T(5) CFTR reporter construct and respective TDP-43 constructs, and incubated at 37˚C for 24 hrs. Total RNA was harvested by QIAGEN RNeasy kit (Cat. #74104) and equal amounts of RNA were used for RT-PCR using 500ng of total RNA. Two micrograms of the resulting cDNA was used for subsequent PCR reactions using primers α2-3 and Bra2. Primer sequences for the Bra2 and a2-3 sequences are 5'-TAGGATCCGGTCACCAGGAAGTTGGTTAAATCA-3', and 5'-CAACTTCAAGCTCCTAAGCCACTGC-3', respectively. PCR conditions were as follows: 95°C for 10 mins (hot start), followed by 35 cycles of denaturing at 95°C for 3s, annealing at 57°C for 30s, and elongation at 72°C for 60s. PCR products were visualized on a 1.5% agarose gel and quantified using ImageJ software. All samples were performed in triplicates and repeated at least 3 times.

2.13 Solubility assay

Cells were washed twice with PBS, lysed with cold radioimmunoprecipitation assay (RIPA) buffer (Santa Cruz, #sc-24948) supplemented with protease and phosphatase inhibitors. Cell lysates were sonicated and cleared by centrifugation at 100,000×g for 30 mins at 4°C. Supernatants were collected as RIPA-soluble fractions. RIPA-insoluble protein pellets were washed by resonication and recentrifugation using the same conditions to prevent carry-over. Only supernatants from first extraction were used. RIPA-insoluble pellets were extracted with Urea buffer (7M urea, 2M thiourea, 4% CHAPS, 30mM Tris, pH 8.5), followed by sonication and centrifugation at 70,000×g for 30 minutes at 22°C. Supernatants collected as RIPA-insoluble fractions and analyzed by standard western blot protocols.

2.14 Immunoprecipitation

Proteins were extracted using lysis buffer (50 mM Tris HCl, pH 7.4, 150 mM NaCl, 1 mM EDTA, 1% Triton X-100, and proteinase inhibitor cocktail (Roche, 04693132001). Protein

concentration was measured and equal amount of protein was loaded for immunoprecipitation using EXview^{TM} Red Anti-Flag® M2 affinity gel (Sigma-Aldrich, F2426).

Firstly, 40µL of the provided 50% slurry was used per reaction. Beads were washed with 500µL of TBS (50 mM Tris HCl, 150 mM NaCl, pH 7.4), vortexed briefly, and centrifuged for 30s at 8,200×g. Supernatant was removed, kept on ice, and repeated a second time as a wash. 200 µL of clarified lysates of denatured proteins and cell debris were loaded into fresh microcentrifuge tubes and filled to 1 mL with lysis buffer. Mixture was incubated overnight in an end-over-end tumbling motion overnight at 4°C. Next day, we centrifuged the mixture for 30 mins at 8,200×g and placed on ice. We collected the supernatants and used as flow-through samples. The remaining pellet was washed three more times with TBS as mentioned above, and beads were incubated with 20 µL of 2x Laemmli sample buffer (125 mM Tris HCl, pH 6.8, 4% SDS, 20% (v/v) glycerol, and 0.004% bromophenol blue). Samples were boiled at 95°C for 5 mins, vortexed briefly, and centrifuged at 8,200×g for 30s. Remaining supernatants were used for SDS-PAGE.

2.15 Stable isotope labeling by amino acids in cell culture

Triplex SILAC labeling was conducted as described previously [222]. Before labeling, HeLa cells were maintained in DMEM supplemented with 10% FBS (v/v), 1% L-Glutamine (v/v) and 1% penicillin/streptomycin (v/v) at 5% CO_2 and 37°C then transferred to SILAC medium with dialyzed FBS plus Lysine (Lys) and Arginine (Arg) isotopologs. Cell populations were amplified 200-fold in the labeling media to achieve complete labeling. Here we refer to the different as ‘0/0’ for the normal isotopic abundance Lys and Arg, ‘4/6’ for $^{2}H_4$-Lys and $^{13}C_6$-Arg and ‘8/10’ for $^{13}C_6{}^{15}N_2$-Lys and $^{13}C_6{}^{15}N_4$-Arg. For each analysis, one 10 cm plates of HeLa cells were used per condition. Labeled cells were then transfected with FLAG-G3BP1 as per

manufacturers protocols (Invitrogen) for 48 hrs. Cells were then starved in pre-warmed HBSS media for mock, 1hr, and 4hrs for 0/0, 4/6 and 8/10, respectively. Cell lysates were collected for each condition and combined at 1:1:1 protein ratio. Co-IP was performed using EZview Red Anti-FLAG® M2 affinity gel beads (Sigma-Aldrich, F2426) as mentioned above. Immunoprecipitated proteins were boiled in 6x sample buffer for 5 minutes at 98°C and samples were run on an SDS gel followed by coomassie staining to visualize protein migration. Protein extraction was performed by gel digestion on the entire lane.

All analyses here involved in solution digestions in 1% SDC (System Development Company, 50 mM Tris, pH 8) with protein sample in the pull-down experiments being solubilized directly in SDC and then subjected to trypsin digestion. Protein solutions were reduced (1 µg DTT/50 µg protein), alkylated (5 µg IAA/50 µg protein) and digested (1 µg trypsin/50 µg protein). For each sample, 5 ug (measured by BCA method) of digested peptides were analyzed by liquid chromatography-tandem mass spectrometry (LC-MS/MS) on a Bruker Impact. The Bruker Impact was on-line coupled to Agilent 1100 Series nanoflow HPLC instruments using a nanospray ionization source (Proxeon Biosystems) holding columns packed into 15-cm-long, 75-µm-inner diameter fused silica emitters (8-µm-diameter opening, pulled on a P-2000 laser puller from Sutter Instruments) using 3-µm-diameter ReproSil Pur C18 beads. Buffer A consisted of 0.5% acetic acid, and buffer B consisted of 0.5% acetic acid and 80% acetonitrile. Gradients were run from 6% B to 30% B over 60 min, then 30% B to 80% B in the next 10 mins, held at 80% B for 5 mins, and then dropped to 6% B for another 15 mins to recondition the column. The LTQ-OrbitrapXL was set to acquire a full-range scan at 60,000 resolution from 350 to 1500 Th in the Orbitrap and to simultaneously fragment the top five peptide ions in each cycle in the LTQ.

Protein identification and quantification were done using MaxQuant and Mascot (v2.3, Matrix Science) to search against the International Protein Index (IPI) Mouse (v3.69, 110,771 sequences - common serum contaminants & human keratins added and all reversed sequences were concatenated) database with the following criteria: electrospray ionization-ion trap fragmentation characteristics, tryptic specificity with up to one missed cleavages; ±10 parts-per-million and ±0.6 Da accuracy for MS and MS/MS measurements respectively; cysteine carbamidomethylation as a fixed modification; N-terminal protein acetylation, methionine oxidation, deamidation (NQ), duplex ($^{2}H_4$-Lys, $^{13}C_6$-Arg) or triplex ($^{13}C_6{}^{15}N_2$-Lys and $^{13}C_6{}^{15}N_4$-Arg) SILAC modifications as appropriate; peptide false discovery rate (FDR) was set at 1%. Quantitation was done using a mass precision of 2 ppm (three times the mass precision is used to create extracted ion chromatograms). After extracting each ion chromatogram, Proteome Discoverer runs several filters to check for, among other things, interfering peaks and the expected isotope pattern, and peptides that do not meet all the criteria are not used in calculating the final ratio for each protein. We consider proteins identified if at least two peptides were observed. Analytical variability of SILAC data in the types of experiments performed here is typically <1% on average and biological variability was addressed in these experiments by performing at least three independent replicates of each experiment.

2.16 Statistical analysis

Quantified results are expressed as means ± standard deviation (SD). Statistical analysis was performed with unpaired Student's *t* test. A value of $p < 0.05$ was considered to be statistically significant. All experiments were repeated at least three times.

Chapter 3: Production of a Dominant-Negative Fragment Due to G3BP1 Cleavage Contributes to the Disruption of Mitochondria-Associated Protective Stress Granules during CVB3 Infection

3.1 Background

In order for CVB3 to successfully replicate, the virus is required to usurp host protein synthesis machinery and evade host innate immunity responses. Previous reports in CVB3 infection show stalled host-protein translation by cleavage of multiple translation factors, including PABP, eIF4G, and eIF5B, by viral protease $2A^{pro}$ and $3C^{pro}$ [223, 224, 225]. CVB3 infection also induces eIF2α phosphorylation, thus reducing the amount of cytoplasmic eIF2-GTP-met-tRNAi ternary complex that may be used to initiate protein translation [226]. Virally-induced shutdown of cap-dependent mRNA protein translation due to cleavage of essential translation factors and eIF2α phosphorylation results in two outcomes: release of ribosomes for viral protein synthesis and a diminished host anti-viral response.

Inhibition of protein synthesis in response to viral infection results in the formation of SGs [122, 149, 182, 227]. SGs are composed of more than 50 known proteins. As previously mentioned, a key component of SGs is the aggregating factor G3BP1, which is widely used as a well-established SG marker under various environmental stress conditions [228]. Other key proteins that localize to SGs include the T-cell restricted intracellular antigen 1/related (TIA1/R) and HuR [131, 142, 227]. Several studies have reported that SGs are compositionally different depending on the type of environmental stresses [192], suggesting that distinct SGs may be regulated differentially and have multiple roles.

Previous studies demonstrated that SG formation can be modulated by infection of several types of viruses, including flaviviruses, dicistroviruses and picornaviruses. SGs have been shown to play both pro- and anti-viral roles in different infections. Multiple viruses have been demonstrated to interfere with different steps of SG assembly [229]. For example, anti-viral SGs are formed in response to PV infection; however SGs are disassembled by viral proteases at late stages of infection in order to promote viral replication [173]. Moreover, studies in Junin virus demonstrated selective inhibition of anti-viral SG formation by inhibiting eIF2α phosphorylation [230]. Other studies showed that anti-viral SGs may require mitochondrial surface proteins to activate downstream interferon pathway [182, 184]. These SGs contain anti-viral proteins including RIG-I, a protein involved in sensing dsRNA for signaling to downstream anti-viral responses by binding interferon-beta promoter stimulator-1 (IPS-1 or also known as MAVS/VISA/Cardif), a mitochondrial surface protein [182, 184]. On the other hand, respiratory syncytial virus and hepatitis C virus have been observed to manipulate SGs for their own benefit by interacting with critical components of the pro-viral SGs during infection [231, 232]. However, the accumulation, function and presence of SGs during CVB3 infection remain largely unclear.

3.2 Objective and specific aims

The objective of this chapter is to investigate the interplay between CVB3 infection and the formation and significance of SGs.

The **SPECIFIC AIMS** include:

Aim 1: To examine the effect of CVB3 infection on SG formation;

Aim 2: To examine the mechanisms by which CVB3 regulates the formation of SGs; and

Aim 3: To examine the significance of SGs in CVB3 infection.

3.3 Results

3.3.1 CVB3 infection induces SG formation at ~3 hrs and disassembly at ~5 hrs post-infection.

As previously mentioned, SG formation has been observed in other viruses including PV and EMCV in the *Picornaviridae* family [173, 184]; however the effect of CVB3 infection on SG formation has not been investigated. In order to visualize SG formation in CVB3 infection, we utilized HeLa cells stably expressing GFP-G3BP1. Confocal imaging showed the punctate accumulation of GFP fluorescence in the cytosol at ~3 hrs post-infection (pi) and disappearance at ~5 hrs pi (**Figure 4A, B, and D**). Using two other well established SG markers, TIA1 and HuR, we demonstrated co-localization of red punctates (dsRed-TIA1 or -HuR) with green punctates (GFP-G3BP1) (**Figure 4A, B, and D**), further suggesting formation and disassembly of SGs during CVB3 infection. Furthermore, we demonstrated the co-localization of G3BP1-SGs with poly(A)-mRNA at 3 hrs pi; however at 5 hrs pi, G3BP1 dissolved homogenously back into the cytoplasm while poly(A)-positive granules persisted (**Figure 4C and E**). The persistence of RNA granules suggests that G3BP1-SGs are specifically targeted during CVB3 infection. Our preliminary results have suggested that the formation and persistence of poly(A)-granules observed at 5 hrs and 7 hrs pi are associated with other RNA granules, i.e. P-bodies (data not shown).

To gain insight into the cellular localization of stalled initiation complexes in CVB3-infected cells, we performed transmission- and immuno-electron microscopy analyses. We chose 4 hrs as an endpoint in this study because SGs are still present at high levels before disassembly at 5 hrs pi. As shown in **Figure 4F**, in sham-infected cells, the ribosomal-like particles (indicated

by arrow heads) were mainly localized to the fiber-like structures that represent the endoplasmic reticulum. However, in CVB3-infected cells, these particles tended to accumulate to form aggregates (~100nm in diameter, indicated by arrow heads), similar to those shown by Gilks *et al.* [161]. Furthermore, immuno-electron microscopy imaging showed that G3BP1 staining was diffuse in sham-infected cells, while CVB3-infected cells comprised of both diffuse and G3BP1-positive aggregates, the latter were primarily observed near mitochondrial surfaces (**Figure 4G**). This observation further supports the presence of G3BP1-positive aggregates in CVB3-infected cells.

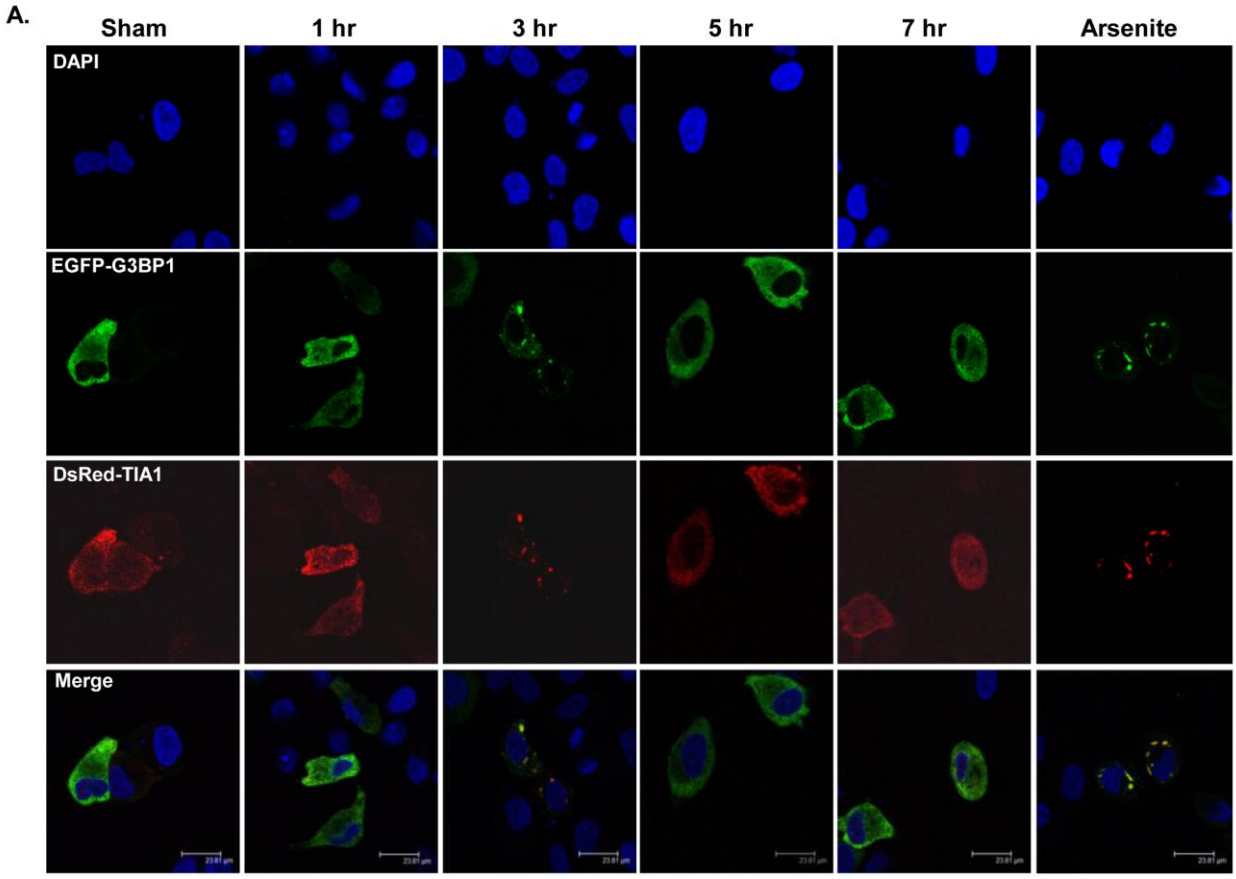
A.
Sham
1 hr
3 hr
5 hr
7 hr
Arsenite
DAPI
EGFP-G3BP1
DsRed-TIA1
Merge

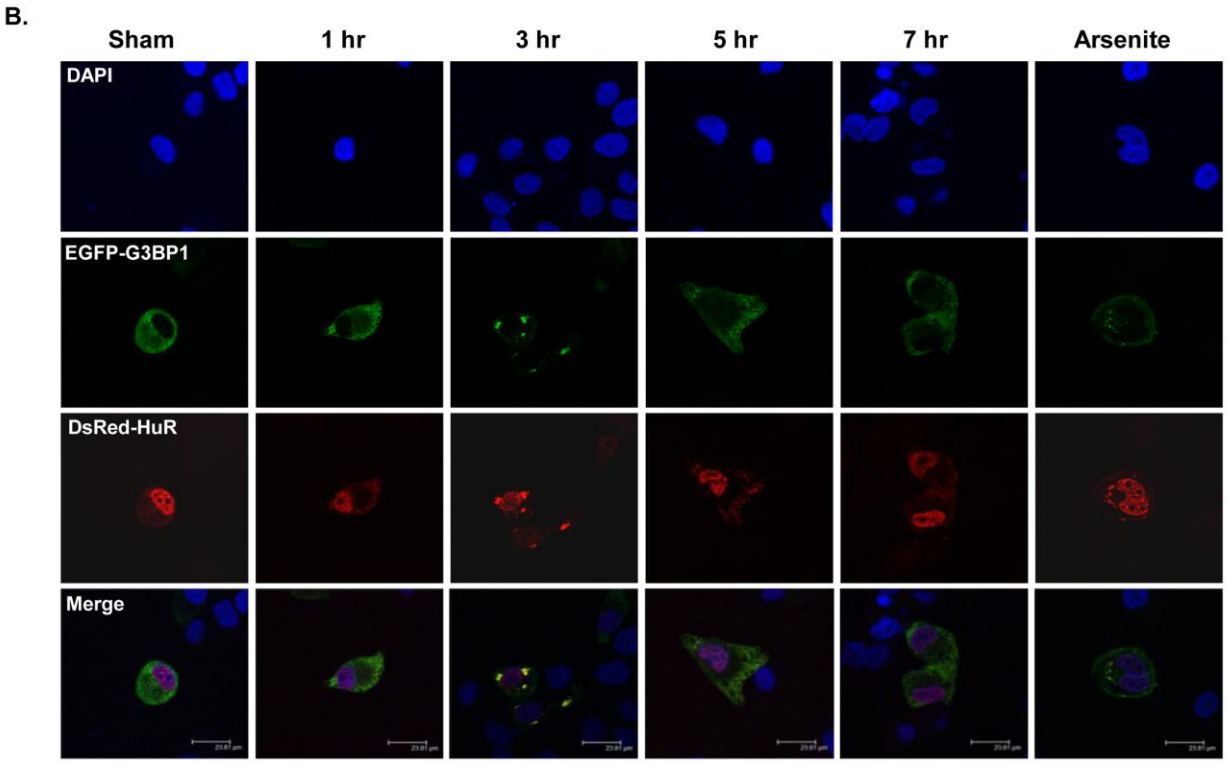
B.
Sham
1 hr
3 hr
5 hr
7 hr
Arsenite
DAPI
EGFP-G3BP1
DsRed-HuR
Merge

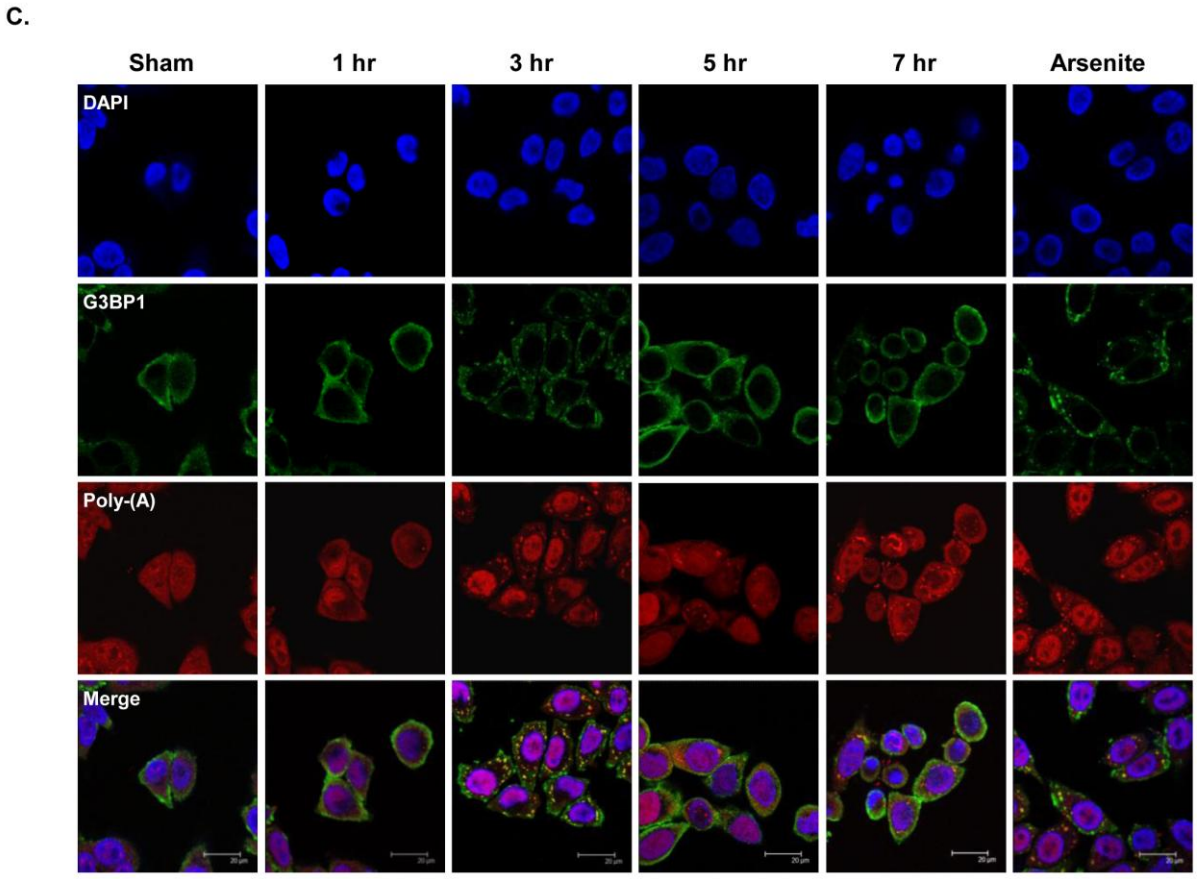
C.
Sham
1 hr
3 hr
5 hr
7 hr
Arsenite
DAPI
G3BP1
Poly-(A)
Merge

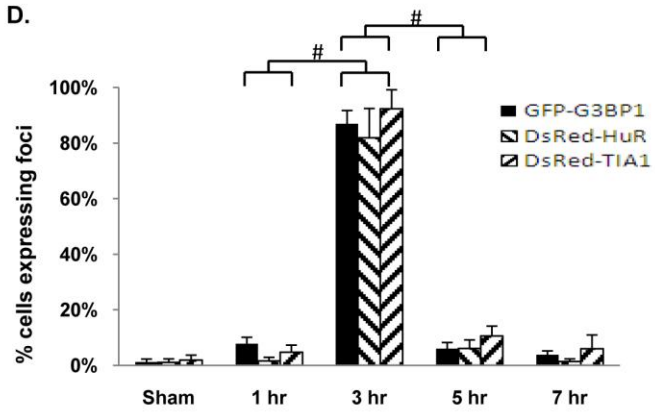
D.
% cells expressing foci
100%
80%
60%
40%
20%
0%
Sham
1 hr
3 hr
5 hr
7 hr
GFP-G3BP1
DsRed-HuR
DsRed-TIA1
#
#

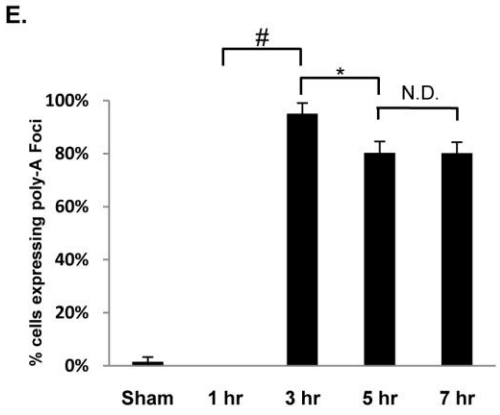
E.
% cells expressing poly-A Foci
100%
80%
60%
40%
20%
0%
Sham
1 hr
3 hr
5 hr
7 hr
#
*
N.D.

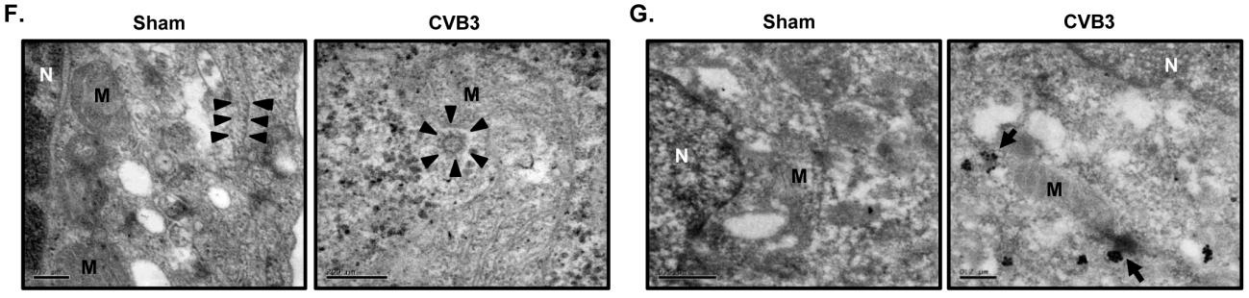
F.
Sham
CVB3
N
M
M
M
G.
Sham
CVB3
N
M
N
M

Figure 4. CVB3 infection induces SG formation at ~3 hrs and disassembly at ~5 hrs post-infection

Representative confocal images of intracellular localization of G3BP1, TIA1 and HuR following CVB3 infection of HeLa cells. HeLa cells were transiently co-transfected with pEGFP-G3BP1 and either pDsRed-TIA1 (A) or pDsRed-HuR (B) for 48 hrs, followed by sham- or CVB3 infection at an MOI of 10 for various time points as indicated. Arsenite treatment at a dose of 50 mM for 1 hr was used as positive controls for inducing SG formation. Cell nuclei were counterstained with DAPI. (C) Representative confocal images of co-localization of poly-(A)-mRNA with G3BP1 during CVB3 infection. HeLa cells were transiently transfected with pEGFP-G3BP1 for 48 hrs, followed by sham- or CVB3 infection at an MOI of 10 for different time points as indicated. Poly-(A)-mRNA was detected by *in situ* hybridization using an oligo-dT probe synthetically conjugated to Cy3, followed by immunostaining for G3BP1. Cell nuclei were counterstained with DAPI. (D) Quantitation of G3BP1-SG formation from (A, B). Percent of cells expressing SGs was quantified as described in Materials and Methods (mean ± SD, n=10 images), #$p<0.001$. (E) Quantitation of poly-(A) granules from (C). Percent of cells expressing poly-(A) punctates was quantified as above. N.D., No statistical difference, *$p<0.01$. (F, G) Representative transmission (F) and immune-electron (G) microscope images. HeLa cells were either sham- or CVB3-infected at an MOI of 10 for 4 hrs. N and M indicate the nucleus and mitochondria, respectively. Arrow heads in (F) indicate ribosomal-like structures. Arrows in (G) indicate cytoplasmic aggregates that were stained positive for endogenous G3BP1.

3.3.2 Coxsackievirus protease 2A cleaves eIF4G and promotes SG formation.

It has been previously demonstrated that CVB3 infection inhibits cap-dependent protein translation, mainly due to eIF4G cleavage and eIF2α phosphorylation [220, 223]. To explore the

potential mechanism by which CVB3 regulates SG formation, we examined the kinetics of eIF4G cleavage and eIF2α phosphorylation. We found that eIF4G cleavage occurred at ~1 hr pi preceding eIF2α phosphorylation at ~5 hrs pi (**Figure 5A**). It should be noted that the correlation of band intensities between full-length and cleaved eIF4G in Figure 6A is likely a result of incomplete transfer of high molecular weight proteins (i.e. full-length eIF4G ~220kDa). Using IRES-driven CVB3 $2A^{pro}$ and $3C^{pro}$ constructs, we showed that eIF4G was cleaved in HeLa cells transfected with pIRES-$2A^{pro}$ (**Figure 5B**). Furthermore, we demonstrated that cells expressing pIRES-$2A^{pro}$, but not pIRES-$3C^{pro}$, displayed increased G3BP1 foci (**Figure 5C**). Together, these results suggest that translation initiation inhibition, which is in part due to eIF4G cleavage by $2A^{pro}$, leads to enhanced SG formation during the early phase of CVB3 infection.

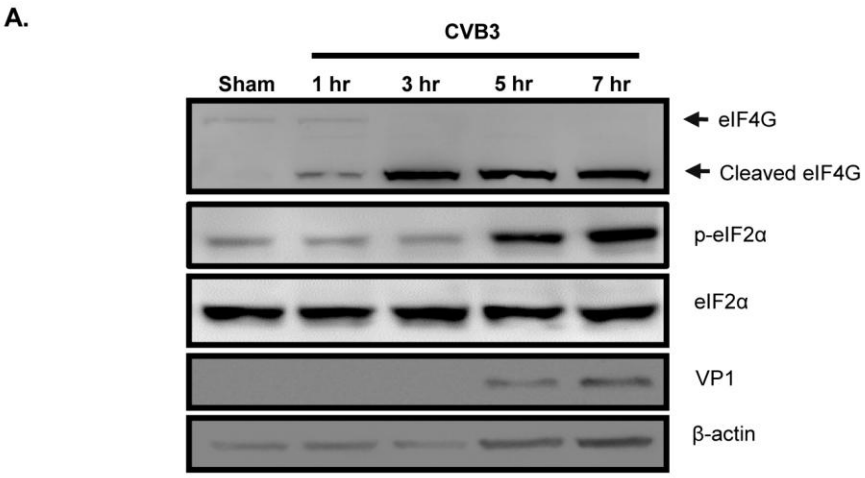

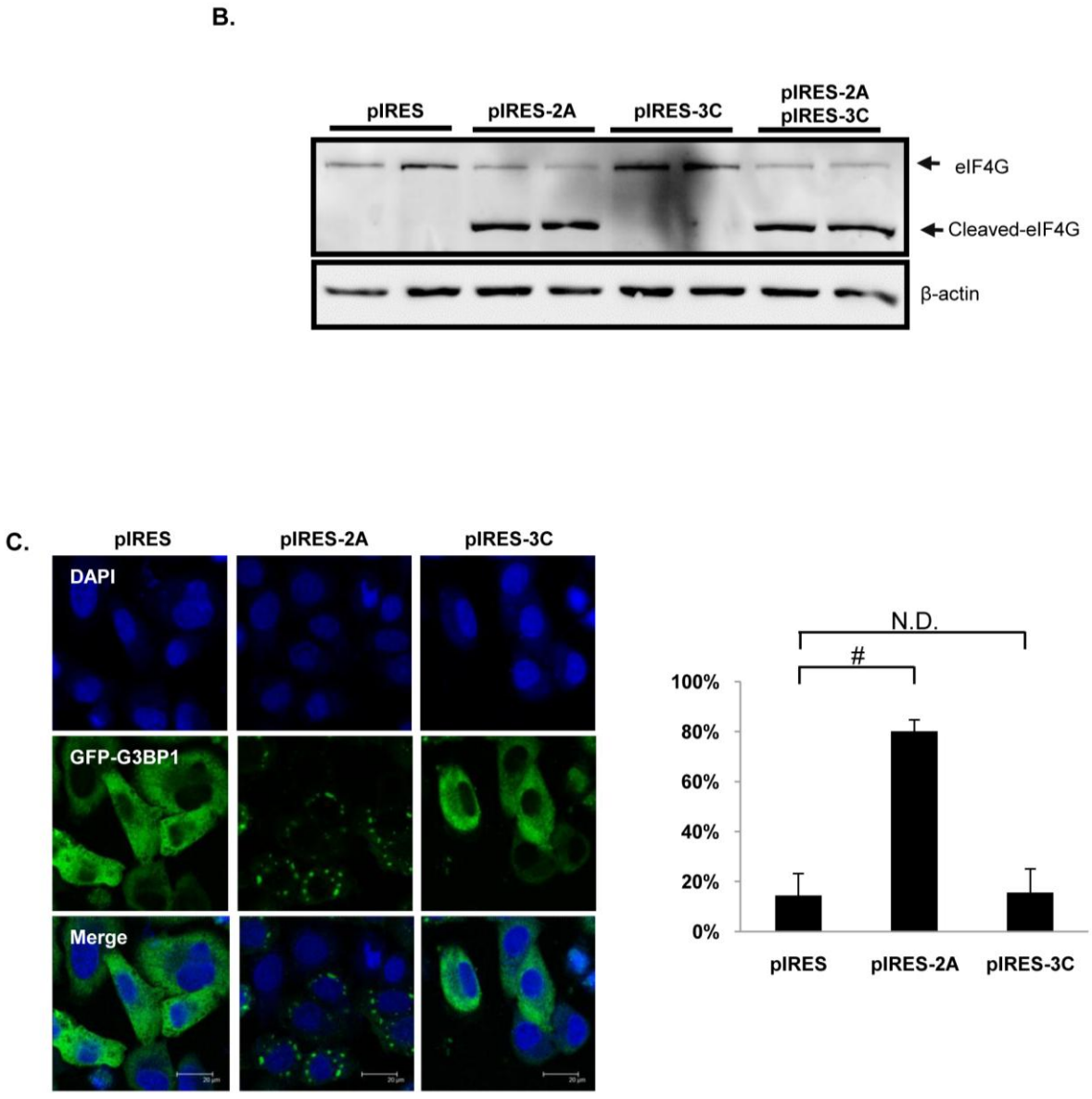

Figure 5. Coxsackieviral protease 2A cleaves eIF4G and promotes SG formation

(A) HeLa cells were either sham- or CVB3-infected at an MOI of 10 for various time points as indicated. Western blotting was performed to assess protein expression of eIF4G, phopho-eIF2α (Ser 51), and total eIF2α. Protein level of viral capsid protein (VP1) and β-actin was also examined as an infection and loading control, respectively. (B) HeLa cells were transfected with pIRES-2A and/or pIRES-3C for 48 hrs. Western blotting was performed to assess protein

expression of eIF4G and β-actin. (C) Representative confocal images of viral protease $2A^{pro}$ inducing G3BP1-SG formation. HeLa cells were co-transfected with pIRES-$2A^{pro}$ or pIRES-$3C^{pro}$ together with GFP-G3BP1 for 24 hrs, followed by confocal microscopy analysis.

3.3.3 CVB3 infection causes G3BP1 cleavage.

To investigate whether disassembly of SGs at the late stage of CVB3 infection is due to an inhibition of the assembly of SGs and/or a result of increased disassembly of SGs, HeLa cells infected with CVB3 were treated with arsenite to induce SG formation and G3BP1-SGs were monitored at 3 hrs and 5 hrs pi. **Figure 6** showed that arsenite-induced G3BP1-SGs were significantly inhibited after 5 hr CVB3 infection, whereas poly-(A)-SGs persisted. This data suggests that G3BP1-SGs are actively and selectively disassembled beyond 5 hrs pi.

We next examined the protein expression of G3BP1 and TIA1 during CVB3 infection in HeLa cells stably expressing GFP-G3BP1. Western blot results showed the reduction in protein expression of full length G3BP1 (exogenous 99kDa, endogenous 71 kDa) at 5 and 7 hrs pi, accompanied by the appearance of a second band with smaller molecular weight (exogenous 82kDa, endogenous 54 kDa) (**Figure 7A**), suggesting that G3BP1 is cleaved at 5 hrs pi. TIA1 remained unchanged along the course of CVB3 infection (**Figure 7B**).

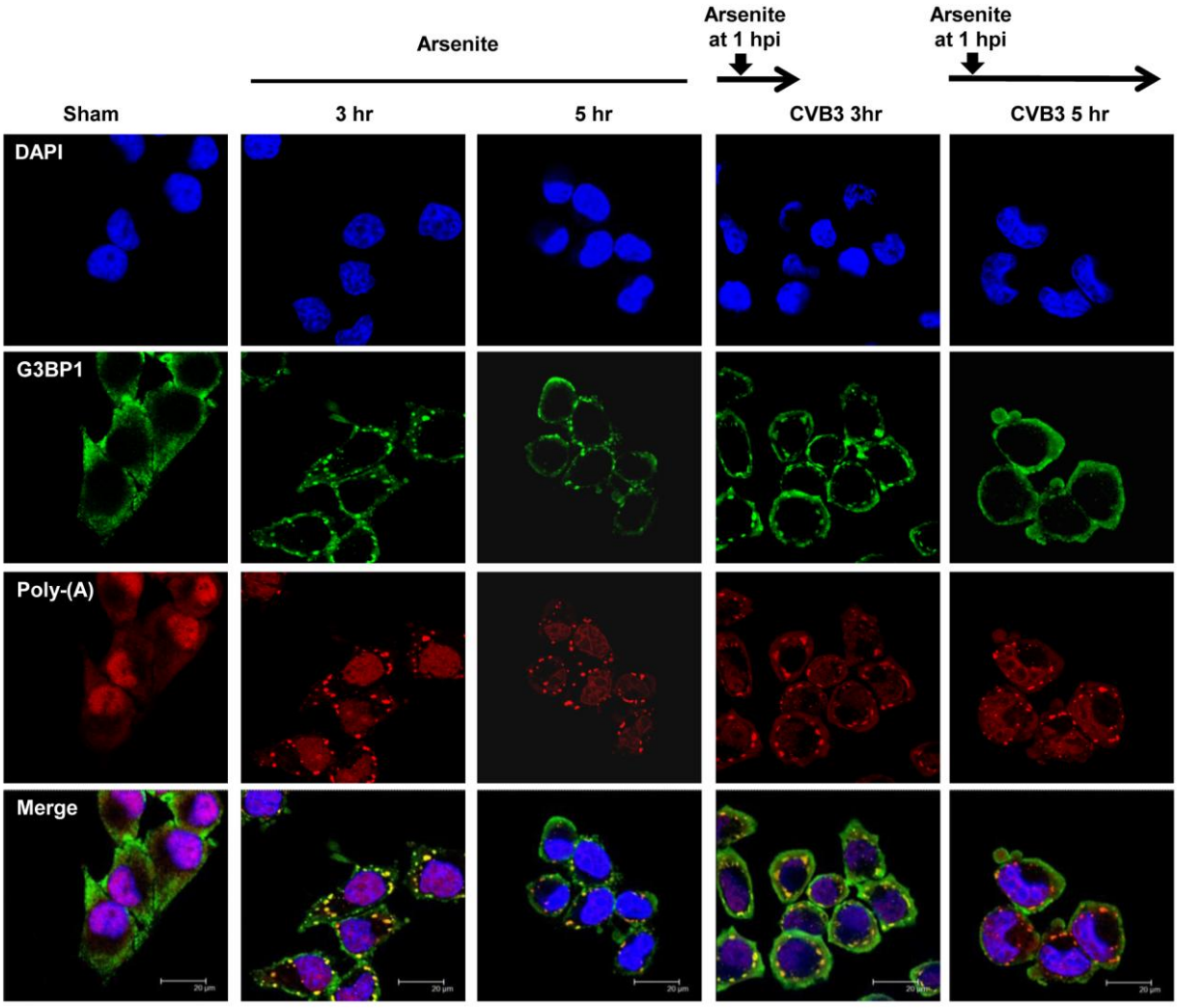
Arsenite
Arsenite at 1 hpi
Arsenite at 1 hpi
Sham
3 hr
5 hr
CVB3 3hr
CVB3 5 hr
DAPI
G3BP1
Poly-(A)
Merge

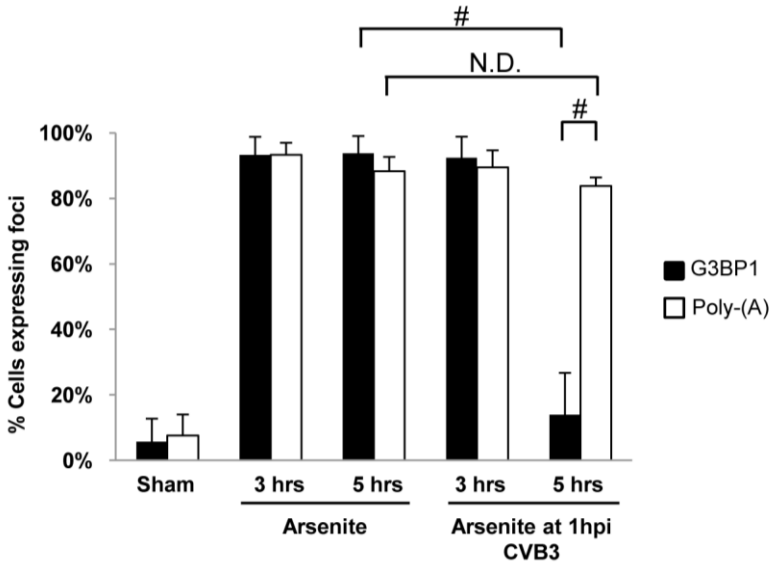

Figure 6. G3BP1-SGs are disassembled while poly-A-SGs remain persistent in CVB3-infected cells

HeLa cells were infected with CVB3 at an MOI of 10 for 3 or 5 hrs. Arsenite was added at 1h post-infection (pi) as indicated. Cells treated with arsenite alone for 3 or 5 hrs were used as negative controls. Cells were fixed and stained for endogenous G3BP1, poly-A mRNA, and nuclei. Percent of cells expressing G3BP1-SGs and poly-A granules was quantified as described in Materials and Methods (mean ± SD, n=5 images), N.D., No statistical difference, #$p<0.001$.

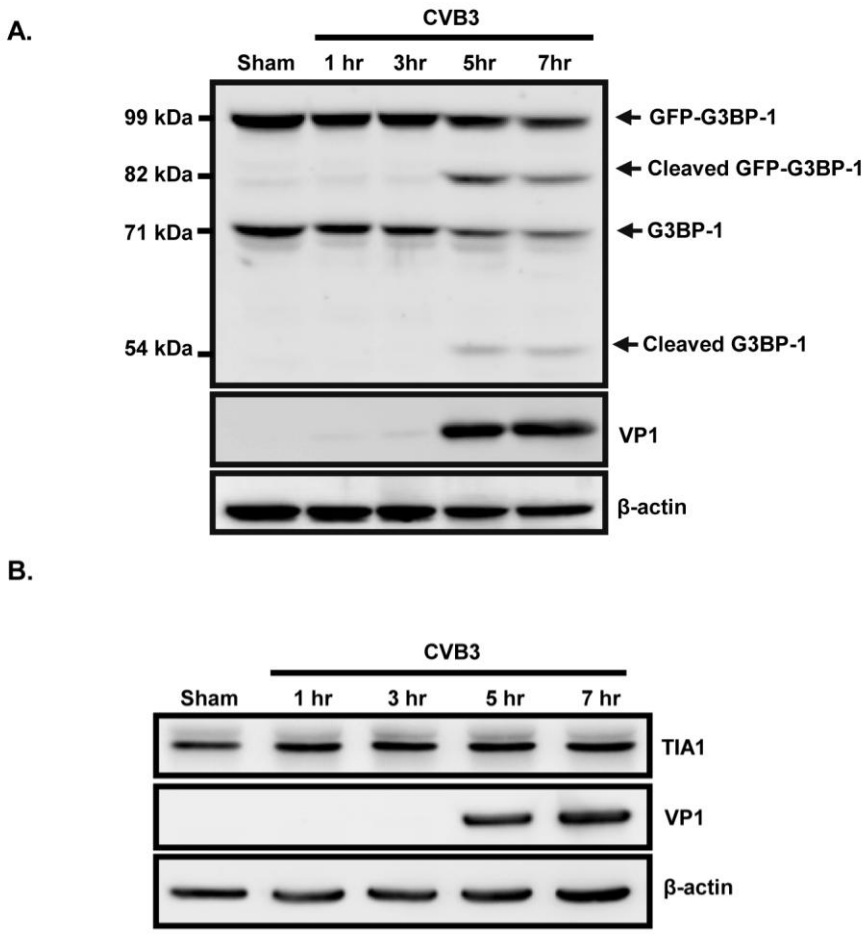

Figure 7. G3BP1 is cleaved at ~5 hrs post-Infection while TIA1 remains unchanged during the course of CVB3 infection

(A) HeLa cells stably expressing exogenous GFP-G3BP1 or (B) regular HeLa cells were either sham- or CVB3-infected at an MOI of 10 for various time points as indicated. Western blotting was performed to assess protein expression of G3BP1 using anti-G3BP1 antibody (A) and TIA1 using anti-TIA1 antibody (B). VP1 expression was used as an infection control and β-actin level was examined as a loading control.

3.3.4 G3BP1 cleavage is due to viral protease 3C.

To explore the mechanism of G3BP1 cleavage, viral proteases, $3C^{pro}$ and $2A^{pro}$, were purified and incubated with uninfected HeLa cell lysates. HeLa cells incubated with $3C^{pro}$ for increasing time points led to decreasing levels of full-length G3BP1 accompanied by an increasing accumulation of G3BP1 cleavage fragments, suggesting that $3C^{pro}$ cleaves G3BP1 (**Figure 8A**). Incubation with purified $2A^{pro}$ failed to induce a similar G3BP1 cleavage fragment, while PABP, a known target of $2A^{pro}$, was cleaved as previously demonstrated [224]. Incubation with a catalytically inactive mutant $2A^{pro}$ ($2Amut^{pro}$), failed to induce PABP cleavage (**Figure 8B**). Furthermore, we found that treatment of HeLa cells with Z-VAD-FMK, a pan-caspase inhibitor, had no effect on CVB3-induced G3BP1 cleavage (data not shown). Taken together, our results indicate that $3C^{pro}$ alone is sufficient to induce G3BP1 cleavage during CVB3 infection.

Figure 8. G3BP1 is cleaved by 3Cpro

HeLa cell lysates were incubated with (A) purified $3C^{pro}$ for 0, 5, 15, 30, and 60 mins or $2A^{pro}$ for 60 mins, or (B) purified $2A^{pro}$ or $2Amut^{pro}$ for 60 mins. *In vitro* cleavage assay was performed as described in Materials and Methods and expression of G3BP1 and PABP was detected by western blotting.

3.3.5 G3BP1 is cleaved at amino acid Q325 and a cleavage resistant mutant restores SG formation.

To identify the cleavage site of G3BP1, we tested whether G3BP1 is cleaved at amino acid 325, a previously identified cleavage site by PV $3C^{pro}$ [173]. We used a mutant G3BP1 with an amino acid mutation (Q325E), a potentially cleavage mutant G3BP1. Western blot results demonstrated the absence of the cleavage product in FLAG-$G3BP1^{Q325E}$-transfected HeLa cells following CVB3 infection, indicating that $G3BP1^{Q325E}$ is cleavage resistant (**Figure 9A**). The cleavage of G3BP1 at Q325 separates its NTF2-like domain from the RRM, which may lead to the disruption of the ability of G3BP1 to bind RNA and protein in order to induce SG formation (**Figure 9B**). Moreover, we conducted immunocytochemistry to determine whether non-cleavable G3BP1 ($G3BP1^{Q325E}$) is able to restore SG formation after 5 hrs CVB3 infection. Results shown in **Figure 9C and D** demonstrated that SG assembly in cells stably expressing GFP-$G3BP1^{Q325E}$ mutant was rescued at 5 hrs and 7 hrs pi. Together, our results suggest that cleavage of G3BP1 at amino acid Q325 contributes to G3BP1-SG disassembly observed during late stage of CVB3 infection.

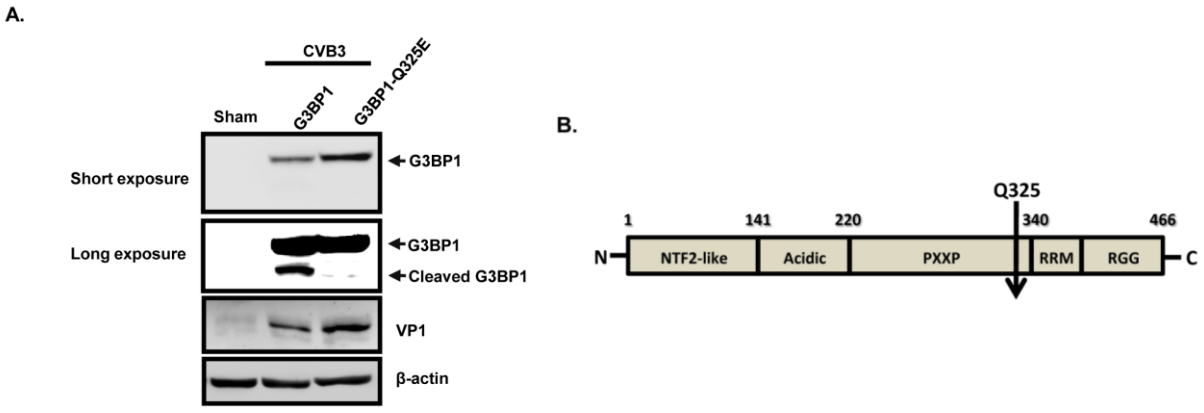

C.

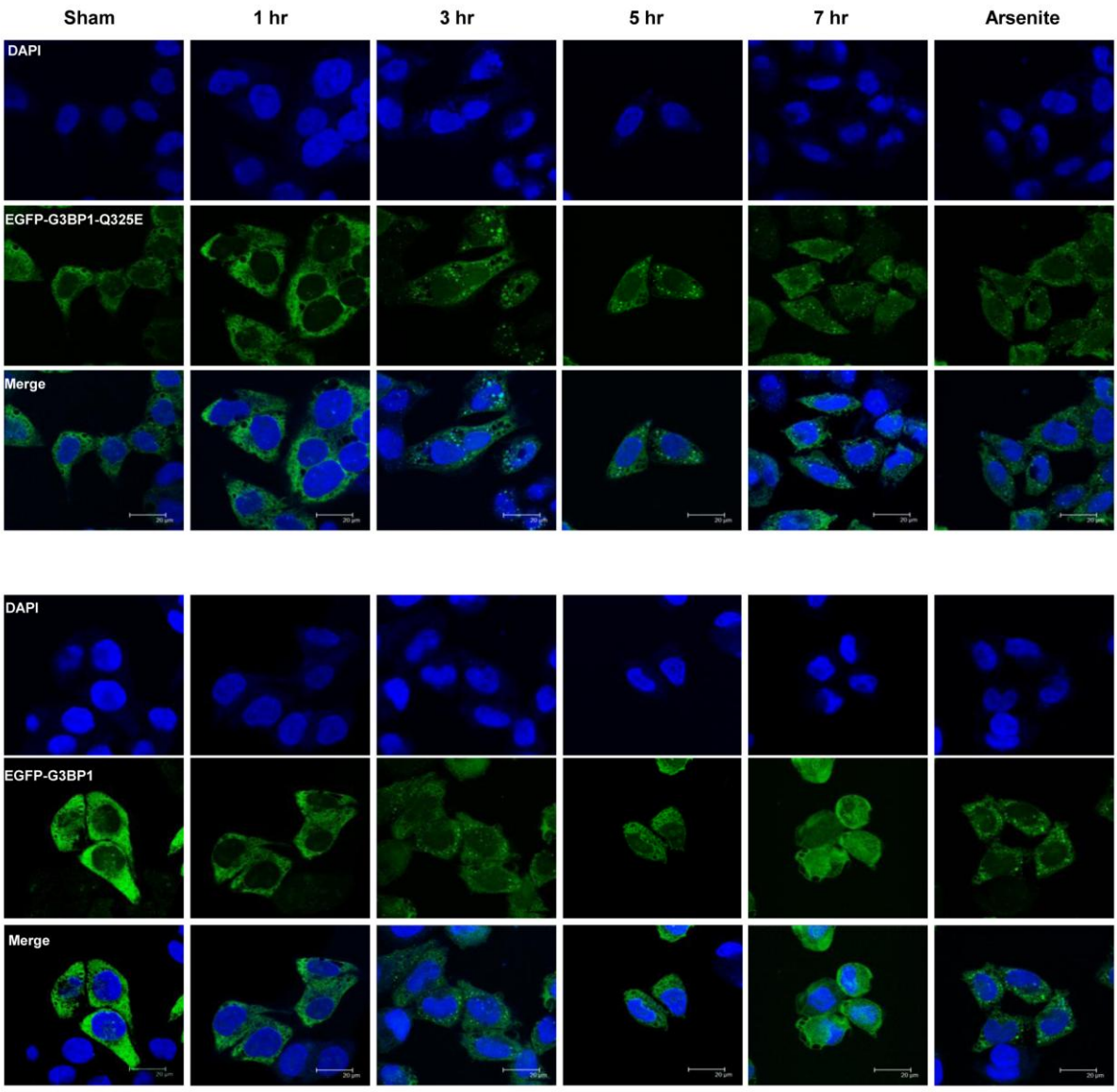
Sham
1 hr
3 hr
5 hr
7 hr
Arsenite
DAPI
EGFP-G3BP1-Q325E
Merge
DAPI
EGFP-G3BP1
Merge

D.

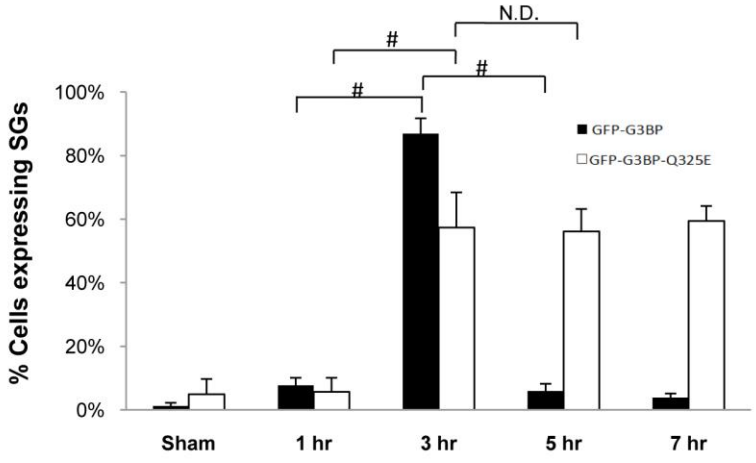
N.D.
#
#
#
100%
80%
60%
40%
20%
0%
% Cells expressing SGs
GFP-G3BP
GFP-G3BP-Q325E
Sham
1 hr
3 hr
5 hr
7 hr

Figure 9. G3BP1 is cleaved at amino acid Q325 and a cleavage-resistant G3BP1 mutant restores SG formation at ~5 hrs post-infection

(A) HeLa cells were transfected with FLAG-G3BP1 or FLAG-G3BP1^{Q325E} mutant for 48 hrs, followed by CVB3 infection at an MOI of 10 for 7 hrs. Western blotting was performed to examine G3BP1 cleavage using an anti-FLAG antibody. Protein expression of VP1 and β-actin was examined as an infection and loading control, respectively. (B) Schematic diagram of full length G3BP1 and the cleavage site. The arrow indicates the cleavage point at amino acid Q325 of G3BP1. NTF2-like, Nuclear Transport Factor 2-like; PXXP, SH3-domain binding domain of Ras-GAP; RRM, RNA Recognition Motif; RGG, Arginine-Glycine-rich region. (C) HeLa cells stably expressing GFP-G3BP1^{Q325E} (upper panels) or GFP-G3BP1 (lower panels) were sham- or CVB3-infected at an MOI of 10 for different times as indicated. Intracellular distribution of G3BP1 was examined using confocal microscopy. Cell nuclei were counterstained with DAPI. Cells treated with 50 mM arsenite for 1 hr were used as positive controls. (D) Quantitation of G3BP1-SG formation from (C). Results are presented as mean ± SD (n=10 images), #$p<0.001$, N.D., No statistical difference.

3.3.6 G3BP1 negatively regulates CVB3 replication.

To determine the significance of SGs in the course of CVB3 infection, G3BP1 was either overexpressed or knocked down in HeLa cells. We showed that overexpression of GFP-G3BP1 increased SG formation (**Figure 10A**), whereas knockdown of G3BP1 by siRNA led to the disappearance of G3BP1-SGs induced by CVB3 infection (**Figure 11A**). We further demonstrated that overexpression of GFP-G3BP1 resulted in marked decreases in VP1 protein expression (~5 fold) (**Figure 10B and C**), viral transcripts (~0.4 fold) (**Figure 10D**), and viral titers (~3 fold) (**Figure 10E**). In contrast, knockdown of G3BP1 resulted in significant increases

in VP1 protein expression (~2.5 fold) (**Figure 11B and C**), viral transcripts (~0.6 fold) (**Figure 11D**), and viral titers (~22 fold) (**Figure 11E**). Our data suggests that G3BP1-SGs negatively regulate CVB3 replication.

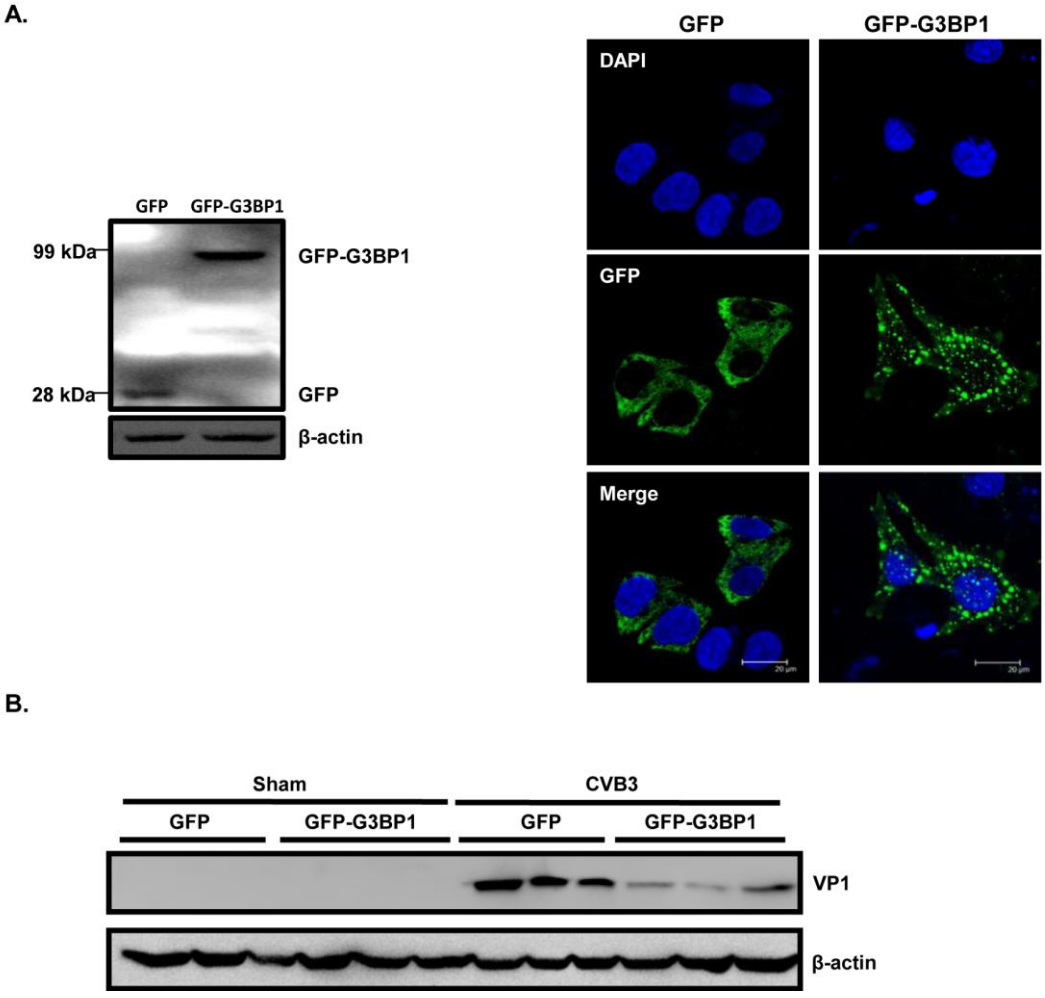

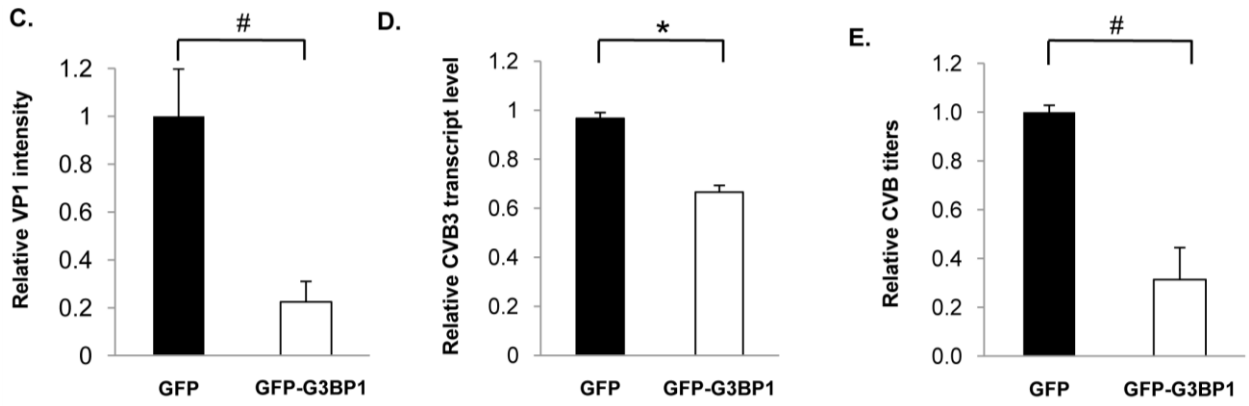

Figure 10. Overexpression of G3BP1 inhibits CVB3 replication.

HeLa cells were transiently transfected with pEGFP-G3BP1 for 24 hrs, followed by CVB3 infection at an MOI of 1 for 16 hrs. (A) Western blotting (left) and confocal microscopy (right) were performed to examine protein level and intracellular distribution of GFP-G3BP1. (B) Western Blotting was performed to assess protein expression of VP1 and β-actin after CVB3 infection. (C) Densitometric analysis using ImageJ was performed on VP1 intensities relative to β-actin intensities of three independent experiments from (B). The value of sham was arbitrarily set as 1. (D) Quantitative RT-PCR was performed to examine viral transcript levels using primers specific to the IRES promoter of the CVB3 RNA transcript. Data is presented as transcript copy number relative to its empty vector control. The value of the empty vector control was arbitrarily set as 1. (E) Plaque assay was performed to examine the effect of G3BP1 overexpression on viral replication and results are presented as relative PFU/ml. The value of the empty vector control was arbitrarily set as 1. Results are presented as mean ± SD (n=3), #$p<0.001$, *$p<0.01$

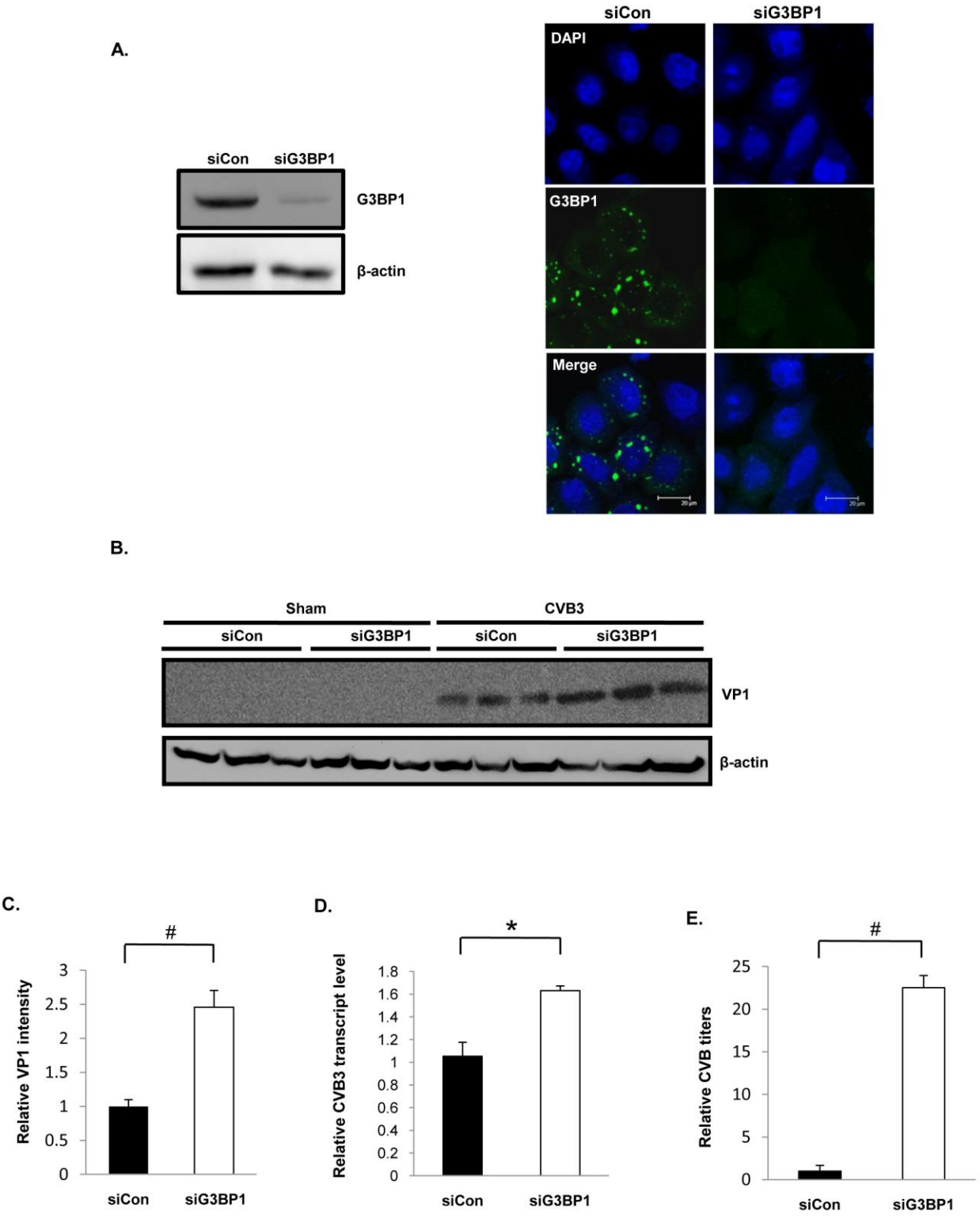
A.
siCon
siG3BP1
G3BP1
β-actin
DAPI
G3BP1
Merge
B.
Sham
CVB3
siCon
siG3BP1
siCon
siG3BP1
VP1
β-actin
C.
Relative VP1 intensity
#
siCon
siG3BP1
D.
Relative CVB3 transcript level
*
siCon
siG3BP1
E.
Relative CVB titers
#
siCon
siG3BP1

Figure 11. Knockdown of G3BP1 enhances CVB3 replication

HeLa cells were transfected with either control siRNA (siCon) or G3BP1-targeted siRNA (siG3BP1), followed by sham- or CVB3-infection at an MOI of 1 for 16 hrs. (A) Western blotting (left) and confocal microscopy (right) were performed to assess protein expression and intracellular distribution of GFP-G3BP1. (B) Western blotting was performed to examine VP1 and β-actin protein expression. (C) Densitometric analysis was performed on VP1 intensities of three independent experiments from (B) as described above. (D) Quantitative RT-PCR was performed to examine viral transcript levels as described above. Data is presented as transcript copy number relative to its empty vector control. The value of the siCon control was arbitrarily set as 1. (E) Plaque assay was performed to assess the effect of G3BP1 knockdown on viral replication and results are presented as relative PFU/ml. The value of the siCon control was arbitrarily set as 1. Results are presented as mean ± SD (n=3), #$p<0.001$, *$p<0.01$.

3.3.7 The C-terminal cleavage fragment of G3BP1 inhibits G3BP1-SG formation and enhances CVB3 replication.

We next explored whether the cleavage fragments of G3BP1 has any effects on SG formation. Confocal microscopy analysis showed that cells co-expressing G3BP1-N_{term} and GFP-G3BP1 displayed similar kinetics of G3BP1-SG assembly and disassembly as previously observed in wild-type G3BP1 expressing cells (data not shown). G3BP1-N_{term}-overexpressing cells also exhibited similar accumulation kinetics of poly(A)-RNA granules throughout infection (data not shown) compared with those expressing wild-type G3BP1 shown in **Figure 4C.** In contrast, cells expressing both G3BP1-C_{term} and GFP-G3BP1 displayed no or much smaller GFP punctates (arrow head) (**Figure 12A and C**), suggesting that the C-terminal fragment of G3BP1

negatively regulates SG formation. Similarly, the number of G3BP1-C_{term} expressing cells with poly(A)-granules at 3 hrs pi was significantly diminished compared to control (**Figure 12B and C**). We also examined the influences of the C-terminal fragment of G3BP1 on arsenite-induced SG formation. **Figure 12D** showed that HeLa cells expressing G3BP1-C_{term} inhibited arsenite-induced SGs, suggesting that the inhibitory effect of G3BP1-C_{term} on SG formation is not CVB3-specific.

Finally, we examined the impacts of the C-terminal portion of G3BP1 on viral replication. **Figure 12E** showed that overexpression of G3BP1-C_{term} resulted in significant increases in virus titres as compared to empty control. Taken together, our results suggest that the C-terminal fragment of G3BP1 acts as a dominant-negative inhibitor for G3BP1-SG formation and positively affects viral growth.

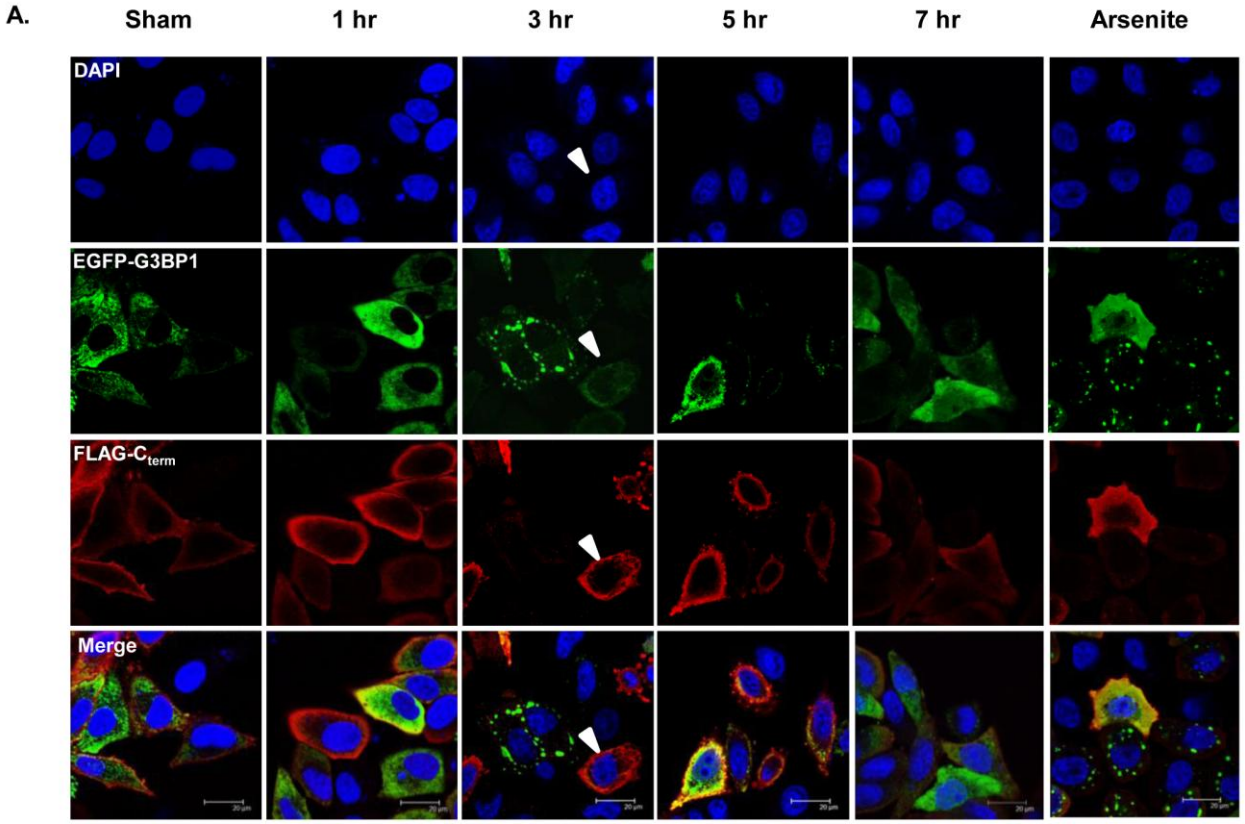

B.

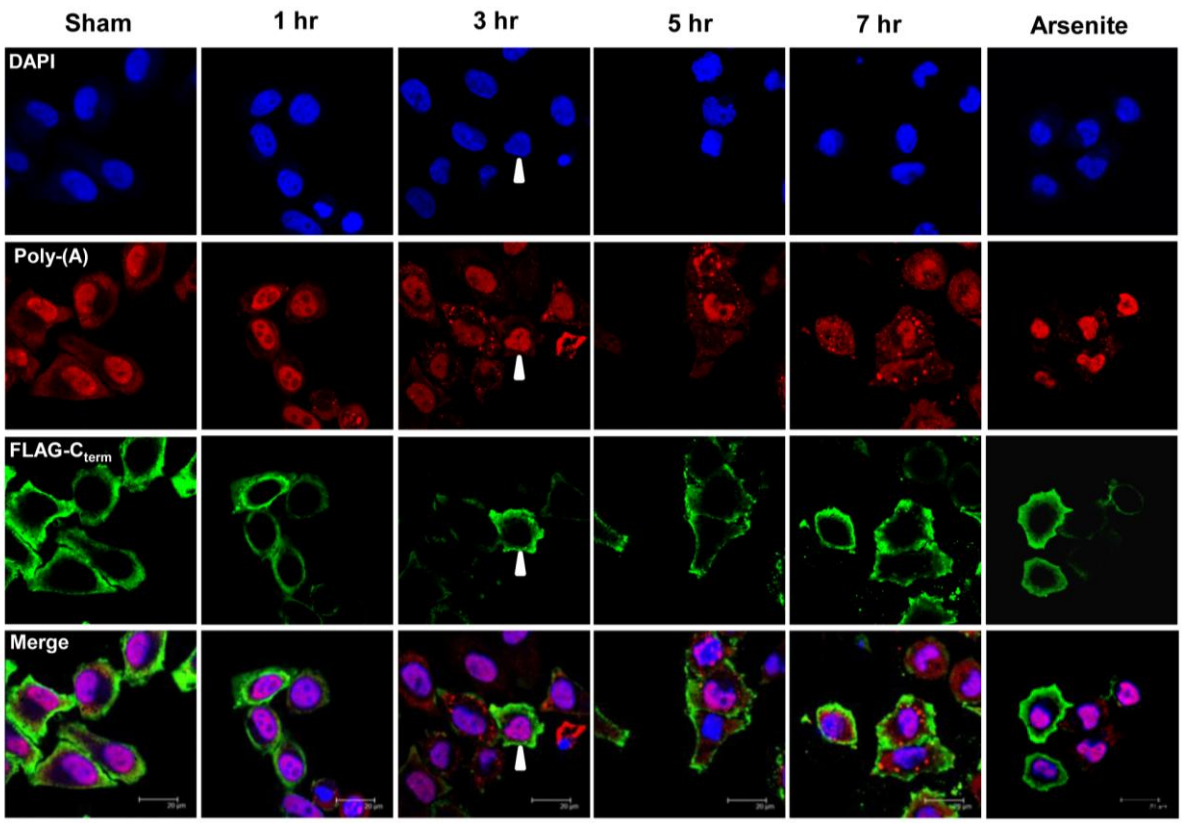
Sham
1 hr
3 hr
5 hr
7 hr
Arsenite
DAPI
Poly-(A)
FLAG-Cterm
Merge

C.

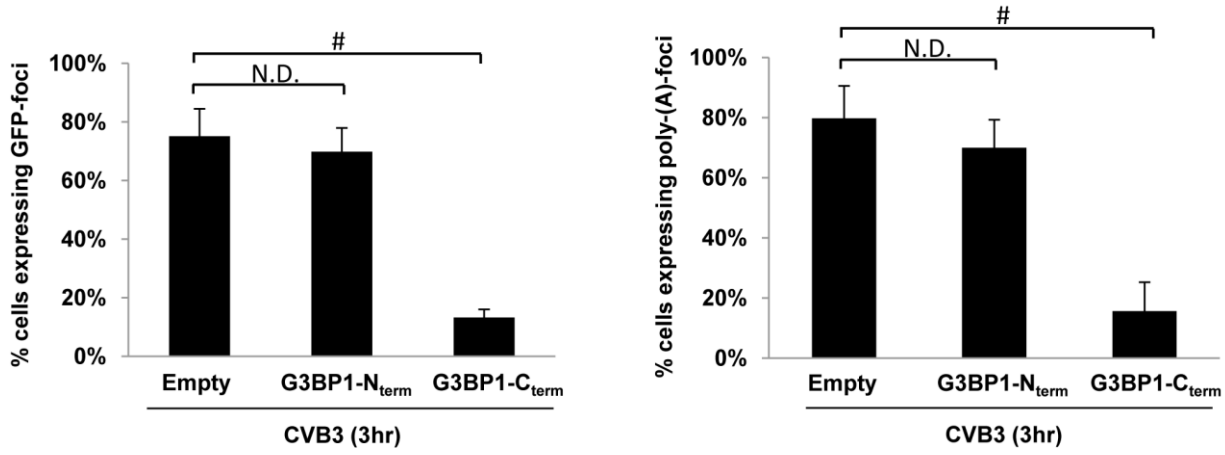
% cells expressing GFP-foci
100%
80%
60%
40%
20%
0%
#
N.D.
Empty
G3BP1-Nterm
G3BP1-Cterm
CVB3 (3hr)
% cells expressing poly-(A)-foci
100%
80%
60%
40%
20%
0%
#
N.D.
Empty
G3BP1-Nterm
G3BP1-Cterm
CVB3 (3hr)

D.

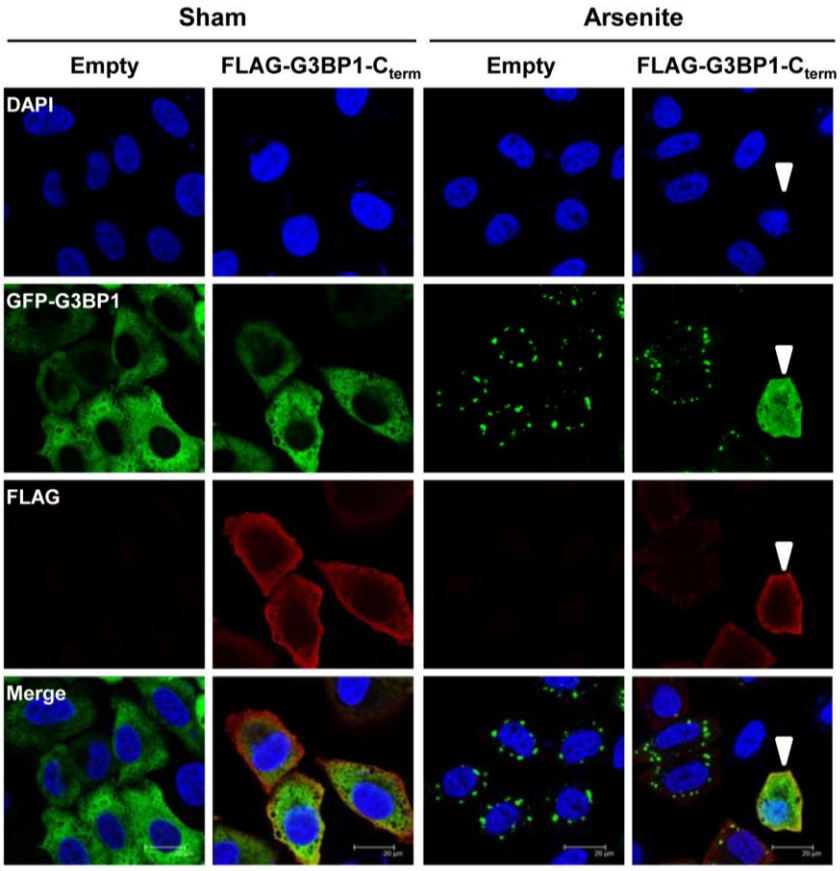
Sham
Arsenite
Empty
FLAG-G3BP1-C$_{term}$
Empty
FLAG-G3BP1-C$_{term}$
DAPI
GFP-G3BP1
FLAG
Merge

E.

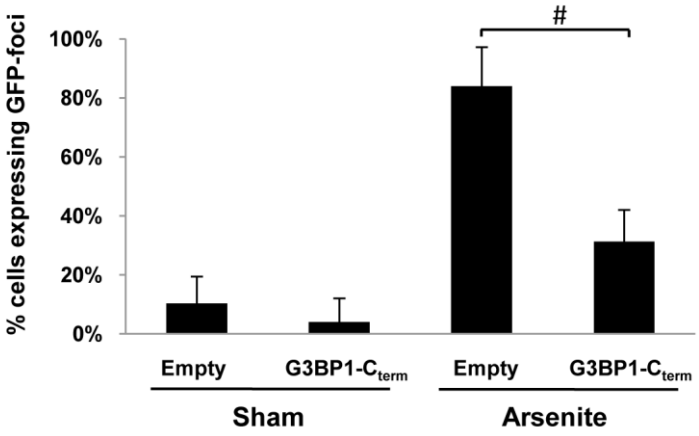
#
100%
80%
60%
40%
20%
0%
% cells expressing GFP-foci
Empty
G3BP1-C$_{term}$
Empty
G3BP1-C$_{term}$
Sham
Arsenite

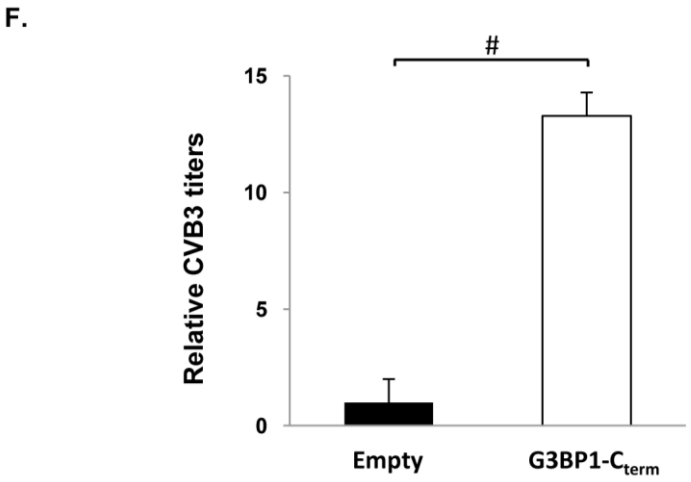

Figure 12. G3BP1-C_{term} fragment reduces SG formation and enhances CVB3 replication

(A, B) HeLa cells were co-transfected with pEGFP-G3BP1 and FLAG-G3BP1-C_{term} for 48 hrs, followed by sham- or CVB3-infection at an MOI of 10 for the indicated time points. G3BP1-C_{term} and G3BP1-N_{term} were stained using an anti-FLAG antibody. Arrow heads indicate cells expressing high levels of G3BP1-C_{term} but lacking distinct G3BP1(+)-SGs or poly-(A) granules. Cells treated with arsenite (50 mM) for 1 hr were used as positive controls. (C) Quantitation of GFP-G3BP1 foci and poly-A granules from (A) and (B) at 3hr pi, respectively. Quantification was performed by counting cells expressing, empty vector, GFP-G3BP1-SGs or poly-A granules together with FLAG, and dividing by the total number of cells expressing FLAG. Results are presented as mean ± SD (n=5 images), #$p<0.001$. N.D., No statistical difference. (D) HeLa cells were co-transfected with pEGFP-G3BP1 and FLAG-G3BP1-C_{term} for 48 hrs, and then treated with 50mM arsenite for 1 hr. Immunostaining was conducted and representative images are displayed. (E) Quantitation of GFP-G3BP1 SGs from (D). The data is presented as mean ± SD (n=5 images), #$p<0.001$. (F) Plaque assay was performed to assess the effect of G3BP1-C_{term} expression on CVB3 replication. Results are presented as relative PFU/ml. The value of the

empty vector control was arbitrarily set as 1. The data is presented as mean ± SD (n=3), #p<0.001.

3.3.8 G3BP1-SGs do not co-localize with CVB3 sense-strand.

To elucidate whether SGs bind to viral transcripts to block the interaction of factors necessary for IRES translation, HeLa cells were sham- or CVB3-infected for the indicated time points, then probed with an oligonucleotide complimentary to the sense-strand of CVB3 transcripts, synthetically conjugated to a Cy-5 fluorescent tag (red), and immunostained for endogenous G3BP1 (green). The sense-strand of CVB3 transcripts was chosen because it is used for both replication as well as protein translation. Results shown in **Figure 13** demonstrated the early formation and late disassembly of G3BP1-SGs over the time course of CVB3 infection, which is in line with the findings in **Figure 4A**; however, red fluorescence signal was found to be homogenously distributed with no co-localization with G3BP1-SGs. Furthermore, this binding is specific to CVB3 sense-strand since no red fluorescence was observed in sham- or arsenite-treated cells, but gradually increased over the time course of CVB3 infection. Our findings that CVB3 sense-strand does not interact with G3BP1-SGs suggest that G3BP1-SGs may function to reduce CVB3 replication by other mechanisms.

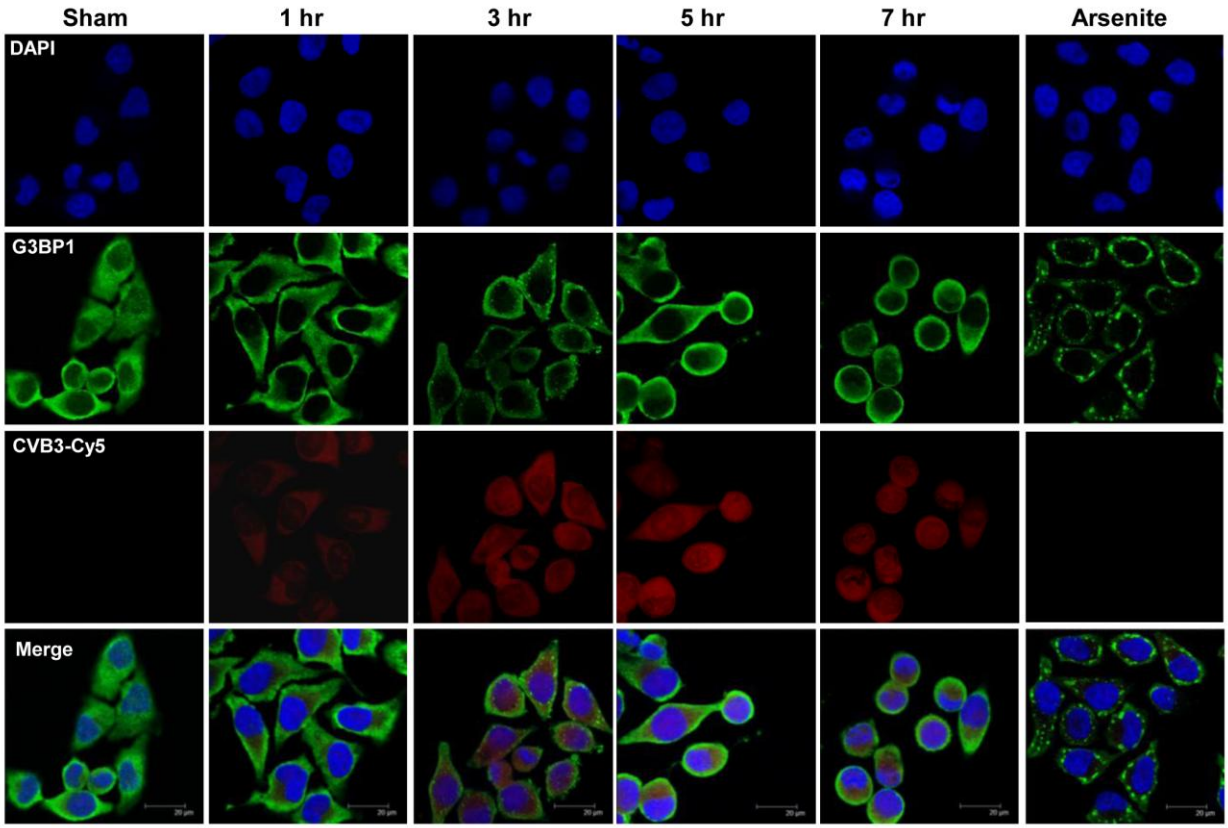

Figure 13. G3BP1-SGs do not localize with CVB3 sense-strand

HeLa cells were infected with CVB3 at an MOI of 10 for the indicated time points, followed by *in situ* hybridization and immunostaining as described in Materials and Methods. Endogenous G3BP1 was detected using an Alexa-488 secondary antibody. CVB3 sense-strand was detected by the synthetically conjugated Cy5 fluorophore.

3.4 Discussion

Viruses are obligated to evolve molecular mechanisms to evade host anti-viral responses as well as hijack host protein machinery for their own benefit. Many viruses have been documented to interact with host SGs [233]. In this chapter, we found that G3BP1-SGs are assembled early following CVB3 infection using multiple SG markers such as G3BP1, TIA1, HuR and Poly-A mRNA via confocal microscopy, live-cell fluorescent imaging, and by both transmission- and immuno-electron microscopy. Furthermore, we demonstrated that G3BP1-SGs are actively disassembled at late times during infection where G3BP1, TIA1 and HuR dissociate from SGs back into the cytoplasm, while poly-A granules persist, suggesting that G3BP1-SGs are specifically targeted while other RNA granules are not. In addition, we observed partial co-localization of G3BP1 and O-linked N-acetylglucosamine (data not shown), a sugar moiety modification recently reported to be localized to SGs during CVB3 infection [234]. Our findings indicate that CVB3-induced SGs may be functionally and compositionally different from those formed under other cellular stresses. Interestingly, by TEM, cytosolic aggregates with ribosomal-like structures around the perimeter were observed adjacent to mitochondrial structures in CVB3-infected cells. Consistent with this finding, IEM showed G3BP1-positive staining for aggregates adjacent to mitochondria. Furthermore, we found that G3BP1-SGs are actively inhibited and disassembled late during CVB3 infection.

CVB3 infection causes shutoff of host protein translation as early as 1 hr after infection [235]. Our data suggests that increased formation of SGs is likely due to active cleavage of eIF4G by $2A^{pro}$, which occurred early during viral infection, rather than the canonical eIF2α phosphorylation which took place at ~5 hrs pi. We observed the cleavage of a primary SG marker protein G3BP1 after CVB3 infection and that the cleavage was independent of host

caspase activity (data not shown) but was directly due to $3C^{pro}$ activity. Like other viruses in the *Picornaviridae* family, such as PV and EMCV [173, 184], $G3BP1^{Q325E}$ was cleavage resistant to $3C^{pro}$ activity. This cleavage separates the NTF2-like domain from the RRM domain of G3BP1, which may lead to the failure to form specific protein-RNA aggregates. We speculate that dissociation of NTF2-like domain from the RRM domain may be a conserved mechanism across *Picornaviridae* viruses. We also demonstrated that overexpression of GFP-G3BP1 resulted in a reduction of viral protein expression, transcripts, and viral titres. In contrast, siRNA knockdown of endogenous G3BP1 led to an increase in VP1 expression, transcripts, and viral titres, indicating that SGs negatively regulate CVB3 replication. It is important to note that the ~22.5 fold increase in viral titres after siG3BP1 treatment may be an additive effect of secreted interferon proteins that were collected in the supernatant of CVB3-infected cells.

Although G3BP1-SGs are disrupted during PV, EMCV and CVB3 infection, the pathological significance of the cleavage fragments remains unclear. Our studies showed that $3C^{pro}$ cleaved G3BP1 at Q325, producing a C-terminal fragment of G3BP1 that inhibits SG formation and promotes CVB3 replication. In contrast, the N-terminal fragment of G3BP1 failed to result in any difference in G3BP1-SG formation and disassembly. Future studies will be required to further explore the molecular mechanism by which G3BP1-C_{term} interferes with G3BP1-SG formation and the molecular basis of the pro-viral action of G3BP1-C_{term}. It is important to note that the cleavage of full-length G3BP1 may not be the primary cause of SG-disassembly, but actually the production of a dominant-negative peptide. Thus complete cleavage of full-length protein may not be entirely necessary to cause G3BP1-SG disassembly.

Our data using a CVB3-Cy5 oligonucleotide showed that G3BP1-SGs and positive-sense viral transcripts failed to co-localize. Furthermore, CVB3 transcripts lack formation of cytosolic

punctates, which may suggest that CVB3 transcripts do not necessarily require any distinct host organelles for replication and protein production. Therefore, G3BP1-SGs may cause activation of downstream effectors such as interferon and NF-κB pathways to negatively impact CVB3 replication.

The observation that SG disassembles due to G3BP1 cleavage by $3C^{pro}$ indicates a crucial anti-viral role of SGs in enteroviral infection. While this study does not provide direct evidence of anti-viral activities regulated by G3BP1-SGs, others have demonstrated that SG accumulation induced by EMCV and PV infection enhances the production of interferon β, IL-6, CXCL10 and RANTES (regulated on activation normal T cell expressed and secreted), leading to reduced viral replication [122, 182].

CVB3 has been demonstrated to interfere with cellular translation, apoptosis/survival, and NF-κB activation through the action of its proteases [89, 223, 225, 236, 237]. The observation in this study of the dominant-negative effect of the G3BP1-C_{term} cleavage fragment on G3BP1-SG formation extends our understanding of how *Picornaviridae* viruses may strategically target proteins critical for cellular responses. This mechanism might serve as a second level of regulation to further reduce SG formation and promote viral replication. Future investigation is warranted to further investigate the anti-viral effects of G3BP1-SGs and how the cleavage fragments may possibly be multifaceted in inhibiting anti-viral responses.

Since the publication of this work, other researchers have also confirmed the cytoprotective role of G3BP1-SGs during viral infections. For example, Reineke et al. [180] demonstrated that G3BP1 actively promotes innate immune responses against several enteroviruses at both the transcriptional and translational levels by recruiting PKR to G3BP1-SGs. In addition, Yoo et al. [149] demonstrated that ATP-dependent RNA helicase plays a critical role in enhancing RIG-I

signaling by facilitating PKR-mediated anti-viral stress granule formation. These studies further confirm the cytoprotective and anti-viral role of G3BP1-SGs due to G3BP1 aggregation during enteroviral infections. Altogether, the observation that multiple enteroviral infections conserved the ability to actively cleave G3BP1 and disrupt G3BP1-SGs suggests that G3BP1 aggregation plays a significant cytoprotective role during enteroviral infection.

Chapter 4: Cytoplasmic Translocation, Aggregation and Cleavage of TDP-43 by Enteroviral Proteases Modulate Viral Pathogenesis

4.1 Background

TDP-43 is an hnRNP that plays a critical role in transcriptional regulation and pre-mRNA maturation of target transcripts through interacting with ribonucleoprotein complexes in the nucleus [197, 198]. Despite being functionally different from G3BP1, TDP-43 also harbors protein-RNA interaction domains (RRM1 and RRM2), and a protein-protein interaction domain (glycine-rich C-terminal domain) for self-aggregation. Furthermore, under various cellular stress condition, TDP-43 was shown to mislocalize from the nucleus to cytoplasmic SGs [156, 238]. While SGs play a cytoprotective role during cellular stress, cytoplasmic redistribution of TDP-43 to SGs has been shown to acquire a toxic gain-of-function [238, 239, 240] and serve as a molecular hallmark for most forms of ALS and FTLD and contribute significantly to disease progression [238, 239, 240]. However, the role of TDP-43 in virus-induced diseases has not been studied. Recent evidence suggests that CVB3-induced pathogenesis resembles the pathological features of neurodegenerative disease, i.e. abnormal accumulation of insoluble, misfolded protein aggregates (also known as proteinopathies) [100, 241, 242], prompting us to hypothesize that dysregulation of TDP-43 during CVB3 infection plays a role in viral pathogenesis, and probably viral infectivity as well.

Although CVB3 replication takes place exclusively in the cytoplasm, viral infection has been demonstrated to lead to cytoplasmic translocation of hnRNPs [243]. For example, hnRNP D has been shown to translocate from the nucleus to the cytoplasm during enteroviral infection [244, 245]. Moreover, hnRNP D is cleaved by $3C^{pro}$ and has an anti-viral function against enteroviral

infection [140, 141]. Cytoplasmic translocation after enteroviral infection has also been demonstrated for several other hnRNPs (A1, C, K and M) [246, 247], however the significance remains unclear. Understanding the mechanism by which CVB3 may alter transcriptional regulators, such as hnRNPs, may aid in understanding viral-pathogen interaction.

In this study, we demonstrate that CVB3 infection causes a cytoplasmic redistribution and aggregation of TDP-43 in a $2A^{pro}$-dependent manner, followed by its cleavage mediated by $3C^{pro}$, leading to the loss-of-function of native TDP-43. Our data also revealed that the N-terminal cleavage fragment of TDP-43 acts as a dominant-negative mutant that inhibits the biological activity of native TDP-43 in regulating RNA splicing. We further demonstrate a host-protective function for TDP-43 against CVB3 infection. Collectively, these results are the first to show TDP-43 proteinopathies in a model outside neurodegenerative disease and suggest a mechanism evolved by enteroviruses to promote viral infection and induce viral pathogenesis.

4.2 Objective and specific aims

The objective of this chapter is to study the interaction between CVB3 infection and the DNA/RNA binding protein TDP-43.

The **SPECIFIC AIMS** include:

Aim 1: To examine the effect of CVB3 infection on TDP-43 localization and protein expression;

Aim 2: To examine the mechanisms by which CVB3 dysregulates TDP-43; and

Aim 3: To examine the significance of TDP-43 in CVB3 infection.

4.3 Results

4.3.1 Coxsackievirus B3 infection induces TDP-43 cleavage

It is well-established that TDP-43 proteinopathies contribute to the pathological progression of motor-neuron diseases [240, 248, 249, 250, 251, 252]; however the interaction between virus infection and the host TDP-43 pathway has not yet been explored. In this study, we first examined the protein expression of TDP-43 in various models of CVB3 infection. We demonstrated the production of a previously undetermined immunoreactive fragment of ~35 kDa in A/J mouse heart challenged with 9 days of CVB3 infection (**Figure 14A**). We then verified this observation in cell culture models where protein expression of TDP-43 was decreased after CVB3 infection, accompanied by the appearance of a similar 35 kDa band in both primary isolated mouse cardiomyocytes (**Figure 14B**) and HeLa cells (**Figure 14C**). To further determine whether the observed fragment is virus-induced, we transiently expressed exogenous HA-TDP-43-GFP in HeLa cells. Following 7 hrs of CVB3 infection, we showed the generation of a similar 35 kDa fragment using an anti-HA antibody, suggesting that TDP-43 is targeted for cleavage following CVB3 infection (**Figure 14D**).

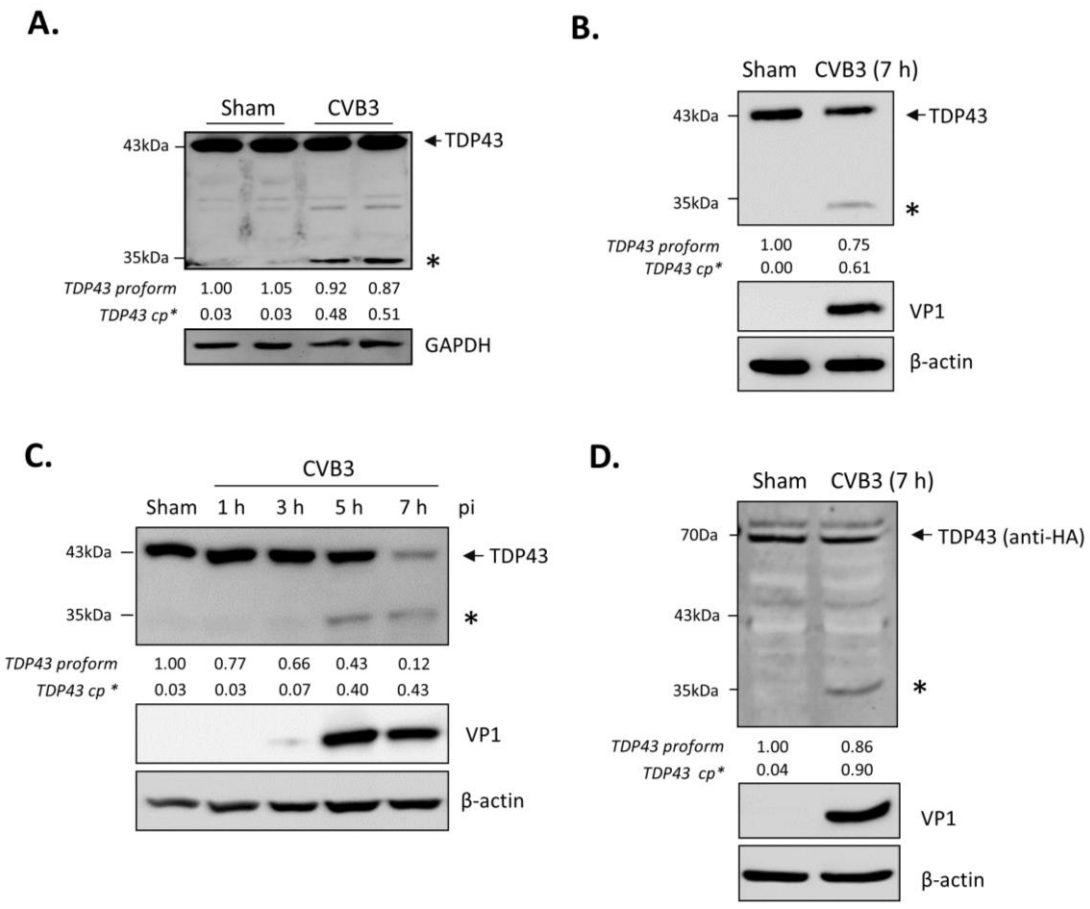

Figure 14. TDP-43 is cleaved following CVB3 infection

A) TDP-43 expression in A/J mouse heart following 9 days of CVB3 infection. Heart extracts were processed for western blot analysis for protein expression of TDP-43 using an anti-N-terminal TDP-43 antibody. GAPDH level was examined as a protein loading control. B, C) TDP-43 protein expression in primary mouse cardiomyocytes B) and HeLa cells C) infected with CVB3 at an MOI of 100 and 10, respectively, for various times as indicated. Western blot analysis was conducted as described above for the detection of protein expression of TDP-43, viral capsid protein VP1, and β-actin (loading control). D) Cleavage of TDP-43 following CVB3 infection. HeLa cells were transiently transfected with a plasmid expressing HA-TDP-43-GFP, followed by 7 hrs of CVB3 infection. Cells were harvested and processed for western blotting

using an anti-HA antibody to detect exogenous TDP-43. * indicates a cleaved TDP-43 band at ~35 kDa. cp, cleavage product. Protein levels of pro- and cleaved TDP-43 were quantified by densitometric analysis using NIH ImageJ, normalized to GAPDH or β-actin, and presented underneath each blot.

4.3.2 Viral protease 3C cleaves TDP-43 at amino acid Q327

To determine whether viral proteases contribute to the cleavage of TDP-43 following CVB3 infection, we carried out an *in vitro* cleavage assay. Our data showed the production of a similar 35 kDa fragment in HeLa cell lysates upon incubation with viral protease 3C in a time-dependent manner (**Figure 15A**). We further demonstrated that the catalytically inactive mutant of 3C failed to cleave TDP-43 (**Figure 15B**). Taken together, our data indicates that 3C is responsible for TDP-43 cleavage.

It was previously reported that TDP-43 could be targeted by caspases, resulting in the generation of pathological C-terminal cleavage fragments [253, 254, 255]. To eliminate the possibility that the above-detected fragment of TDP-43 is due to caspase-induced cleavage, we pharmacologically inhibited caspase activity using Z-VAD-FMK. **Figure 15C** showed that treatment with Z-VAD-FMK did not block the generation of the ~35kDa cleavage products at 7 hrs post-infection. This is expected since caspase-3 was not activated at this time point (**Figure 15D**). It was previously shown that CVB3 infection induces caspase activation at a late stage of viral infection [256, 257, 258]. We then extended the period of viral infection to 9 h. **Figure 15D** showed that caspase-3 was activated at this time point as evidenced by the cleavage of caspase-3 and addition of Z-VAD-FMK inhibited this cleavage. As show in **Figure 15E**, three cleavage fragments, that is, ~35 kDa, ~32 kDa, and ~25 kDa, were detected in CVB3-infected cells. The

lower two bands were undetected, while the upper band accumulated in cells treated with caspase inhibitor (**Figure 15E**). Collectively, our results suggest that the production of the ~35 kDa bands is not a result of caspase activation.

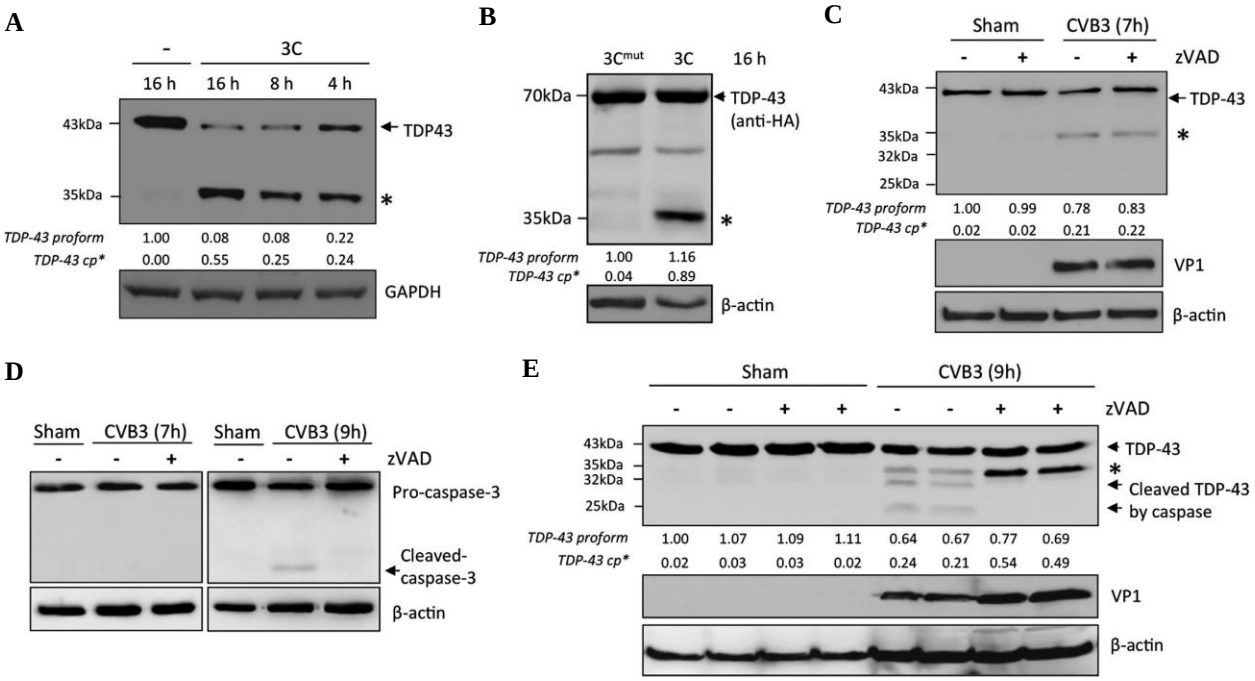

Figure 15. TDP-43 is cleaved by viral protease 3C

A and B) Cleavage of TDP-43 by viral protease 3C. A) HeLa cell lysates (50 μg) were incubated with or without viral protease 3C (0.1 μg) for different times as indicated. B) Protein extracts from HeLa cells transiently expressing HA-TDP-43-GFP were incubated with wild-type or catalytically inactive mutant of 3C (3Cmut) for 16 hrs. *In vitro* cleavage assay was performed as described in the 'Materials and Methods'. Expression of TDP-43 was examined using an anti-N-terminal TDP-43 A) or anti-HA antibody B). C–E) Effects of general caspase inhibition on CVB3-mediated TDP-43 cleavage. HeLa cells were infected with CVB3 for 7 hrs C) or 9 hrs E) in the presence or absence of Z-VAD-FMK (zVAD, 50 μM). Western blotting was performed to examine the expression of TDP-43 using an anti-N-terminal TDP-43 antibody and the cleavage of caspase-3 by an anti-caspase-3 antibody D). VP1 and β-actin was detected as described above. * indicates a cleaved TDP-43 band at ~ 35 kDa. '-', vehicle control (treated with DMSO). Densitometric analysis was carried out as in Figure 15.

Using netpicoRNA V1.0 algorithm, several potential cleavage sites on TDP-43 were predicted. On the basis of the predicted sites, point mutants of TDP-43 were constructed by site-directed mutagenesis. Among these mutants, TDP-43-Q327L, in which the glutamine (Q) at position 327 was replaced with leucine (L), was cleavage resistant, indicating TDP-43 is cleaved at 327 (**Figure 16A**). *In vitro* cleavage assay further confirmed that TDP-43-Q327L failed to be cleaved by $3C^{pro}$, while wild-type TDP-43 was proteolytically processed by $3C^{pro}$, but not $2A^{pro}$ (**Figure 16B**). Collectively, our data suggest that TDP-43 is cleaved by $3C^{pro}$ at Q327, generating a 35 kDa N-terminal (TDP-43-N) and an 8 kDa C-terminal cleavage fragment (TDP-43-C) (**Figure 16C**).

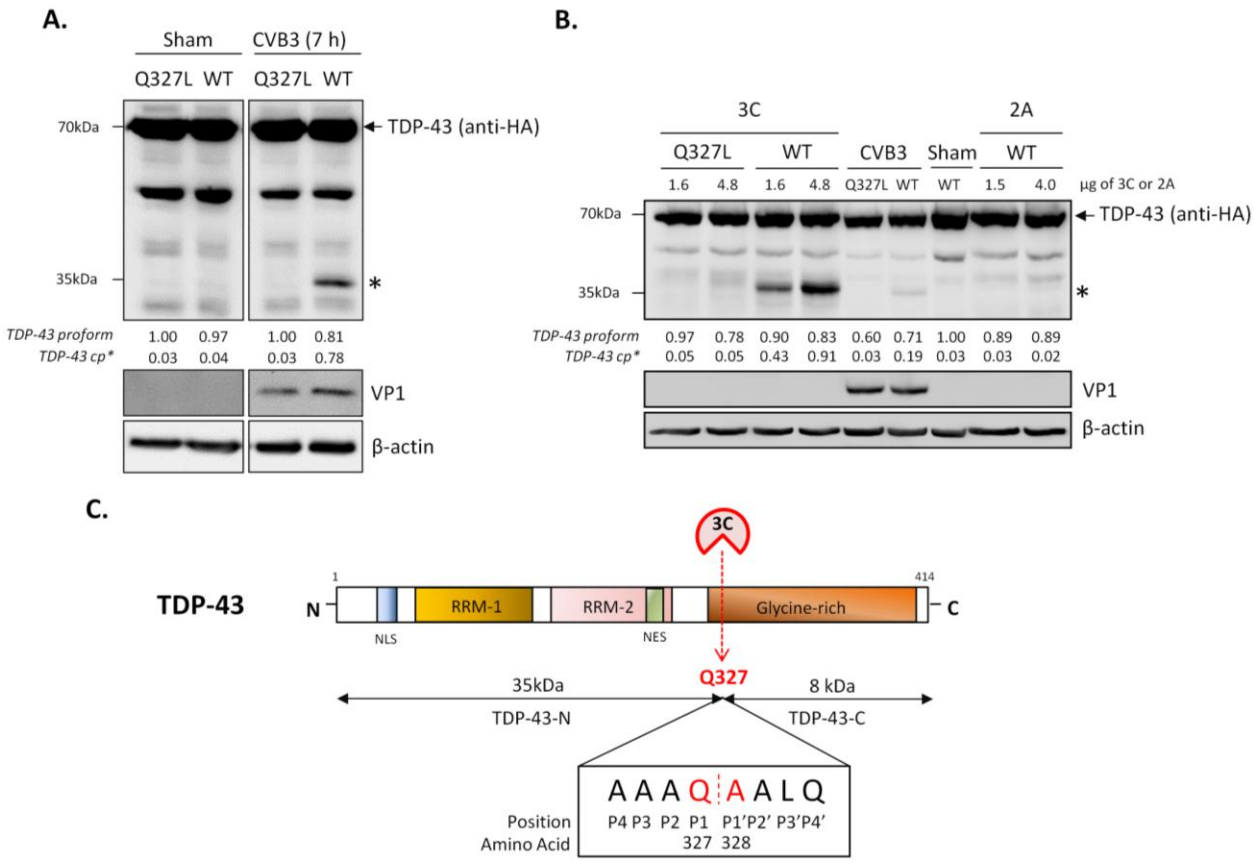

Figure 16. TDP-43 is cleaved at Q327

A) HeLa Cells transiently transfected with HA-TDP-43-GFP (WT) or HA-TDP-43^{Q327L}-GFP (Q327L) were either sham or CVB3-infected for 7 hrs. Cells were harvested for western blot analysis of the expression of TDP-43 using anti-HA antibody, VP1, and β-actin. Densitometric analysis was carried out as in Figure 15. B) Fifty microgram of protein extracts from HeLa cells transiently expressing WT or HA-TDP-43^{Q327L}-GFP was incubated with increasing concentrations of viral protease 3C or 2A as indicated for 8 hrs. CVB3-infected HeLa lysates were used as a control to compare the generation of similar 35 kDa cleavage fragments. Protein expression of TDP-43, VP1, and β-actin was detected as described above. * indicates a cleaved TDP-43 band at ~35 kDa. C) Schematic diagram of the functional domains, the identified

cleavage site, and the resulting cleavage fragments of TDP-43. RRM, RNA-recognition motif; NLS, nuclear localization signal; and NES, nuclear export signal.

4.3.3 Viral protease 2A is responsible for cytoplasmic translocation and aggregation of TDP-43

Cytoplasmic translocation and aggregation of TDP-43 are the pathological hallmarks for ALS and FTLD [259]. To understand the effect of CVB3 infection on TDP-43 localization, we utilized a fluorescent mCherry tagged TDP-43. As shown in **Figure 17A**, TDP-43 was localized exclusively in the nucleus in sham-infected cells, upon infection TDP-43 was translocated from the nucleus to the cytosol. Increasing evidence has shown that cytoplasmic TDP-43 localizes to stress granules (SGs) to form protein aggregates [218, 260, 261]. Here we used a construct expressing EGFP tagged G3BP1 as previously mentioned in Chapter 3. Similar to our previous findings [121], CVB3 infection induced the formation of SGs at 3 hrs post-infection. Interestingly, we found that ~83% of cells infected with CVB3 exhibited punctate cytoplasmic staining patterns of TDP-43, co-localizing to G3BP1-SG aggregates (**Figure 17A**). We further determined whether viral proteases are responsible for the translocation of TDP-43. **Figure 17B** demonstrated that transient expression of $2A^{pro}$, but not $3C^{pro}$, elicited significant cytoplasmic redistribution and aggregate formation of TDP-43, similar to those observed during viral infection, indicating that $2A^{pro}$ expression is sufficient and responsible for cytoplasmic translocation and aggregation of TDP-43 during CVB3 infection.

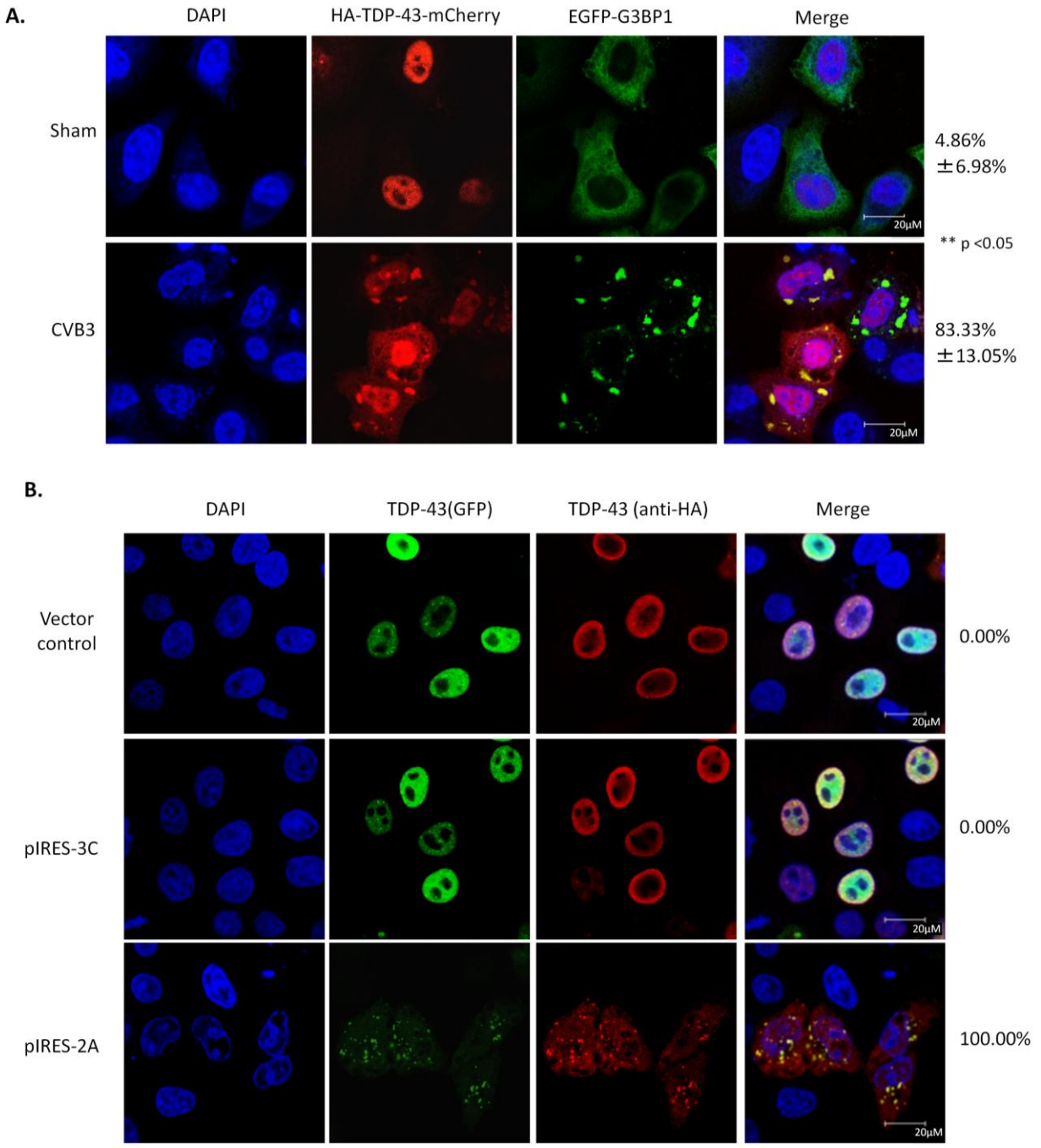

Figure 17. Viral protease 2A is responsible for cytoplasmic relocalization and aggregation of TDP-43 during CVB3 infection

A) Cytoplasmic redistribution and aggregation of TDP-43 after CVB3 infection. HeLa cells transiently co-expressing HA-TDP-43-mCherry and EGFP-G3BP1 were sham- or CVB3-infected for 3 hrs. Confocal fluorescence images are presented (TDP-43, red; G3BP1, green; nucleus, DAPI (blue)). Percentage of cells expressing cytoplasmic TDP-43 was quantified over 10 different images as described in "Materials and Methods" B) Localization of TDP-43 after viral protease expression. HeLa cells were transiently co-transfected with HA-TDP-43-GFP and viral protease 2A, 3C or empty vector for 24 hrs. Immunostaining was carried out for the detection of TDP-43 using anti-HA antibody (Alexa-fluor-594, red). Cell nuclei were counterstained with DAPI (blue). Percentages of TDP-43-positive cells expressing cytoplasmic TDP-43 in 10 different images are shown to the right.

4.3.4 TDP-43 solubility is reduced following CVB3 infection

It was previously reported that, under disease condition, the solubility of TDP-43 is changed and altered solubility is correlated with cytoplasmic translocation and aggregation of TDP-43 and disease progression [240, 262, 263]. To determine whether CVB3 infection affects TDP-43 solubility, cells were infected with CVB3 for 7 h and cellular proteins were extracted sequentially using RIPA and urea buffers. In CVB3-infected cells, both native and cleavage forms of TDP-43 were transferred to the RIPA-insoluble, urea-soluble fractions (**Figure 18**), suggesting that the solubility of TDP-43 is decreased after CVB3 infection.

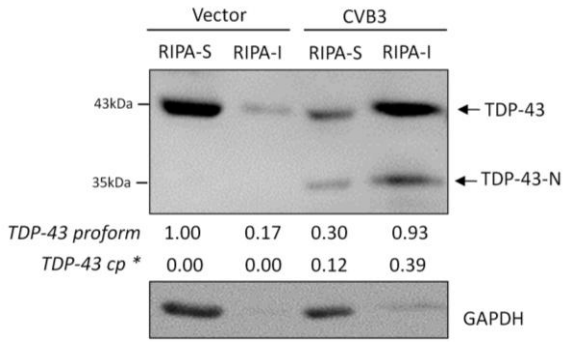

Figure 18. TDP-43 solubility is reduced in cells infected by CVB3

HeLa cells were infected with CVB3 for 7 hrs, cell lysates were harvested and proteins were sequentially extracted using RIPA and Urea buffers. Western blotting was performed using an anti-N-terminal TDP-43 antibody for the detection of full-length and the N-terminal cleaved form of TDP-43. Expression of GAPDH was examined to evaluate the purity of protein extraction (GAPDH is presented in RIPA-soluble fraction) and as a loading control. * indicates the N-terminal fragment of TDP-43. RIPA-S, RIPA buffer-soluble; RIPA-I, RIPA buffer-insoluble. Densitometric analysis was carried out as in Figure 15.

4.3.5 TDP-43-N localizes to stress granules to form protein aggregates while TDP-43-C is rapidly degraded via the proteasomal pathway

To explore the possible significance of TDP-43 cleavage during CVB3 infection, we cloned the human TDP-43 N- (amino acids 1-327) and C- (amino acids 328-414) terminal cleavage products into a vector expressing an HA tag. Western blotting verified the protein expression of full-length and N-terminal TDP-43 after transient transfection (**Figure 19A**). However, TDP-43-C failed to be detected following transfection (**Figure 19A**). Previous studies have demonstrated degradation of caspase-induced cleavage products of TDP-43 by the proteasome [264]. To determine whether TDP-43-C is rapidly degraded following transient

transfection, HeLa cells were treated with bafilomycin or MG132 to inhibit autophagic and proteasomal pathways, respectively. **Figure 19B** showed that treatment with MG132, but not bafilomycin, rescued TDP-43-C protein expression. This data suggests that the C-terminal fragment is quickly turned over through proteasome-mediated proteolysis, contributing to the loss-of-function of TDP-43 following CVB3 infection. Furthermore, we examined the localization of the cleavage products. TDP-43-C signal was undetectable by confocal microscopy, which is likely due to its instability (**data not shown**). TDP-43-N was localized to the nucleus in sham-infected or vector control cells, but translocated to SG aggregates in the cytoplasm upon CVB3 infection or 2A expression (**Figure 19C**). These results indicate that, in addition to full-length TDP-43 (**Figure 17B**), the TDP-43-N fragment is also able to localize to G3BP1-SGs.

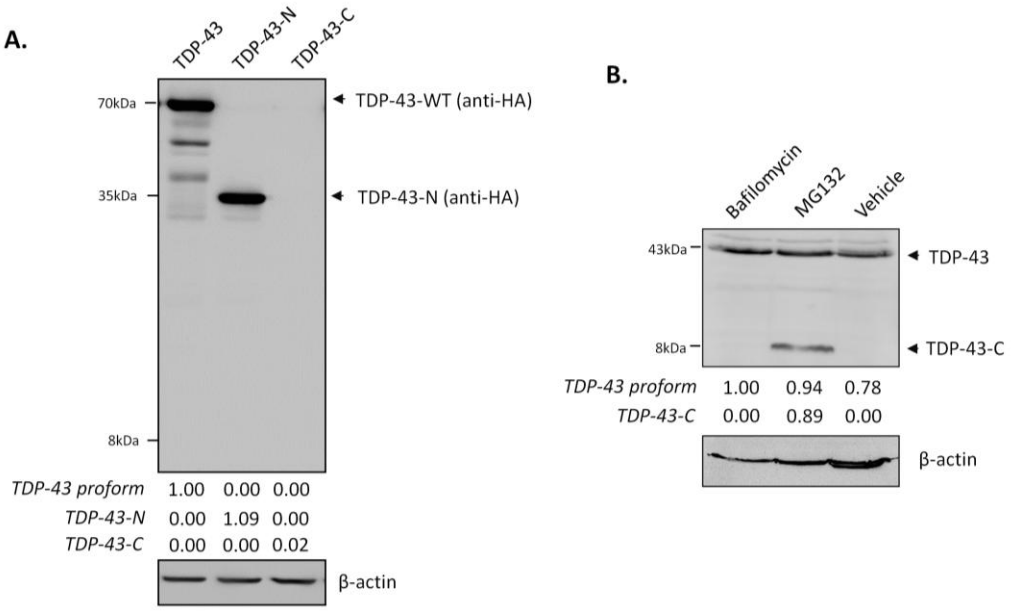

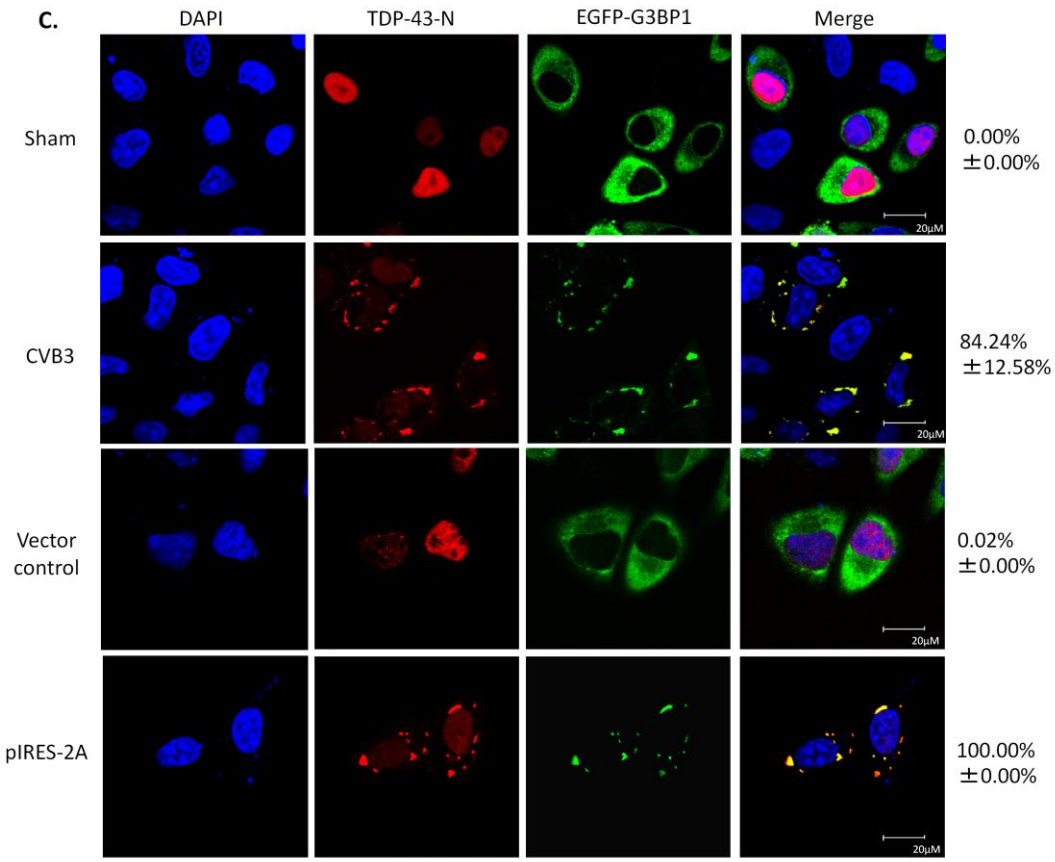

Figure 19. TDP-43-C is rapidly degraded by the proteasome pathway and TDP-43-N localizes to stress granules to form protein aggregates after CVB3 infection

A) Protein expression of full-length and truncated forms of TDP-43. HeLa cells were transiently transfected with HA-TDP-43-GFP, HA-TDP-43-N, or HA-TDP-43-C as indicated. Protein expression of various types of TDP43 was detected using an anti-HA antibody. The level of β-actin was examined as a loading control. B) TDP-43-C is degraded through the proteasome pathway. HeLa cells were transiently transfected with HA-TDP-43-C in the presence of 200 nM bafilomycin (a lysosome inhibitor), 1 μM MG132 (a proteasome inhibitor), or equal volume of DMSO as a vehicle control for 24 h. Western blotting was performed using an anti-C-terminal TDP-43 antibody which detects both endogenous TDP-43 (~43 kDa) and exogenous HA-TDP-43-C (~8 kDa). Densitometric analysis of TDP-43 proform, TDP-43-N and TDP-43-C was

carried out as in Figure 15. C) Cytoplasmic localization and aggregation of TDP-43-N following either CVB3 infection or viral protease 2A expression. HeLa cells were transiently co-transfected with HA-TDP-43-N and EGFP-G3BP1 for 24 h, followed by either CVB3 infection for 3 hrs or second-round of transfection with viral protease 2A as indicated. Immunostaining was performed for the detection of TDP-43-N using anti-HA antibody (Alexa-fluor-594, red). Cell nuclei were counterstained with DAPI (blue). GFP signal of EGFP-G3BP1 is shown in green. Percentage of cells expressing cytoplasmic TDP-43 was quantified as in Figure 18.

4.3.6 TDP-43-N compromises the function of native TDP-43 in *CFTR* exon 9 skipping

TDP-43 plays an important role in the regulation of alternative splicing [265, 266, 267]. To determine whether TDP-43-N has an impact on the function of native TDP-43 in RNA splicing, we utilized a well-established technique, Cystic fibrosis transmembrane conductance regulator (*CFTR)* exon 9 skipping [240, 265]. TDP-43 facilitates exon 9 skipping by interacting with UG repeats in intron 8 of *CFTR* pre-mRNA, thus generating an exon 9-deficient transcript at resting states [197, 198, 265]. HeLa cells were transiently transfected with a *CFTR* minigene reporter construct (TG(13)T(5)) [240, 265], together with empty vector, full-length TDP-43 or TDP-43-N. Transfection was carried out for 24 hrs to achieve desired expression levels of TDP-43-N similar to those observed in virus-infected cells. RT-PCR was performed to detect the transcripts of *CFTR* reporter plasmid. We found that expression of TDP-43-N resulted in a significant decrease in *CFTR* exon 9 skipping (decreased ratio of spliced to unspliced exon 9) relative to vector controls (**Figure 20**). These results suggest that the N-terminal cleavage fragment of TDP-43 functions as a dominant-negative mutant that inhibits the activity of native TDP-43 in regulating RNA splicing. It was noted that transient transfection of full-length TDP-43 did not further increase

CFTR splicing compared to empty-vector control (**Figure 20**), in contrast to an early report [254]. The discrepancy is likely due to the differences in the basal levels of endogenous TDP-43 activity and the amount of exogenous TDP-43 transfected between two studies. The endogenous TDP-43 exon skipping activity in our study appeared to be already high (higher than that in their study [254]). Thus, modest increase of exogenous TDP43 due to a shorter term of transfection (24 hrs in our study *versus* 48 hrs in their report [254]) may not be sufficient to promote further increase in exon 9 exclusion. Our result is consistent with an early report with the same period of TDP-43 transfection (24 hrs) showing that exon skipping activity in cells expressing exogenous TDP-43 is comparable to cells expressing empty-vector, but significantly higher compared to cells depleted of TDP-43 [240].

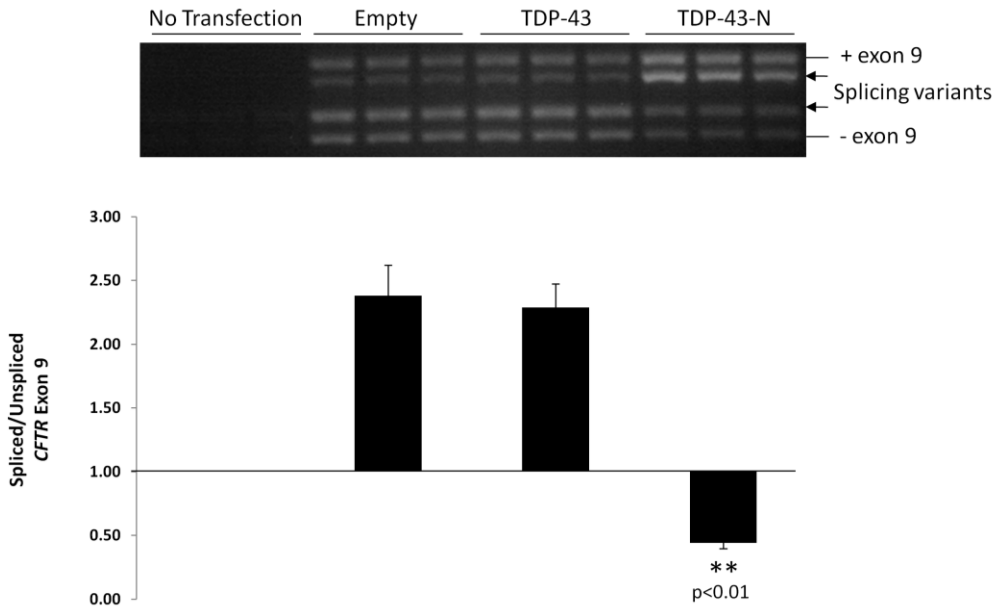

Figure 20. TDP-43-N compromises the function of native TDP-43 in *CFTR* splicing

HeLa cells were transiently co-transfected with *CFTR* reporter construct (TG(13)T(5)) with empty vector control, full-length TDP-43 or TDP-43-N for 24 hrs. RNA was extracted and RT-PCR was performed to examine *CFTR* exon 9 skipping. PCR products were visualized on 1.5% agarose gels (upper panel) and quantified by NIH imageJ software and presented as ratios of spliced to unspliced exon 9 (mean ± SD, n=3) (lower panel). ** $p < 0.01$. Arrows indicate previously documented splicing variants. Exon 9 inclusion (+) and exclusion (-) are shown.

4.3.7 TDP-43 knockdown promotes CVB3 replication

To determine whether TDP-43 plays a role in CVB3 infection, HeLa cells were treated with siRNA specific for TDP-43 mRNA, followed by viral infection. **Figure 21A & B** showed that gene-silencing of TDP-43 resulted in an approximately 2-fold increase in virus titers as compared with control, indicating a host protective effect of TDP-43 against CVB3 infection. To

further understand the potential mechanism by which knockdown of TDP-43 enhances viral replication, immunostaining was performed to determine whether TDP-43 interacts directly with the viral RNA. We utilized a double-stranded RNA (dsRNA) antibody to monitor the accumulation of viral replication intermediates. Confocal microscope images and Pearson's correction analysis showed that TDP-43 signal did not significantly co-localize with dsRNA staining (**Fig. 22C**), suggesting that the anti-viral activity of TDP-43 may not be through direct binding with CVB3 RNA and subsequent interfering with its replication, rather than an indirect mechanism.

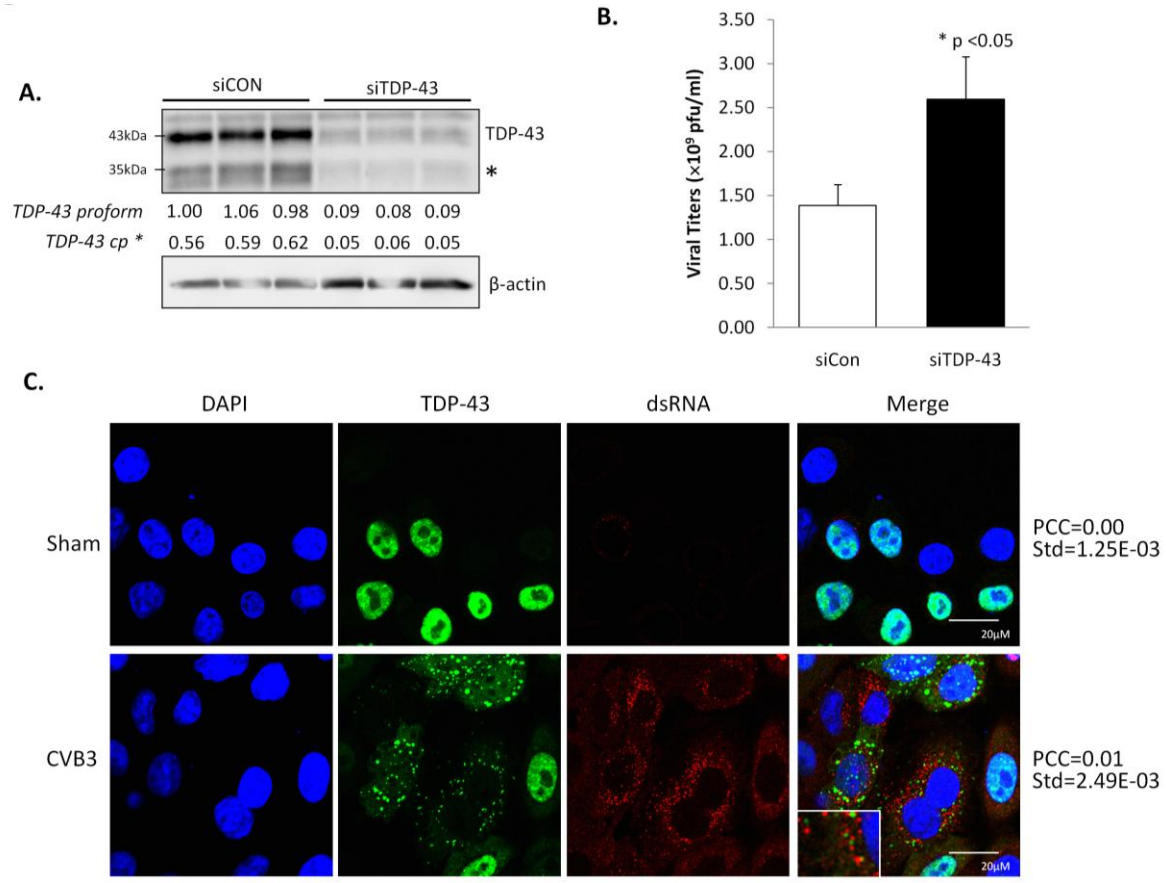

Figure 21. Knockdown of TDP-43 enhances CVB3 replication

HeLa cells were transfected with siRNA targeting TDP-43 (siTDP-43) or a scramble siRNA (siCon) for 48 hrs followed by CVB3 infection for 16 hrs at an MOI of 1. A) Western blotting was conducted to examine protein expression of TDP-43 and β-actin (loading control). Densitometric analysis was performed as in Figure 15. * indicates the N-terminal cleavage fragment of TDP-43. B) Plaque assay was carried out to assess viral titers in the supernatant. Viral titers were expressed as plaque formation units (pfu) per milliliter and presented as mean ± SD (n=3), * $p < 0.05$. C) Localization of TDP-43 and dsRNA in the cytoplasm of CVB3-infected cells. HeLa cells were transfected with HA-TDP-43 for 24 hrs, followed by CVB3 infection for 3 hrs. Immunostaining was carried out for the detection of TDP-43, using an anti-HA antibody

(green) and dsRNA using anti-dsRNA antibody (red). Cell nuclei were counterstained with DAPI (blue). Pearson's Correlation Coefficient (PCC) was calculated using Volocity software Version 5.2.1 over at least 3 images.

4.4 Discussion

In this study, we provide the first evidence that TDP-43 is manipulated by enteroviruses to contribute to viral pathogenesis and viral replication. TDP-43 is a nuclear-cytoplasmic shuttling protein passing across the nuclear membrane through the activity of its intrinsic nuclear localization signal (NLS) and nuclear export signal (NES). However, under normal conditions, TDP-43 is predominantly localized to the nucleus. In neurodegenerative diseases, patients suffering from ALS or FTLD exhibit cytoplasmic translocation of TDP-43 [240, 250, 251, 259, 262]. In this study, we showed a similar translocation pattern of TDP-43 from the nucleus to the cytoplasm following CVB3 infection. As enteroviral protease 2A was previously shown to cleave key components of the nuclear pore complex, resulting in the disruption of nuclear import pathways and consequent cytoplasmic redistribution of selective nuclear proteins, including several members of the hnRNPs [108, 246, 268, 269], we asked whether expression of 2A is sufficient to induce similar cytoplasmic translocation patterns of TDP-43. Our data indicates that transient expression of 2A in cells recapitulates this phenomenon, indicating that 2A is responsible for the cytoplasmic translocation of TDP-43. Identification of TDP-43 as another member of hnRNPs undergoing cytoplasmic relocalization during CVB3 infection suggests that modulation of hnRNP distribution may be a common strategy exploited by enteroviruses to allow for efficient viral production. Although 3C can directly cleave TDP-43 and the cleavage products tend to promote aggregation, expression of 3C alone was unable to induce cytoplasmic translocation and

aggregation of TDP-43. This is because the absence of viral infection or viral protease 2A, TDP-43 remains in the nucleus, inaccessible to 3C that is mainly present in the cytoplasm.

TDP-43 proteinopathies are characterized by reduced solubility and increased cytoplasmic accumulation of TDP-43 as ubiquitinated protein aggregates [259]. Here we demonstrated that CVB3 infection causes a decrease in solubility of both native and the N-terminal cleaved form of TDP-43. These findings are accompanied by the observations that CVB3 infection or ectopic expression of 2A induces cytoplasmic redistribution and aggregation of full-length and N-terminal TDP-43. In addition to reduced solubility, a number of studies have shown that mutated TDP-43 and caspase-derived C-terminal TDP-43 fragments that are often detected in the brain of ALS and FTLD patients are highly prone to aggregation [240, 254, 262, 263]. Furthermore, it was reported that wild-type TDP-43 and cytoplasmically restricted TDP-43 (mutated at its NLS) are also able to form protein aggregates in the cytoplasm, which are associated with increased TDP-43 phosphorylation and ubiquitination, and co-localized with SG markers [261, 270]. The exact mechanism leading to decreased solubility and increased aggregation of TDP-43 following CVB3 infection is still not known, but could be related to cytoplasmic translocation of TDP-43, which allows for direct interaction of the two RNA-recognition motifs (RRM 1 and 2) on full length TDP-43 and TDP-43-N, with cytosolic SGs containing various RNA transcripts and proteins that are involved in protein ubiquitination and phosphorylation.

SGs are dynamic cytoplasmic aggregates of stalled initiation complexes that play an anti-viral role against enteroviral infection [121, 122, 173]. We have previously demonstrated that shutoff of host protein translation upon CVB3 infection triggers the formation of SGs at ~3 hrs post-infection and protease 3C-mediated cleavage of G3BP1 contributes, at least in part, to SG disassembly at ~5 hrs post-infection (**Chapter 3**) [121]. Similar to these findings, cytosolic

aggregates of TDP-43 are formed and co-localize to SGs at ~3 hrs (**Figure 17A**) and then disassembled at late stage of viral infection (data not shown). Cytoplasmic TDP-43 has been identified as a component of SGs in response to stress; it is thus plausible that formation and disappearance of TDP-43 aggregates are the consequences of SG assembly and disassembly. Whether TDP-43 also plays a role in coxsackieviral modulation of the formation and disassembly of SGs and the significance of TDP-43 accumulation in SGs are still unknown and warrant future investigations.

While both the ubiquitin-proteasome system and autophagy are implicated to play a role in the disposal of TDP-43, TDP-43 is a relatively stable protein with a half-life between 12 to 34 hrs depending on the cell types [259]. In this study, we found that the 3C-induced TDP-43-C is highly labile and undetectable in cells either infected by CVB3 or transiently expressing TDP-43-C. We further demonstrated that TDP-43-C is rapidly degraded through the proteasome pathway as treatment with the proteasome inhibitor restores the protein level of TDP-43-C. This finding is consistent with previous observation that caspase-induced C-terminal truncation product of TDP-43 has a much shorter half-life (~4 hrs) compared with full-length TDP-43 [259]. The molecular basis leading to increased turnover of TDP-43-C remains unclear. It is postulated that cleavage may cause conformational change of TDP-43-C, which enables it for direct and quick access to the chamber of the 20S proteasome [271]. Since TDP-43-C contains a portion of the glycine-rich region that is required for its interaction with other hnRNPs, and for the regulation of alternative splicing and transcriptional activity [248], we propose that rapid removal of TDP-43-C contributes to the loss-of-function of TDP-43 following CVB3 infection.

In addition to loss-of-function, our results also suggest a gain-of-toxic-function for TDP-43-N. We demonstrated that expression of TDP-43-N in HeLa cells, which contain abundant

endogenous TDP-43, results in a significant reduction of *CFTR* splicing, indicating that TDP-43-N inhibits the biological functions of native TDP-43 as a dominant-negative mutant. TDP-43-N comprises both RRM 1 and 2, but lacks the C-terminal glycine-rich region that plays a key role in modulating RNA splicing [248]. Thus, we speculate that TDP-43-N negatively regulates the activity of native TDP-43 by competing for substrate RNA binding without being able to regulate RNA maturation. However, the significance of TDP-43 function during viral infection remains unknown.

Our finding that knockdown of TDP-43 results in a significant increase in viral titers suggests an anti-viral function for TDP-43 against CVB3 infection. Like other viral pathogens, enteroviruses have evolved to manipulate host proteins to provide a favorable environment for productive viral infections. Among them, several members of the hnRNPs family have been previously shown to play a role in regulating viral replication [108, 244, 245, 272, 273, 274, 275]. For examples, hnRNP C and K were documented to interact with the non-coding regions of enteroviral RNA to facilitate translation initiation and RNA synthesis [272, 273, 275]. Similar to our findings in the current study, enteroviral infection causes cytoplasmic redistribution and cleavage of hnRNP D and deletion of this protein results in enhanced viral replication, suggesting that hnRNP D acts as a host restriction factor against enterovirus infection [108, 244, 245]. The anti-viral mechanisms of hnRNP D appear to involve negative regulation of IRES-mediated translation of viral RNA via direct interaction with the IRES of enteroviruses [244, 274], and viral RNA degradation by targeting the 3'-UTR of enteroviral genome [108, 276]. The exact mechanism of TDP-43 suppressing CVB3 replication remains to be clarified. In this study, we tested our hypothesis that TDP-43 interacts directly with the viral RNA through its RRM domains, leading to the inhibition of viral translation and RNA replication. However, our data does not support

this notion since TDP-43 and viral RNA intermediates do not appear to co-localize, indicating an indirect mechanism of TDP-43 action. We speculate that TDP-43 inhibits CVB3 replication by regulating its host RNA substrates that have either pro- or anti-viral functions, instead of direct targeting on viral genome. It is important to note that TDP-43 functions as a complex of transcriptional regulators and hnRNPs. Thus, we argue that single knockdown of TDP-43 may only moderately ameliorate viral replication as observed in the current study, whereas collective modulation of multiple hnRNPs would yield a greater impact on viral replication.

On the basis of the results in the present study, we propose a model by which CVB3 manipulates the TDP-43 pathway, contributing to viral pathogenesis (**Figure 22A-E**). Under normal conditions, TDP-43 participates in regulating RNA maturation in the nucleus. Upon CVB3 infection, viral protease 2A induces redistribution of TDP-43 from the nucleus to the cytoplasm (**Figure 22A**), where TDP-43 is targeted by viral protease 3C for cleavage at Q327 to yield two previously undiscovered cleavage fragments, TDP-43-N and TDP-43-C (**Figure 22B**). Cytoplasmic translocation of TDP-43 causes decreased solubility and increased aggregation of TDP-43 (**Figure 22C**). The TDP-43-C fragment is rapidly degraded through the proteasomal pathway, leading to its loss-of-function (**Figure 22D**), whereas TDP-43-N is prone to form aggregates (**Figure 22C**) and negatively regulates the function of native TDP-43 in alternative RNA splicing, possibly through competing for substrate RNA binding (**Figure 22E**). Taken together, our findings are the first to document enteroviral manipulation of TDP-43 during infection, leading to a phenotype similar to TDP-43 proteinopathies observed in neurodegenerative diseases. Whether aggregation of TDP-43 plays a cytoprotective or detrimental role during viral infection remains to be further elucidated, however our studies

indicate that the cytoplasmic aggregation, misfolding and cleavage of TDP-43 during CVB3 infection may alter proper mRNA maturation, contributing to virus-induced cardiomyopathy.

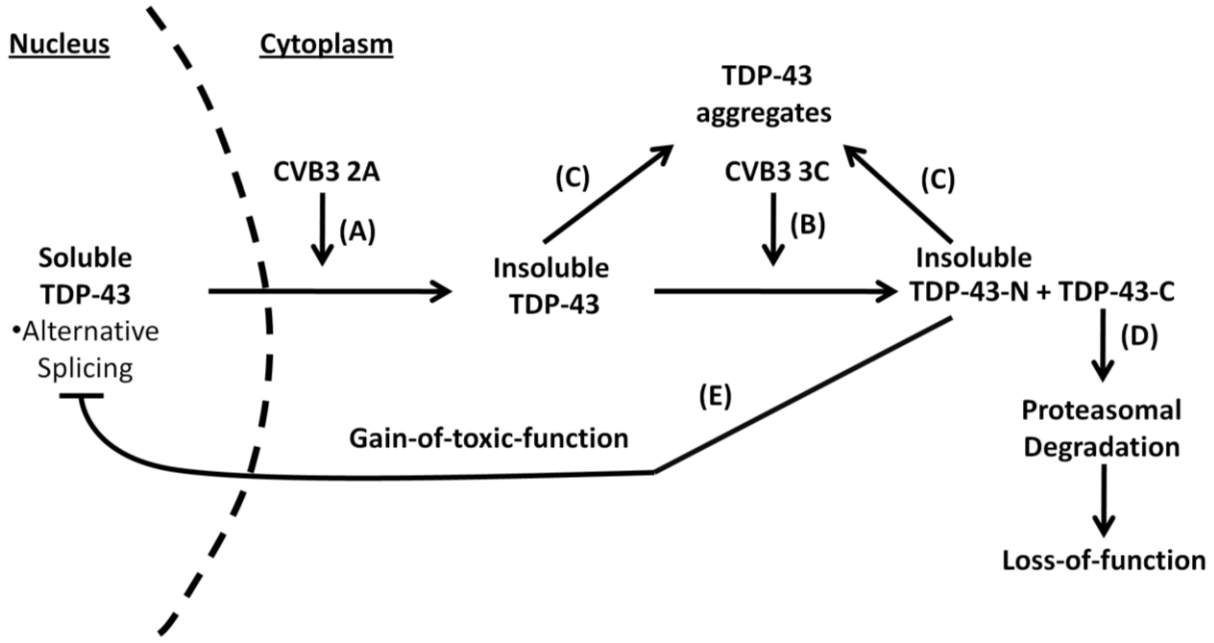

Figure 22. Proposed model of CVB3 manipulation of TDP-43 pathway

Nuclear TDP-43 participates in the regulation of RNA metabolism under normal condition. A) Upon CVB3 infection, viral protease $2A^{pro}$ causes the translocation of TDP-43 from the nucleus to the cytoplasm, where B) TDP-43 is cleaved at amino acid Q327 by viral protease $3C^{pro}$ to generate TDP-43-N and TDP-43-C. C) The solubility of cytoplasmic full-length TDP-43 and TDP-43-N is reduced and prone to aggregation. D) TDP-43-C is rapidly degraded via the proteasomal degradation pathway, leading to its loss-of-function, whereas E) TDP-43-N functions as a dominant-negative mutant, which inhibits the biological activity of TDP-43 in RNA splicing.

Chapter 5: G3BP1 Negatively Regulates Autophagy Potentially via Direct Recruitment of STAT3

5.1 Background

Cells are tasked with maintaining a constant internal environment conducive for vital biochemical processes while counteracting endogenous and environmental stresses. Examples of such cellular stresses include hypoxia, heat-shock, oxidative stress, viral infection, and starvation. Cells have developed intricate, multi-faceted mechanisms to counteract such stressful conditions and reinforce survivability. Failure to cope with internal and external stresses can lead to metabolic dysregulation, genetic instability, and ultimately cell death. As a result, understanding how stress-response mechanisms are orchestrated provides the fundamental knowledge required to understand the development and pathogenesis of diseases, including virus-induced diseases.

Autophagy, as mentioned earlier, is a cellular self-digestion process that removes misfolded proteins and damaged organelles and plays critical roles in numerous forms of cellular stress responses. Autophagy was previously reported to have an important function in the clearance of SGs in yeast and mammalian systems [163]. However, the influence of SGs themselves on autophagic function has not yet been explored. In this study, we investigated the possible co-regulation between the two stress mechanisms.

A properly coordinated stress response is critical to maintaining cell viability. All cells can experience stress; however, those that are quiescent, such as cardiomyocytes and neuronal cells, and experiencing prolonged, unresolved stress pose the greatest risk of permanent tissue damage. The findings in this study may contribute to future therapeutics development for

bolstering cell defenses against stress, thereby salvaging functional tissue from acute stressors or chronic degenerative disease.

5.2 Objective and specific aims

The objective of this chapter is to investigate the influence of G3BP1-SGs on autophagic activation.

The **SPECIFIC AIMS** include:

Aim 1: To examine the effect of G3BP1 overexpression and knockdown on autophagic activation; and

Aim 2: To examine the mechanisms by which G3BP1 regulates autophagy.

5.3 Results

5.3.1 Optimization of starvation-induced autophagy in HEK293 cells

In this study, HEK293 cells were used due to their lower basal level of autophagy as compared to HeLa cells [277]. In order to study the effects of G3BP1 on autophagy, we first characterized autophagy dynamics in HEK293 cells by measuring p62 degradation (a substrate protein of autophagy-mediated degradation) and LC3-I lipidation to LC3-II (also known as LC3-I/LC3-II conversion, a marker of autophagosome formation) under starvation stress. HEK293 cells starved with HBSS for 0 to 6 hrs in 30 min intervals showed a decreasing level of p62 protein as starvation progressed (half-life ~4 hrs) (**Figure 23A**). In addition, LC3-II level rapidly peaked after 1 hr starvation, and slowly decreased as starvation progressed. Thus, our subsequent studies in this chapter will use 6 hrs and 1 hr starvation to analyze p62 degradation and conversion of LC3-I to LC3-II, respectively. BAF, as mentioned earlier, is a well-established

inhibitor of vacuolar-type H^+-ATPase [278], and blocks acidification and protein degradation in lysosomes. BAF was used as a positive control to restore p62 and LC3 protein levels during prolonged starvation. Furthermore, titration experiments of BAF concentrations in HEK293 cells after 6 hrs starvation demonstrated that treatment with 80.0 nM BAF is sufficient to saturate p62 and LC3-II protein expression (**Figure 23B**). Therefore, the dosage of 80.0 nM BAF will be used in the subsequent experiments.

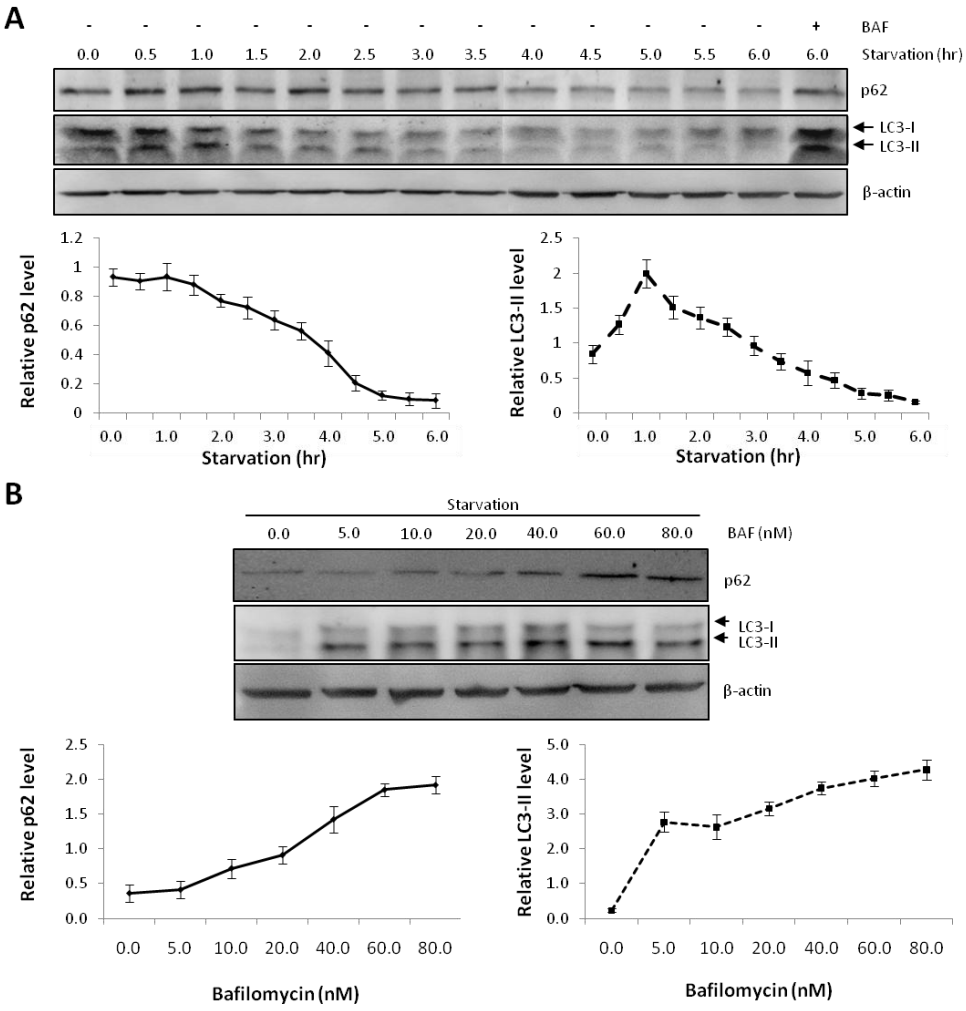

Figure 23. Starvation induces p62 degradation by 6 hrs, and LC3-I lipidation by 1 hr, which can be restored optimally with 80.0 nM Bafilomycin

A) HEK293 cells were starved in HBSS buffer for up to 6 hrs in 30 min intervals. Cells treated with 80.0 nM BAF were used as a positive control. B) HEK293 cells starved for 6 hrs were treated with titrating amounts of BAF as indicated above. Protein lysates were collected for western blot analysis of protein expression of p62, LC3-I and -II, and β-actin (loading control). Densitometry was performed on triplicate samples, normalized to β-actin, and is shown as relative values compared to non-treated controls (mean ± SD, n=3).

5.3.2 G3BP1 knockdown promotes autophagy

To determine whether G3BP1-SGs play a role in regulating autophagy, we examined the influence of knocking down G3BP1 on autophagic activities in response to starvation. HEK293 cells were treated with a pool of siRNA specific for G3BP1 (siG3BP1) mRNA transcripts or scramble siRNA (siCon) for 48 hrs, followed by starvation for various time-points as indicated (**Figure 24**). Independent expression of each siRNA used in our siG3BP1 pool specific for the G3BP1 transcript was not tested individually to investigate off-target effects. However, we showed that siG3BP1-treated HEK293 cells yielded decreased G3BP1 protein level (**Figure 24A, left panel**), and failed to form G3BP1-SGs under starvation stress (**Figure 24A, right panel**). Upon starvation for up to 6 hrs, siCon-treated cells exhibited similar p62 degradation and LC3-I lipidation kinetics as shown in Figure 23A (**Figure 24B**). However, we found that p62 degradation was increased (half-life ~2.5 hrs) upon siG3BP1 treatment as compared to siCon treated cells (half-life ~4 hrs) (**Figure 24C**). In addition, siG3BP1 treatment induced early LC3-I lipidation to LC3-II at resting states, followed by rapid LC3-II degradation by 1 hr starvation. When comparing cells starved for 6 hrs, siG3BP1-treated cells showed significant decrease in p62 protein expression both with and without BAF treatment, before and after G3BP1 knockdown (**Figure 24D**). LC3-I lipidation was also rapidly increased in siG3BP1 cells at resting states, while 1 hr starvation demonstrated significant decrease in LC3-II protein expression as compared to siCon treated cells (**Figure 24E**) suggesting that G3BP1 knockdown results in an increase in autophagic activity as measured by p62 degradation and LC3-I lipidation. Furthermore, overexpression of TIA-1 and HuR did not alter p62 degradation and LC3-I lipidation kinetics during cellular stress (data not shown). Altogether, these data suggest that G3BP1 plays a role in negatively regulating autophagic activity during cellular stress.

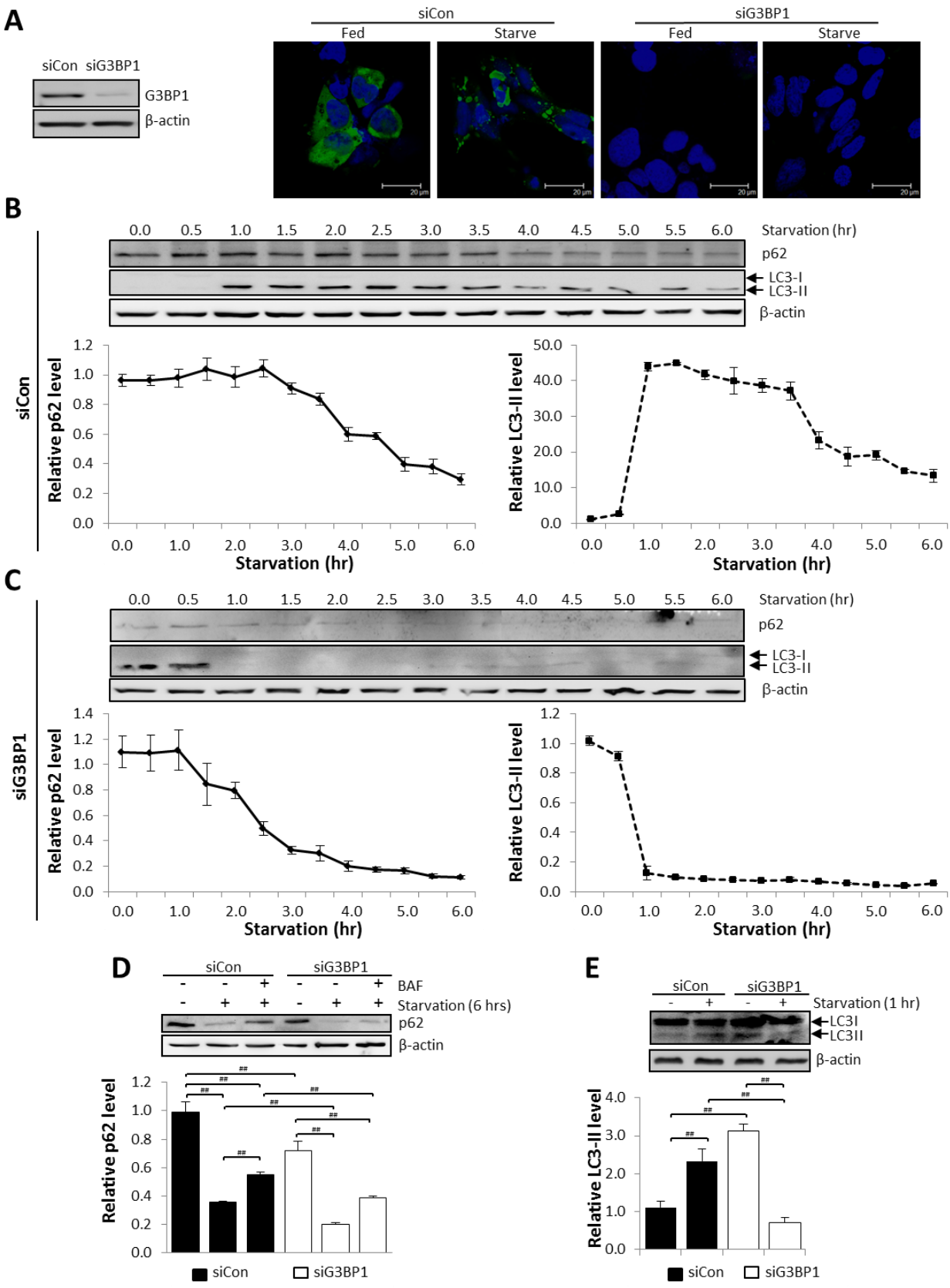
A
siCon siG3BP1
G3BP1
β-actin
siCon
siG3BP1
Fed
Starve
Fed
Starve
B
siCon
Starvation (hr)
p62
LC3-I
LC3-II
β-actin
Relative p62 level
Relative LC3-II level
Starvation (hr)
C
siG3BP1
Starvation (hr)
p62
LC3-I
LC3-II
β-actin
Relative p62 level
Relative LC3-II level
Starvation (hr)
D
siCon
siG3BP1
BAF
Starvation (6 hrs)
p62
β-actin
Relative p62 level
siCon
siG3BP1
E
siCon
siG3BP1
Starvation (1 hr)
LC3I
LC3II
β-actin
Relative LC3-II level
siCon
siG3BP1

Figure 24. G3BP1 knockdown promotes p62 degradation and LC3-I lipidation

A) HEK293 cells were treated with either siCon or siG3BP1 for 48 hrs and analyzed for successful knockdown of G3BP1 protein (left panel) and the lack of G3BP1-SGs in siG3BP1-treated cells during starvation stress (right panel). HEK293 cells treated with B) siCon or C) siG3BP1 were starved for up to 6 hrs in 30 minute intervals and protein lysates were collected to analyze protein expression of p62, LC3-I and -II, and β-actin (loading control). Cells treated with siCon or siG3BP1 were starved for D) 6 hrs and E) 1 hr to analyze p62 and LC3 protein expression, respectively. BAF (80.0 nM) was used as a positive control. Densitometry was performed in triplicates, normalized to β-actin and shown as relative values to siCon-treated controls (mean ± SD, n=3). ## $p < 0.01$.

5.3.3 G3BP1 overexpression blocks autophagy

In contrast to G3BP1 knockdown, we transfected a Flag tagged G3BP1 (Flag-G3BP1) into HEK293 cells to overexpress G3BP1 (**Figure 25A, left panel**), which induces the formation of G3BP1-SGs (**Figure 25A, right panel**) at resting states, consistent with those of previous report by Reineke et al. [279]. HEK293 cells transfected with an empty vector control showed similar p62 degradation (half-life ~4 hrs) and LC3-I lipidation to LC3-II (peak at 1 hr starvation) kinetics as previously demonstrated in Figure 23A (**Figure 25B**). However, HEK293 cells overexpressing G3BP1 showed significant retardation of p62 degradation with a half-life of ~6 hrs under starvation (**Figure 25C**). Furthermore, LC3-I lipidation to LC3-II peaked at 1 hr starvation and LC3-II failed to degrade as starvation progressed. When comparing starvation at 6 hrs, p62 accumulated significantly in G3BP1 overexpressing cells as compared to the empty vector transfected controls both before and after starvation (**Figure 25D**). G3BP1 overexpressing

cells starved for 1 hr also demonstrated a significant accumulation of LC3-II both before and after starvation (**Figure 25E**). Taken together, these data are consistent with Figure 24 and suggest that G3BP1 negatively regulate autophagic activity as observed by an attenuated degradation of p62, LC3-II, and ubiquitinated proteins in G3BP1 overexpressing cells.

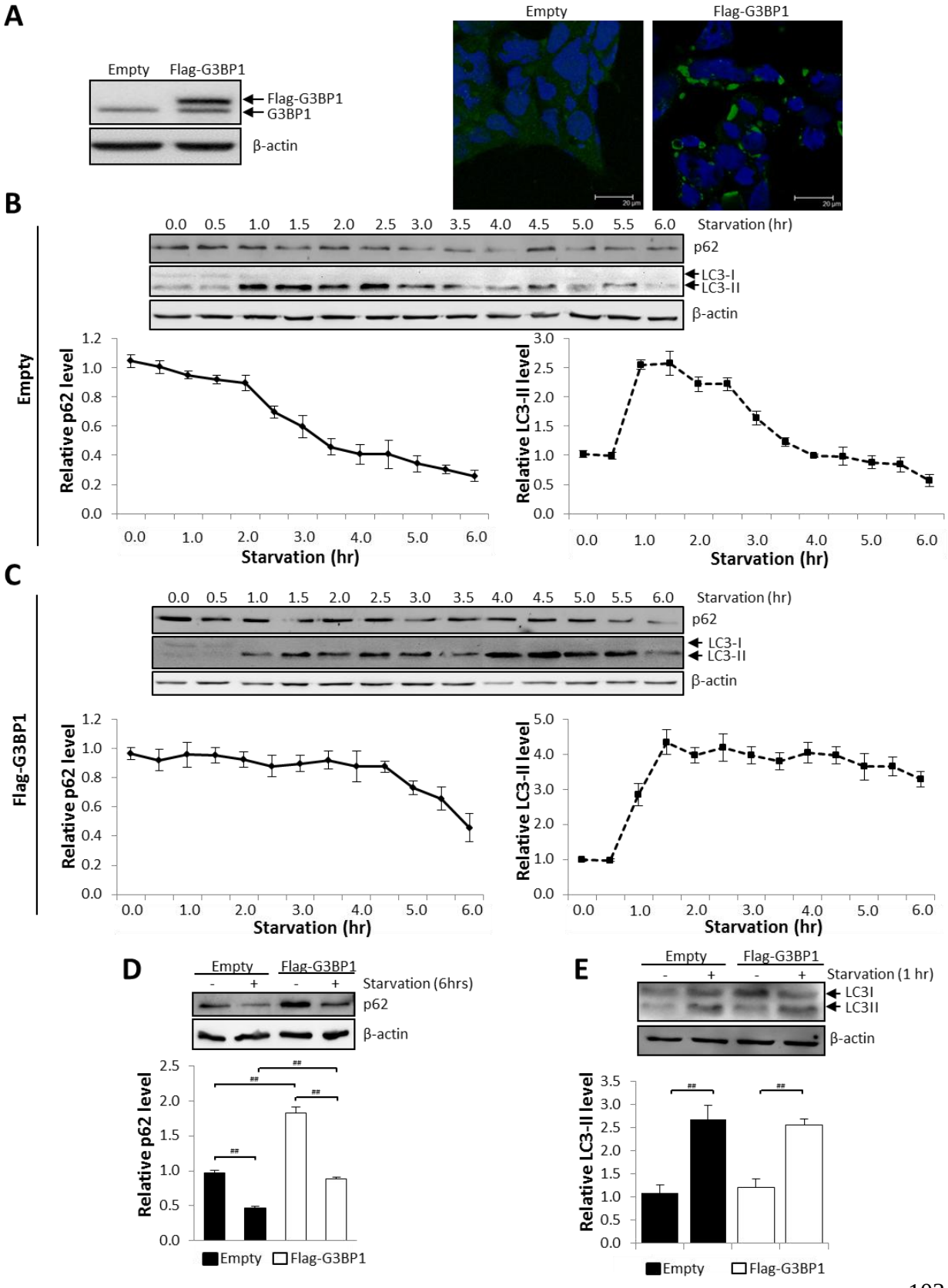
A
Empty
Flag-G3BP1
Flag-G3BP1
G3BP1
β-actin
Empty
Flag-G3BP1
B
Empty
0.0 0.5 1.0 1.5 2.0 2.5 3.0 3.5 4.0 4.5 5.0 5.5 6.0 Starvation (hr)
p62
LC3-I
LC3-II
β-actin
Relative p62 level
Starvation (hr)
Relative LC3-II level
Starvation (hr)
C
Flag-G3BP1
0.0 0.5 1.0 1.5 2.0 2.5 3.0 3.5 4.0 4.5 5.0 5.5 6.0 Starvation (hr)
p62
LC3-I
LC3-II
β-actin
Relative p62 level
Starvation (hr)
Relative LC3-II level
Starvation (hr)
D
Empty
Flag-G3BP1
- + - +
Starvation (6hrs)
p62
β-actin
Relative p62 level
##
Empty
Flag-G3BP1
E
Empty
Flag-G3BP1
- + - +
Starvation (1 hr)
LC3I
LC3II
β-actin
Relative LC3-II level
##
Empty
Flag-G3BP1

Figure 25. G3BP1 overexpression attenuates p62 degradation and LC3-I lipidation

A) HEK293 cells were transfected with either empty vector or Flag-G3BP1 for 48 hs and analyzed for successful overexpression of G3BP1 (left panel) and formation of G3BP1-SGs (right panel). HEK293 cells overexpressing B) empty vector or C) Flag-G3BP1 were starved for up to 6 hrs in 30 minute intervals and protein lysates were collected to analyze protein expression of p62, LC3-I and -II, and β-actin (loading control). D) Cells treated with empty vector or Flag-G3BP1 were starved for D) 6 hrs and E) 1 hr to analyze p62 and LC3 protein expression, respectively. Densitometry was performed in triplicates, normalized to β-actin and shown as relative values to empty vector controls (mean ± SD, n=3) ## $p < 0.01$.

5.3.4 G3BP1 negatively regulates autophagosome fusion with lysosomes

To further understand the exact effects of G3BP1 on autophagic flux, we utilized a GFP-RFP-LC3 tandem construct as previously described by Mizushima et al. [280]. This technique enables the visualization of autophagosomes as cytoplasmic yellow puncta, and autolysosomes as red puncta due to quenching of GFP fluorescence in acidic environments. Therefore, quantification of visible yellow and red puncta per cell allows us to gain insight into autophagic flux during cellular stress. Accumulation of red puncta indicates proper autophagosome-lysosome fusion to form autolysosomes devoid of GFP fluorescence, while accumulation of yellow puncta indicates an inhibition of autophagic flux. Using this technique, we overexpressed or knocked down G3BP1 and starved HEK293 cells stably expressing GFP-RFP-LC3 and quantified yellow and red puncta by confocal microscopy. BAF treatment was used as a positive control to demonstrate effective blockage of autophagic flux as observed by an accumulation of yellow puncta. siG3BP1-treated cells showed a significant increase in RFP puncta as compared

to siCon-treated cells, while levels of yellow puncta were not statistically different both before and after starvation (**Figure 26A**). Pearson's correlation coefficient (PC) of visible puncta was decreased in siG3BP1 treated cells (PC=0.147) as compared to siCon treated cells (PC=0.234). Treatment with BAF showed significant accumulation of yellow puncta, and was used as a positive control to block autophagosome-lysosome fusion. These data suggests that siG3BP1 treatment promoted formation of autolysosomes and GFP quenching. In contrast, we found that G3BP1 overexpression blocked autolysosome formation as observed by the significant accumulation of yellow puncta, as compared to the accumulation of red puncta in empty vector controls (**Figure 26B**). Also, starved G3BP1 overexpressing cells yielded an increased PC (PC=0.442) as compared to empty vector controls (PC=0.281), suggesting that G3BP1 blocks autolysosome formation. Altogether, these data reveal a previously undiscovered negative regulation of G3BP1 in autophagy during cellular stress.

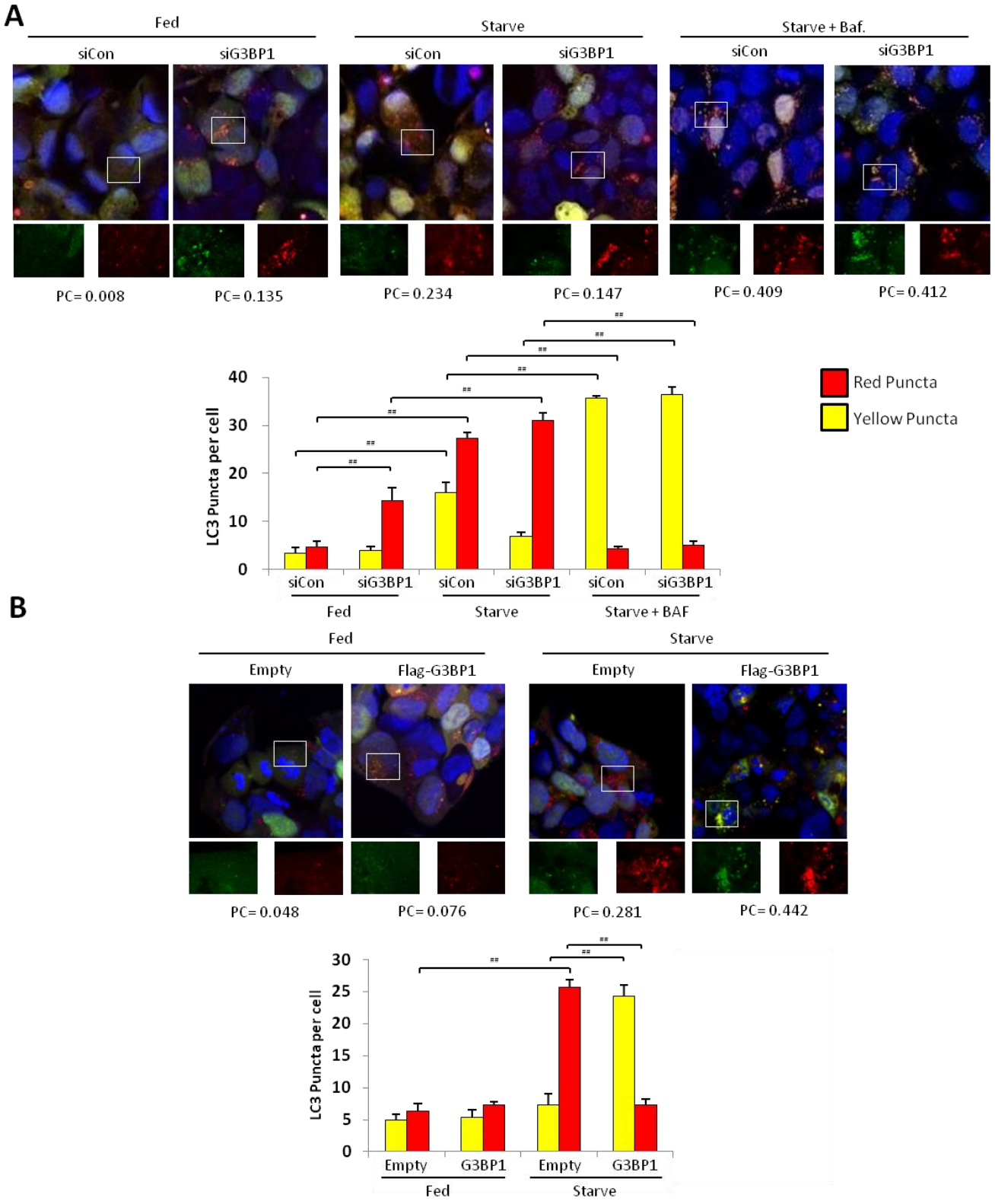
A
Fed
Starve
Starve + Baf.
siCon
siG3BP1
siCon
siG3BP1
siCon
siG3BP1
PC= 0.008
PC= 0.135
PC= 0.234
PC= 0.147
PC= 0.409
PC= 0.412
LC3 Puncta per cell
0
10
20
30
40
Red Puncta
Yellow Puncta
siCon
siG3BP1
siCon
siG3BP1
siCon
siG3BP1
Fed
Starve
Starve + BAF
B
Fed
Starve
Empty
Flag-G3BP1
Empty
Flag-G3BP1
PC= 0.048
PC= 0.076
PC= 0.281
PC= 0.442
LC3 Puncta per cell
0
5
10
15
20
25
30
Empty
G3BP1
Empty
G3BP1
Fed
Starve

Figure 26. G3BP1 negatively regulates autophagosome fusion with lysosomes

HEK293 cells stably expressing GFP-RFP-LC3 tandem reporter was either treated with A) siCon or siG3BP1, or B) empty vector or Flag-G3BP1 for 48 hrs and starved for 4 hrs. BAF was used as a positive control to block autolysosome formation in A). Yellow and red puncta were quantified by Volocity software version 5.2.1 over at least 5 images that contain 10 or more cells. Pearson's Correlation Coefficient (PC) was calculated similarly using Volocity software. (mean ± SD, n=5) ## $p < 0.01$.

5.3.5 G3BP1 binds STAT3

To further understand the mechanisms by which G3BP1 regulates autophagy, we performed quantitative proteomics (i.e. SILAC) to identify potential G3BP1 binding partners before and after starvation stress. After ratio analysis of a list of identified candidate peptides, selecting for peptides with high-confidence, and a 1% false discover rate with 2 or more unique peptides, we identified a total of 219 proteins that interacted with G3BP1 either before or after starvation stress. Protein ratios before and after cellular stress were represented as Z-scores; high Z-values indicate SG localization during starvation stress, while proteins with low Z-score values indicate proteins that disassociated from G3BP1 upon cellular stress. Among these 219 proteins, our analysis identified STAT3 as a novel interacting partner with G3BP1 at resting states (**Figure 27A**). Previously, a study by Shen et al. revealed a novel mechanism by which STAT3 represses autophagy by inhibiting PKR activity in the cytoplasm [209]. G3BP1 has also been demonstrated to interact with PKR to promote innate immune responses [180] via the phosphorylation of eIF2α [281], a critical mechanism required for autophagy and SGs activation. Thus, G3BP1 may negatively regulate autophagy via interaction with cytoplasmic STAT3 at

resting states. To confirm the interaction between G3BP1 and STAT3, we performed a co-immunoprecipitation assay and showed that G3BP1 co-immunoprecipitated with STAT3 at resting states, but not under starvation stress (**Figure 27B**). These data suggests that cytoplasmic STAT3 interacts with G3BP1 at resting states, and disassociates from G3BP1 upon cellular stress.

To better characterize the biochemical interaction between G3BP1 and STAT3, we performed docking analyses *in silico* using Cluspro 2.0 (http;//cluspro.bu.edu) and 3D imaging software, PyMOL. G3BP1 NTF2-like domain was selected for this analysis since this domain is crucial for protein-protein interactions. After screening 29 potential interacting models by which G3BP1 NTF2-like domain may possibly bind STAT3, we propose a model by which G3BP1 and STAT3 form strong hydrogen bonds between R17 and Q18 of G3BP1, with D334, S554 and T556 of STAT3 (**Figure 27C**). Cross-species analysis of amino acid sequences yielded a 91.2% sequence homology where D334. S554 and T556 are conserved (**Figure 27D**). Mutational analysis of these critical amino acids would be important in further confirming the direct interaction of G3BP1 with STAT3 and the downstream effects on autophagy. Taken together, these data propose a novel regulatory mechanism where G3BP1 may negatively regulate autophagy via direct interaction with cytoplasmic STAT3.

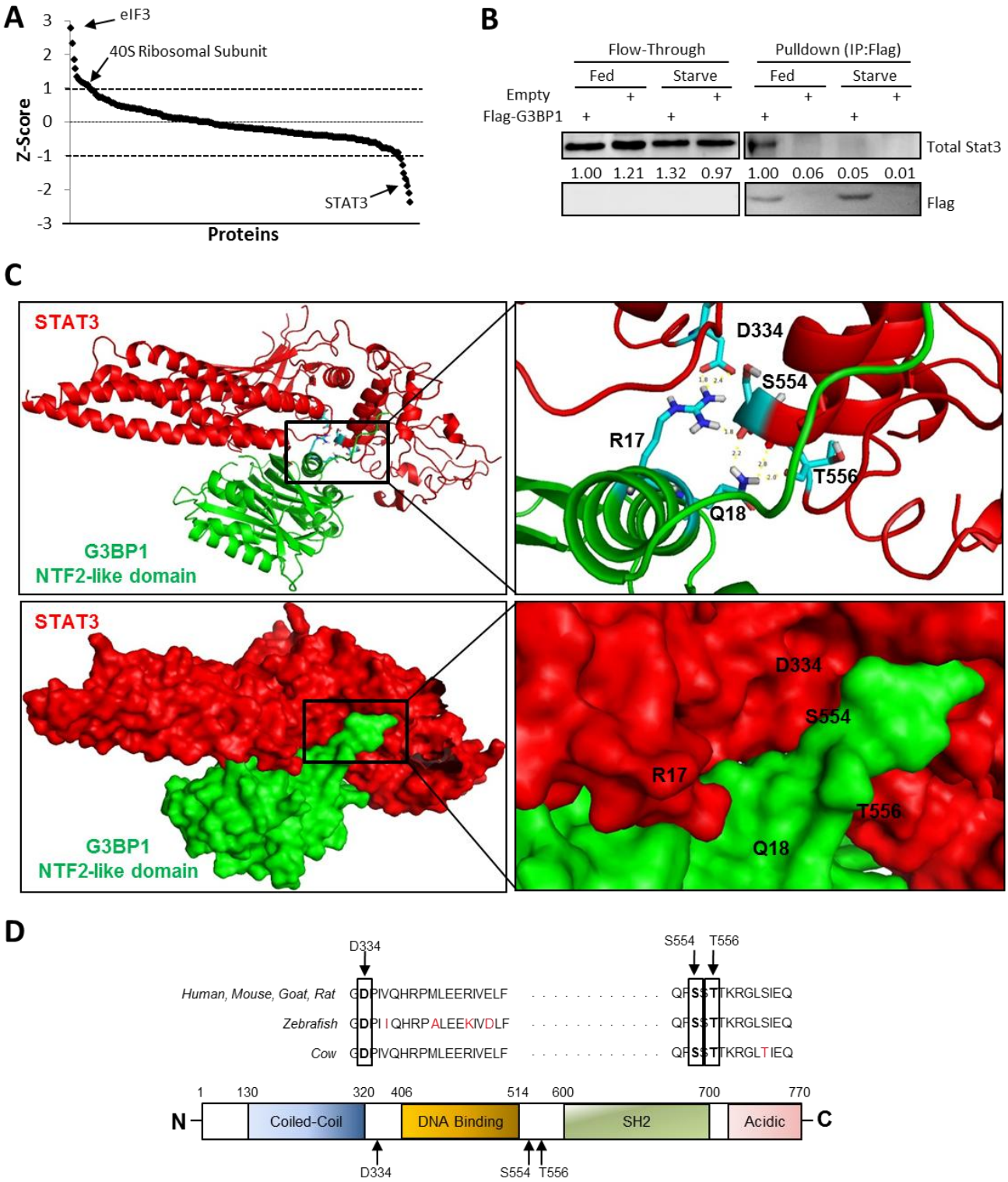

Figure 27. G3BP1 binds cytoplasmic STAT3

A) SILAC identified STAT3 as a protein disassociated from G3BP1 upon starvation stress in HEK293 cells. Z-scores of heavy to light binding ratios were plotted in decreasing order; low Z-scores indicate G3BP1 disassociation, and high Z-scores indicate increased association upon starvation stress. B) HEK293 cells were either transfected with empty vector or Flag-G3BP1 and starved for 4 hrs, followed by immunoprecipitation of the Flag epitope and detection of Flag and endogenous STAT3. STAT3 band intensities were quantified by densitometry and shown below. C) A molecular model of the STAT3 and G3BP1 interaction. A ribbon model (upper panel) and a surface model (lower panel) are shown on the left. Inserts on the right highlight residues that may contribute at the interaction surface. D) Cross-species homology and schematic diagram of STAT3. Residues D334, S554 and T556 are indicated with arrowheads. Red residues indicate amino acid variations across species. SH2; Src-homology 2 domain.

5.4 Discussion

In this chapter, we show that a key nucleating factor of SGs, G3BP1, negatively regulates autophagy, and interacts with a cytoplasmic repressor of autophagy, STAT3. We propose a potential mechanism by which G3BP1 interacts with cytoplasmic STAT3, and subsequently inhibits autophagy at resting states. This study contributes to the overall understanding of well-orchestrated cellular stress response pathways that are fundamental to various stresses and degenerative diseases. Dysregulation of STAT3 may contribute significantly to pathological disease progression of all types. More specifically, studies have previously demonstrated the significance of the STAT3 pathway in regulating vascular diseases [282], inflammatory bowel disease [283], neurodegenerative diseases [284], metastasis and progression of various cancers [285], and

viral infections [286], thus understanding the role of G3BP1 in regulating STAT3 activity may contribute to novel therapeutics to combat disease progression.

In this study, our data demonstrated that knockdown of G3BP1 promoted autophagic flux as observed by the increased degradation of p62 and early induction of LC3-I lipidation to LC3-II (**Figure 24C, D and E**)**.** In contrast, G3BP1 overexpression blocks autophagic flux as observed by the accumulation of p62 and LC3-II during starvation stress (**Figure 25C, D and E**). These results were further supported by accumulation of RFP puncta in siG3BP1 knockdown cells stably expressing the tandem construct GFP-RFP-LC3 during starvation stress (**Figure 26A**). Conversely, G3BP1 overexpression resulted in the accumulation of yellow puncta further demonstrating that G3BP1 blocks autolysosome formation (**Figure 26B**).

Previous studies have demonstrated G3BP1 and PKR as interacting partners to regulate innate immunity during viral-induced stress [180], and that PKR kinase activity to phosphorylate eIF2α is suppressed via direct sequestration by STAT3 at resting states [209]. In this study, our data showed a potential regulatory role of G3BP1 on autophagy activation using SILAC to identify STAT3 as an interacting partner (**Figure 27A and B**). Of interest, other proteins identified in our SILAC included key pathological proteins involved in neurodegenerative diseases such as Fragile X mental retardation protein 1/2, TDP-43 and RNA-binding protein fused to sarcoma (FUS), various hnRNPs, and canonical SG factors such as eIF3 and 40S ribosomal subunits. These findings are not surprising since abnormal cytoplasmic aggregation of the above mentioned proteins into G3BP1-SGs are well-established as pathological hallmarks of degenerative diseases [200]. Surprisingly, PKR was not identified as an interacting partner with G3BP1 amongst the 219 other proteins. However, the vicinity by which G3BP1 may be

interacting with STAT3, and thus indirectly to PKR, may be within a reasonable limit (< 40nm) to yield a positive signal using proximity ligation assay as previously demonstrated [180].

By *in silico* docking analysis of G3BP1 NTF2-like domain with unphosphorylated STAT3 monomer, we propose a model by which G3BP1 interacts with STAT3 (**Figure 27C**). This model was chosen based on its high conservation of critical amino acids in secondary structures that are involved in intermolecular hydrogen bonding. We showed that G3BP1-R17 and -Q18 participate in intermolecular hydrogen bonding with STAT3-D334, -S554 and -T556. Site-directed mutagenesis of such key residues on either G3BP1 or STAT3 remains to be completed to further demonstrate a cause-effect relationship between G3BP1-STAT3 interactions and autophagy activation. In order to fully determine a strong causal relationship between G3BP1 and autophagy repression, more mechanistic studies will be required.

It is important to note that our conclusions do not sufficiently associate the regulatory role of G3BP1-SGs on autophagy (i.e. whether the observed inhibition of autophagy is due to G3BP1 alone, or G3BP1-SGs). To address this issue, a stable cell-line expressing G3BP1-S149E, a mutant incapable of aggregation and SG formation, must be used. However, no reliable cell line models have been established. Future studies will be required to attribute the observed regulatory roles on autophagy to either G3BP1 alone, or G3BP1-SGs. In addition, these data do not exclude the possibility of a cell-type specific effect of G3BP1 on autophagy. Also studies involving models of STAT3 mutants may yield vital information about the integrated response between autophagy and SGs before and after cellular stress. Taken together, future studies using various cell lines and mutant STAT3 models will be required to confirm the significance of G3BP1 on autophagy.

The significance of STAT3 in autophagy regulation has been gaining interest this past decade. Mammucari et al. [287] has shown that STAT3 cytoplasmically represses forkhead box O1 (FOXO1) and FOXO3 at resting states via direct sequestration. Upon STAT3 phosphorylation, FOXO1 and FOXO3 translocate to the nucleus and induce transcriptional activation of autophagy-related genes such as *ULK2, BECN1, PIK3C3, BNIP3L, ATG12, ATG4B, and MAP1LC3A* [287]. STAT3 has also been shown to partially localize to mitochondria and plays a vital role in reducing autophagy-mediated degradation of mitochondria (termed mitophagy) induced by oxidative stress [288]. In addition, STAT3 is not the only cytoplasmic repressors that rely on post-translational modifications leading to autophagy activation. In a study by Tasdemir et al. [289], p53 has been demonstrated to inhibit autophagy presumably via a direct inhibitory interaction with high mobility group box 1, a protein responsible for the positive regulation of Beclin 1 [290], and with RB1CC1/FIP200, the human ortholog of yeast ATG17 [291]. Therefore, the integrated crosstalk between G3BP1 and autophagy activation may be part of a larger, more complicated, interconnected network of stress response activators that play a crucial role in mounting a sufficient autophagic response via post-translational modifications of cytoplasmic inhibitory proteins and transcriptional activation of autophagy-related genes.

While the role of SGs during cellular stress is generally cytoprotective, a clear linkage between SGs and autophagy has not yet been demonstrated as our studies do not fully associate the inhibitory effect of G3BP1 on autophagy to be due to G3BP1 alone, or cellular SGs. In this study, we provide evidence of a potential mechanism by which G3BP1 may negatively regulate autophagic activity (**Figure 28**). At resting states, G3BP1 binds STAT3 to inhibit the activation of autophagy (**Figure 28A**). Upon cellular stress, G3BP1 disassociation leads to the phosphorylation of PKR and STAT3 (**Figure 28B**). Dimerized p-STAT3 undergoes nuclear

translocation and functions as a transcriptional regulator (**Figure 28C**) while p-PKR phosphorylates eIF2α (**Figure 28D**). Phosphorylation of eIF2α induces the formation of SGs (**Figure 28E**) and activation of autophagy (**Figure 29F**). SGs inhibit autophagic flux by preventing the fusion of autophagosomes (AP) with lysosomes (L) to form autolysosomes (AL) in an unknown mechanism (**Figure 29G**). Taken together, our study proposes a potential mechanism by which G3BP1 negatively regulates autophagy. A deeper understanding of the integral roles of SGs, in particular G3BP1-SGs, and autophagy may contribute significantly to disease pathologies that involve STAT3, including hepatocarcinogenesis [292], Crohn's disease [293], oncogenesis [294], and various viral infections [181, 286].

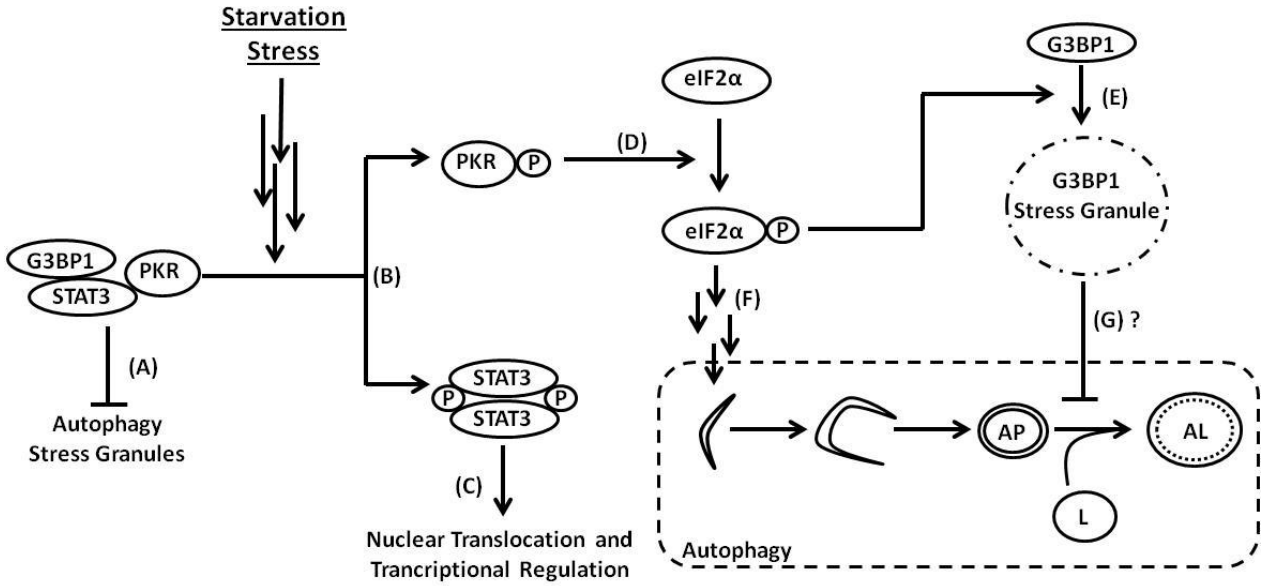

Figure 28. Potential model of the interplay between G3BP1, SGs and autophagic activity

A) G3BP1 binds to cytoplasmic STAT3 and inhibits autophagy and SG activation at resting states. B) Upon cellular stress, G3BP1 disassociates from STAT3, leading to PKR and STAT3 phosphorylation. C) Dimerized p-STAT3 undergoes nuclear translocation and functions as a transcriptional regulator, while D) p-PKR phosphorylates eIF2α, leading to the formation of SGs

E) and the activation of autophagy F). SGs inhibit autophagic flux by preventing the fusion of autophagosomes (AP) with lysosomes (L) to form autolysosomes (AL) in an unknown mechanism.

Chapter 6: Conclusion

6.1 Research summary and conclusions

Chapter 3: Production of a dominant-negative fragment due to G3BP1 cleavage contributes to the disruption of mitochondria-associated protective stress granules during CVB3 infection. My major findings in this chapter are:

1. CVB3 infection induces SG formation at early time points of infection.
2. CVB3 infection disassembles G3BP1-SGs at late time points of infection by cleaving G3BP1 at Q325 via $3C^{pro}$.
3. The cleavage of G3BP1 generates a C-terminal fragment that further inhibits G3BP1-SG formation during viral infection.
4. G3BP1-SGs play an anti-viral cytoprotective role during CVB3 infection.

Chapter 4: Cytoplasmic translocation, aggregation and cleavage of TDP-43 by enteroviral proteases modulate viral pathogenesis. My major findings in this chapter are:

1. CVB3 infection induces TDP-43 cleavage in mice and *in vitro* at amino acid Q327 by $3C^{pro}$.
2. $2A^{pro}$ induces cytoplasmic translocation and aggregation of TDP-43.
3. Full length and N-terminal TDP-43 translocates from the nucleus to the cytoplasmic G3BP1-SGs during CVB3 infection.
4. TDP-43-N compromises the function of native TDP-43 in *CFTR* exon 9 skipping.
5. TDP-43 knockdown promotes CVB3 replication.

Chapter 5: G3BP1-SGs negatively regulate autophagy potentially via direct recruitment of STAT3.

1. G3BP1 negatively regulates p62 and LC3-II degradation.
2. G3BP1 inhibits autolysosome formation.
3. G3BP1 binds cytoplasmic STAT3.

Taken together, my research demonstrated that CVB3 infection results in the formation via the activity of $2A^{pro}$ and late disruption of G3BP1-SGs through $3C^{pro}$ and G3BP1 possess an anti-viral function against CVB3 infection. My study also showed that CVB3 infection promotes TDP-43 translocation, aggregation and cleavage to benefit viral replication and contribute to virus-induced pathogenesis. Finally, I provide evidence of a potential mechanism by which G3BP1 negatively regulates autophagic activity.

6.2 Research significance

Virus-induced cardiomyopathy has been largely underestimated due to the protean nature of the disease [295]. To date, there is no cure for viral myocarditis and the chronic form, DCM. The research findings shown in this dissertation contribute to our understanding of how CVB3 interacts with the cellular stress response machinery and RNA binding proteins to promote viral infection and induce viral pathogenesis. Our results may aid in the discovery of potential therapeutic targets for the treatment of viral myocarditis/DCM.

Given that SGs are vital to mounting a sufficient innate immune response against viral infection, new techniques to bolster SG formation and function may be useful to limit viral replication. Furthermore, pharmacological inhibitors of $3C^{pro}$ activity could potentially block $3C^{pro}$-mediated cleavage of G3BP1, leading to the rescue of anti-viral SGs and subsequent attenuation of CVB3 pathogenesis. Therefore, identification of novel therapeutics to promote SG

function and block $3C^{pro}$ activity may result in persistent SG formation and function until viral clearance is complete.

TDP-43 translocation to cytoplasmic SGs upon CVB3 infection may possess detrimental consequences. Thus, blocking TDP-43 translocation to cytoplasmic SGs may be a promising therapeutic strategy in the management of viral myocarditis and TDP-43 proteinopathies. In addition, pharmacological inhibitors of $2A^{pro}$ activity may be developed to prevent destruction of the nuclear pore complex and cytoplasmic translocation of not only TDP-43, but also many other nuclear proteins involved in transcription regulation and mRNA processing that have been shown to be regulated during enteroviral infection to benefit viral replication and pathogenesis. Such proteins include hnRNP M and AUF1 [91, 108]. Furthermore, pharmacological inhibitors of $3C^{pro}$ may prevent CVB3-induced TDP-43 cleavage and the formation of a TDP-43 dominant-negative cleavage fragment that may contribute to the altered transcriptional dynamics during viral cardiomyopathy.

Given that CVB3 infection utilizes autophagic vesicles as replication sites [220], the newly discovered interaction of G3BP1 with STAT3 to negatively regulate autophagy suggests that targeting G3BP1 to strategically manipulate the accumulation of autophagosomes may be an approach to limit viral replication. Together, our findings contribute to the understanding of integrated cellular stress responses, and may aid in the development of novel therapeutics to regulate SGs and autophagy levels to minimize cardiomyocyte damage and disease progression during viral cardiomyopathy.

6.3 Limitations and future directions

Due to the focal nature of CVB3 infection in the myocardium, G3BP1 cleavage was undetectable in mouse hearts. This is in stark contrast to both primary and secondary cardiomyocyte cultures where near 100% infection can be achieved in a synchronized manner. A method of addressing this issue is to use recombinant GFP- tagged CVB3, thus allowing for direct isolation of CVB3-infected cells by fluorescent-activated cell sorting techniques, followed by western blot detection of target cleavage proteins. Moreover, the formation of SGs has not been investigated *in vivo* using conventional microscopy techniques. However, proteolytic cleavage of TDP-43 has been demonstrated in primary mouse neonatal cardiomyocytes and in the myocardium of CVB3-infected A/J mice.

Another limitation in these studies involves the indirect determination of viral protease cleavage sites on G3BP1 and TDP-43. While site-directed mutagenesis is widely accepted in the literature as a method of identifying potential cleavage sites, the possibility of significant conformational changes that sterically hinder proteolytic sites on the candidate protein cannot be excluded. A method to address this issue is to perform traditional Edman degradation sequencing where the C-terminal cleavage band of interest is isolated and digested from either a coomassie-stained SDS-PAGE gel or nitrocellulose membrane and sequenced from the free amino-termini. However the limitation of this method is that it requires sufficient isolation (> 3 picomole) of cleavage peptides to obtain discernible results. Of note, while attempting to isolate the 8 kDa C-terminal cleavage band of TDP-43 during CVB3 infection, all attempts of using Edman degradation failed to identify a discernible amino-acid primary sequence due to insufficient amounts of protein. In addition, our results demonstrated that the C-terminal cleavage fragment of TDP-43 was rapidly degraded by the ubiquitin-proteasome pathway. Edman degradation is

also restricted to free amino-terminus that is not post-translationally modified. The amino-terminal of TDP-43 C-terminal cleavage product has not been previously demonstrated to be post-translationally modified; however this possibility cannot be excluded. TAILS is a possible method of directly identifying target proteins and their respective cleavage sites even in the midst of post-translational modifications.

My studies are also limited by the lack of *in vivo* models to further confirm the role of TDP-43 and SGs in viral cardiomyopathy. Studies that may address this limitation include the use of a knock-in mouse strain that expresses cardiac-specific, non-cleavable G3BP1 (i.e. G3BP1-Q325E) in an A/J mouse line background. Upon CVB3 infection, we expect that G3BP1-Q325E would rescue the formation of SGs, and consequently rescue cytoprotective and anti-viral activities of SGs, leading to ameliorated heart function and anti-viral responses. In addition, simple immunohistochemical studies may be used to detect the formation of G3BP1-SGs in CVB3-infected mouse myocardium. In contrast, in order to understand the role of cytoplasmic translocation and cleavage of TDP-43 in *in vivo* models, the use of a noncleavable TDP-43 knock-in mouse model may not be sufficient as it may also translocate to the cytoplasm due to $2A^{pro}$ induced disruption of nuclear pore complexes. Therefore, a mouse strain that possesses a TDP-43 knockout mutation may be useful in addressing the role of TDP-43 in viral cardiomyopathy. Previous studies have attempted to generate full-body knockout of TDP-43 and have reported embryonic lethality [296]. Interestingly, there was a report showing that partial loss of TDP-43 by transgenic RNAi resulted in premature death, likely due to dilated cardiomyopathy [297]. A mouse model with conditional cardiac-specific knockout of TDP-43 has not yet been established and would be of great interest to the study of TDP-43 in viral cardiomyopathy.

Due to the heterogeneous nature of SGs, it is important to note that our studies are limited to the most well-established G3BP1-SGs. Other future directions are to further confirm the composition of G3BP1-SGs reported by Jain et al. [127]. In addition, while my studies propose a novel mechanism by which G3BP1 cytoplasmically represses STAT3 in the cytoplasm, these studies have not been repeated during CVB3 infection and would yield interesting avenues of future research.

Altogether, these studies contribute significantly to the understanding of the role of SGs and TDP-43 in CVB3 infection and propose promising new avenues of future research to better understand the orchestrated integration of cellular stress responses of viral cardiomyopathy.

Bibliography

1. Richardson P, McKenna W, Bristow M, Maisch B, Mautner B, O'Connell J, *et al.* Report of the 1995 World Health Organization/International Society and Federation of Cardiology Task Force on the Definition and Classification of cardiomyopathies. *Circulation* 1996, **93**(5)**:** 841-842.

2. Caforio AL, Pankuweit S, Arbustini E, Basso C, Gimeno-Blanes J, Felix SB, *et al.* Current state of knowledge on aetiology, diagnosis, management, and therapy of myocarditis: a position statement of the European Society of Cardiology Working Group on Myocardial and Pericardial Diseases. *Eur Heart J* 2013, **34**(33)**:** 2636-2648, 2648a-2648d.

3. Maron BJ, Towbin JA, Thiene G, Antzelevitch C, Corrado D, Arnett D, *et al.* Contemporary definitions and classification of the cardiomyopathies: an American Heart Association Scientific Statement from the Council on Clinical Cardiology, Heart Failure and Transplantation Committee; Quality of Care and Outcomes Research and Functional Genomics and Translational Biology Interdisciplinary Working Groups; and Council on Epidemiology and Prevention. *Circulation* 2006, **113**(14)**:** 1807-1816.

4. Elliott P, Andersson B, Arbustini E, Bilinska Z, Cecchi F, Charron P, *et al.* Classification of the cardiomyopathies: a position statement from the European Society Of Cardiology Working Group on Myocardial and Pericardial Diseases. *Eur Heart J* 2008, **29**(2)**:** 270-276.

5. Heidecker B, Kittleson MM, Kasper EK, Wittstein IS, Champion HC, Russell SD, *et al.* Transcriptomic biomarkers for the accurate diagnosis of myocarditis. *Circulation* 2011, **123**(11)**:** 1174-1184.

6. Felker GM, Boehmer JP, Hruban RH, Hutchins GM, Kasper EK, Baughman KL, *et al.* Echocardiographic findings in fulminant and acute myocarditis. *J Am Coll Cardiol* 2000, **36**(1)**:** 227-232.

7. Cooper LT, Baughman KL, Feldman AM, Frustaci A, Jessup M, Kuhl U, *et al.* The role of endomyocardial biopsy in the management of cardiovascular disease: a scientific statement from the American Heart Association, the American College of Cardiology, and the European Society of Cardiology. Endorsed by the Heart Failure Society of America and the Heart Failure Association of the European Society of Cardiology. *J Am Coll Cardiol* 2007, **50**(19)**:** 1914-1931.

8. Kindermann I, Barth C, Mahfoud F, Ukena C, Lenski M, Yilmaz A, *et al.* Update on myocarditis. *J Am Coll Cardiol* 2012, **59**(9)**:** 779-792.

9. Klingel K, Sauter M, Bock CT, Szalay G, Schnorr JJ, Kandolf R. Molecular pathology of inflammatory cardiomyopathy. *Med Microbiol Immunol* 2004, **193**(2-3)**:** 101-107.

10. Crowell RL, Landau BJ. A short history and introductory background on the coxsackieviruses of group B. *Curr Top Microbiol Immunol* 1997, **223:** 1-11.

11. Breinholt JP, Moulik M, Dreyer WJ, Denfield SW, Kim JJ, Jefferies JL, *et al.* Viral epidemiologic shift in inflammatory heart disease: the increasing involvement of parvovirus B19 in the myocardium of pediatric cardiac transplant patients. *J Heart Lung Transplant* 2010, **29**(7)**:** 739-746.

12. Schultz JC, Hilliard AA, Cooper LT, Jr., Rihal CS. Diagnosis and treatment of viral myocarditis. *Mayo Clin Proc* 2009, **84**(11)**:** 1001-1009.

13. Yilmaz A, Klingel K, Kandolf R, Sechtem U. A geographical mystery: do cardiotropic viruses respect national borders? *J Am Coll Cardiol* 2008, **52**(1)**:** 82; author reply 82-83.

14. Andreoletti L, Venteo L, Douche-Aourik F, Canas F, Lorin de la Grandmaison G, Jacques J, *et al.* Active Coxsackieviral B infection is associated with disruption of dystrophin in endomyocardial tissue of patients who died suddenly of acute myocardial infarction. *J Am Coll Cardiol* 2007, **50**(23)**:** 2207-2214.

15. Matsumori A, Shimada T, Chapman NM, Tracy SM, Mason JW. Myocarditis and heart failure associated with hepatitis C virus infection. *J Card Fail* 2006, **12**(4)**:** 293-298.

16. Bratincsak A, El-Said HG, Bradley JS, Shayan K, Grossfeld PD, Cannavino CR. Fulminant myocarditis associated with pandemic H1N1 influenza A virus in children. *J Am Coll Cardiol* 2010, **55**(9)**:** 928-929.

17. Kandolf R, Klingel K, Mertsching H, Canu A, Hohenadl C, Zell R, *et al.* Molecular studies on enteroviral heart disease: patterns of acute and persistent infections. *Eur Heart J* 1991, **12 Suppl D:** 49-55.

18. Griffin LD, Kearney D, Ni J, Jaffe R, Fricker FJ, Webber S, *et al.* Analysis of formalin-fixed and frozen myocardial autopsy samples for viral genome in childhood myocarditis and dilated cardiomyopathy with endocardial fibroelastosis using polymerase chain reaction (PCR). *Cardiovascular pathology : the official journal of the Society for Cardiovascular Pathology* 1995, **4**(1)**:** 3-11.

19. Bowles NE, Ni J, Kearney DL, Pauschinger M, Schultheiss HP, McCarthy R, *et al.* Detection of viruses in myocardial tissues by polymerase chain reaction. evidence of adenovirus as a common cause of myocarditis in children and adults. *J Am Coll Cardiol* 2003, **42**(3)**:** 466-472.

20. Kuhl U, Pauschinger M, Seeberg B, Lassner D, Noutsias M, Poller W, *et al.* Viral persistence in the myocardium is associated with progressive cardiac dysfunction. *Circulation* 2005, **112**(13)**:** 1965-1970.

21. Caforio AL, Calabrese F, Angelini A, Tona F, Vinci A, Bottaro S, *et al.* A prospective study of biopsy-proven myocarditis: prognostic relevance of clinical and aetiopathogenetic features at diagnosis. *Eur Heart J* 2007, **28**(11)**:** 1326-1333.

22. Gaaloul I, Riabi S, Harrath R, Hunter T, Hamda KB, Ghzala AB, *et al.* Coxsackievirus B detection in cases of myocarditis, myopericarditis, pericarditis and dilated cardiomyopathy in hospitalized patients. *Mol Med Rep* 2014, **10**(6)**:** 2811-2818.

23. Cooper LT Jr KK. Myocarditis. In: Mann Dl ZD, Libby P, Bonow RO, eds. (ed). *Braunwald's Heart Disease: A Textbook of Cardiovascular Medicine*. Elsevier: Philadelphia, PA, 2015, pp 1589-1602.

24. Seko Y, Takahashi N, Yagita H, Okumura K, Yazaki Y. Expression of cytokine mRNAs in murine hearts with acute myocarditis caused by coxsackievirus b3. *J Pathol* 1997, **183**(1)**:** 105-108.

25. Godeny EK, Gauntt CJ. Murine natural killer cells limit coxsackievirus B3 replication. *J Immunol* 1987, **139**(3)**:** 913-918.

26. Fuse K, Chan G, Liu Y, Gudgeon P, Husain M, Chen M, *et al.* Myeloid differentiation factor-88 plays a crucial role in the pathogenesis of Coxsackievirus B3-induced myocarditis and influences type I interferon production. *Circulation* 2005, **112**(15)**:** 2276-2285.

27. Seko Y, Matsuda H, Kato K, Hashimoto Y, Yagita H, Okumura K, *et al.* Expression of intercellular adhesion molecule-1 in murine hearts with acute myocarditis caused by coxsackievirus B3. *J Clin Invest* 1993, **91**(4)**:** 1327-1336.

28. Esfandiarei M, McManus BM. Molecular biology and pathogenesis of viral myocarditis. *Annual review of pathology* 2008, **3:** 127-155.

29. Kyu B, Matsumori A, Sato Y, Okada I, Chapman NM, Tracy S. Cardiac persistence of cardioviral RNA detected by polymerase chain reaction in a murine model of dilated cardiomyopathy. *Circulation* 1992, **86**(2)**:** 522-530.

30. Li Y, Bourlet T, Andreoletti L, Mosnier JF, Peng T, Yang Y, *et al.* Enteroviral capsid protein VP1 is present in myocardial tissues from some patients with myocarditis or dilated cardiomyopathy. *Circulation* 2000, **101**(3)**:** 231-234.

31. Chow LH, Gauntt CJ, McManus BM. Differential effects of myocarditic variants of Coxsackievirus B3 in inbred mice. A pathologic characterization of heart tissue damage. *Lab Invest* 1991, **64**(1)**:** 55-64.

32. Klingel K, Hohenadl C, Canu A, Albrecht M, Seemann M, Mall G, *et al.* Ongoing enterovirus-induced myocarditis is associated with persistent heart muscle infection: quantitative analysis of virus replication, tissue damage, and inflammation. *Proc Natl Acad Sci U S A* 1992, **89**(1)**:** 314-318.

33. Matsumori A, Yamada T, Suzuki H, Matoba Y, Sasayama S. Increased circulating cytokines in patients with myocarditis and cardiomyopathy. *Br Heart J* 1994, **72**(6)**:** 561-566.

34. Boehmer JP, Starling RC, Cooper LT, Torre-Amione G, Wittstein I, Dec GW, *et al.* Left ventricular assist device support and myocardial recovery in recent onset cardiomyopathy. *J Card Fail* 2012, **18**(10)**:** 755-761.

35. Atluri P, Ullery BW, MacArthur JW, Goldstone AB, Fairman AS, Hiesinger W, *et al.* Rapid onset of fulminant myocarditis portends a favourable prognosis and the ability to bridge mechanical circulatory support to recovery. *Eur J Cardiothorac Surg* 2013, **43**(2)**:** 379-382.

36. Chen JM, Spanier TB, Gonzalez JJ, Marelli D, Flannery MA, Tector KA, *et al.* Improved survival in patients with acute myocarditis using external pulsatile mechanical ventricular assistance. *J Heart Lung Transplant* 1999, **18**(4)**:** 351-357.

37. Cooper LT, Jr. Myocarditis. *N Engl J Med* 2009, **360**(15)**:** 1526-1538.

38. Makarov VA, Riabova OB, Granik VG, Wutzler P, Schmidtke M. Novel [(biphenyloxy)propyl]isoxazole derivatives for inhibition of human rhinovirus 2 and coxsackievirus B3 replication. *J Antimicrob Chemother* 2005, **55**(4)**:** 483-488.

39. Fohlman J, Pauksen K, Hyypia T, Eggertsen G, Ehrnst A, Ilback NG, *et al.* Antiviral treatment with WIN 54 954 reduces mortality in murine coxsackievirus B3 myocarditis. *Circulation* 1996, **94**(9)**:** 2254-2259.

40. Pevear DC, Tull TM, Seipel ME, Groarke JM. Activity of pleconaril against enteroviruses. *Antimicrobial agents and chemotherapy* 1999, **43**(9)**:** 2109-2115.

41. Desmond RA, Accortt NA, Talley L, Villano SA, Soong SJ, Whitley RJ. Enteroviral meningitis: natural history and outcome of pleconaril therapy. *Antimicrobial agents and chemotherapy* 2006, **50**(7)**:** 2409-2414.

42. Daliento L, Calabrese F, Tona F, Caforio AL, Tarsia G, Angelini A, *et al.* Successful treatment of enterovirus-induced myocarditis with interferon-alpha. *J Heart Lung Transplant* 2003, **22**(2)**:** 214-217.

43. Aradottir E, Alonso EM, Shulman ST. Severe neonatal enteroviral hepatitis treated with pleconaril. *Pediatr Infect Dis J* 2001, **20**(4)**:** 457-459.

44. Cao Y, Xu X, Zhang P. Advances in the Traditional Chinese Medicine-Based Management of Viral Myocarditis. *Cell Biochem Biophys* 2015.

45. Wojnicz R, Nowalany-Kozielska E, Wojciechowska C, Glanowska G, Wilczewski P, Niklewski T, *et al.* Randomized, placebo-controlled study for immunosuppressive treatment of inflammatory dilated cardiomyopathy: two-year follow-up results. *Circulation* 2001, **104**(1)**:** 39-45.

46. Amabile N, Fraisse A, Bouvenot J, Chetaille P, Ovaert C. Outcome of acute fulminant myocarditis in children. *Heart* 2006, **92**(9)**:** 1269-1273.

47. Xiao J, Shimada M, Liu W, Hu D, Matsumori A. Anti-inflammatory effects of eplerenone on viral myocarditis. *Eur J Heart Fail* 2009, **11**(4)**:** 349-353.

48. Wang YX, da Cunha V, Vincelette J, White K, Velichko S, Xu Y, *et al.* Antiviral and myocyte protective effects of murine interferon-beta and -{alpha}2 in coxsackievirus B3-induced myocarditis and epicarditis in Balb/c mice. *Am J Physiol Heart Circ Physiol* 2007, **293**(1)**:** H69-76.

49. Lenzo JC, Shellam GR, Lawson CM. Ganciclovir and cidofovir treatment of cytomegalovirus-induced myocarditis in mice. *Antimicrobial agents and chemotherapy* 2001, **45**(5)**:** 1444-1449.

50. Bailey TR, Diana GD, Kowalczyk PJ, Akullian V, Eissenstat MA, Cutcliffe D, *et al.* Antirhinoviral activity of heterocyclic analogs of Win 54954. *J Med Chem* 1992, **35**(24)**:** 4628-4633.

51. Zhang Y, Zhu H, Huang C, Cui X, Gao Y, Huang Y, *et al.* Astragaloside IV exerts antiviral effects against coxsackievirus B3 by upregulating interferon-gamma. *J Cardiovasc Pharmacol* 2006, **47**(2)**:** 190-195.

52. Chen P, Xie Y, Shen E, Li GG, Yu Y, Zhang CB, *et al.* Astragaloside IV attenuates myocardial fibrosis by inhibiting TGF-beta1 signaling in coxsackievirus B3-induced cardiomyopathy. *Eur J Pharmacol* 2011, **658**(2-3)**:** 168-174.

53. Zhang Y, Zhu H, Ye G, Huang C, Yang Y, Chen R, *et al.* Antiviral effects of sophoridine against coxsackievirus B3 and its pharmacokinetics in rats. *Life Sci* 2006, **78**(17)**:** 1998-2005.

54. Wang YF, Wang XY, Ren Z, Qian CW, Li YC, Kaio K, *et al.* Phyllaemblicin B inhibits Coxsackie virus B3 induced apoptosis and myocarditis. *Antiviral Res* 2009, **84**(2)**:** 150-158.

55. Wang WZ, Matsumori A, Yamada T, Shioi T, Okada I, Matsui S, *et al.* Beneficial effects of amlodipine in a murine model of congestive heart failure induced by viral myocarditis. A possible mechanism through inhibition of nitric oxide production. *Circulation* 1997, **95**(1)**:** 245-251.

56. Yuan J, Cheung PK, Zhang H, Chau D, Yanagawa B, Cheung C, *et al.* A phosphorothioate antisense oligodeoxynucleotide specifically inhibits coxsackievirus B3 replication in cardiomyocytes and mouse hearts. *Lab Invest* 2004, **84**(6)**:** 703-714.

57. Costanzo-Nordin MR, Reap EA, O'Connell JB, Robinson JA, Scanlon PJ. A nonsteroid anti-inflammatory drug exacerbates Coxsackie B3 murine myocarditis. *J Am Coll Cardiol* 1985, **6**(5)**:** 1078-1082.

58. Khatib R, Reyes MP, Smith FE. Enhancement of Coxsackievirus B3 replication in Vero cells by indomethacin. *J Infect Dis* 1990, **162**(4)**:** 997-998.

59. Crocker SJ, Frausto RF, Whitmire JK, Benning N, Milner R, Whitton JL. Amelioration of coxsackievirus B3-mediated myocarditis by inhibition of tissue inhibitors of matrix metalloproteinase-1. *Am J Pathol* 2007, **171**(6)**:** 1762-1773.

60. Godsel LM, Leon JS, Wang K, Fornek JL, Molteni A, Engman DM. Captopril prevents experimental autoimmune myocarditis. *J Immunol* 2003, **171**(1)**:** 346-352.

61. Reyes MP, Khatib R, Khatib G, Ho KL, Smith F, Kloner RA. Prolonged Captopril Therapy in Murine Viral Myocarditis. *J Cardiovasc Pharmacol Ther* 1998, **3**(1)**:** 43-50.

62. Bahk TJ, Daniels MD, Leon JS, Wang K, Engman DM. Comparison of angiotensin converting enzyme inhibition and angiotensin II receptor blockade for the prevention of experimental autoimmune myocarditis. *Int J Cardiol* 2008, **125**(1)**:** 85-93.

63. Seko Y. Effect of the angiotensin II receptor blocker olmesartan on the development of murine acute myocarditis caused by coxsackievirus B3. *Clin Sci (Lond)* 2006, **110**(3)**:** 379-386.

64. Yuan Z, Shioji K, Kihara Y, Takenaka H, Onozawa Y, Kishimoto C. Cardioprotective effects of carvedilol on acute autoimmune myocarditis: anti-inflammatory effects associated with antioxidant property. *Am J Physiol Heart Circ Physiol* 2004, **286**(1)**:** H83-90.

65. Yuan J, Stein DA, Lim T, Qiu D, Coughlin S, Liu Z, *et al.* Inhibition of coxsackievirus B3 in cell cultures and in mice by peptide-conjugated morpholino oligomers targeting the internal ribosome entry site. *J Virol* 2006, **80**(23)**:** 11510-11519.

66. Zhang HM, Wang F, Qiu Y, Ye X, Hanson P, Shen H, *et al.* Emodin Inhibits Coxsackievirus B3 Replication via Multiple Signaling Cascades Leading to Suppression of Translation. *Biochem J* 2015.

67. Zhang HM, Dai H, Hanson PJ, Li H, Guo H, Ye X, *et al.* Antiviral activity of an isatin derivative via induction of PERK-Nrf2-mediated suppression of cap-independent translation. *ACS Chem Biol* 2014, **9**(4)**:** 1015-1024.

68. Yanagawa B, Spiller OB, Proctor DG, Choy J, Luo H, Zhang HM, *et al.* Soluble recombinant coxsackievirus and adenovirus receptor abrogates coxsackievirus b3-mediated pancreatitis and myocarditis in mice. *J Infect Dis* 2004, **189**(8)**:** 1431-1439.

69. Yanagawa B, Spiller OB, Choy J, Luo H, Cheung P, Zhang HM, *et al.* Coxsackievirus B3-associated myocardial pathology and viral load reduced by recombinant soluble human decay-accelerating factor in mice. *Lab Invest* 2003, **83**(1)**:** 75-85.

70. Goodfellow IG, Evans DJ, Blom AM, Kerrigan D, Miners JS, Morgan BP, *et al.* Inhibition of coxsackie B virus infection by soluble forms of its receptors: binding affinities, altered particle formation, and competition with cellular receptors. *J Virol* 2005, **79**(18)**:** 12016-12024.

71. Pinkert S, Westermann D, Wang X, Klingel K, Dorner A, Savvatis K, *et al.* Prevention of cardiac dysfunction in acute coxsackievirus B3 cardiomyopathy by inducible expression of a soluble coxsackievirus-adenovirus receptor. *Circulation* 2009, **120**(23)**:** 2358-2366.

72. Dalldorf G. The Coxsackie group of viruses. *Science* 1949, **110**(2866)**:** 594.

73. Dalldorf G, Sickles GM. An Unidentified, Filtrable Agent Isolated From the Feces of Children With Paralysis. *Science* 1948, **108**(2794)**:** 61-62.

74. Grist NR, Reid D. General Pathogenicity and Epidemiology. In: Bendinelli M, Friedman H (eds). *Coxsackieviruses: A General Update*. Springer US: Boston, MA, 1988, pp 221-239.

75. Dalldorf G. The Coxsackie viruses. *Annu Rev Microbiol* 1955, **9:** 277-296.

76. Gauntt CJ, Paque RE, Trousdale MD, Gudvangen RJ, Barr DT, Lipotich GJ, *et al.* Temperature-sensitive mutant of coxsackievirus B3 establishes resistance in neonatal mice that protects them during adolescence against coxsackievirus B3-induced myocarditis. *Infect Immun* 1983, **39**(2)**:** 851-864.

77. Sabin AB. Characteristics and genetic potentialities of experimentally produced and naturally occurring variants of poliomyelitis virus. *Ann N Y Acad Sci* 1955, **61**(4)**:** 924-938; discussion, 938-929.

78. Salk JE. Principles of immunization as applied to poliomyelitis and influenza. *Am J Public Health Nations Health* 1953, **43**(11)**:** 1384-1398.

79. Toyoda H, Franco D, Fujita K, Paul AV, Wimmer E. Replication of poliovirus requires binding of the poly(rC) binding protein to the cloverleaf as well as to the adjacent C-rich spacer sequence between the cloverleaf and the internal ribosomal entry site. *J Virol* 2007, **81**(18)**:** 10017-10028.

80. Klump WM, Bergmann I, Muller BC, Ameis D, Kandolf R. Complete nucleotide sequence of infectious Coxsackievirus B3 cDNA: two initial 5' uridine residues are regained during plus-strand RNA synthesis. *J Virol* 1990, **64**(4)**:** 1573-1583.

81. Flanegan JB, Petterson RF, Ambros V, Hewlett NJ, Baltimore D. Covalent linkage of a protein to a defined nucleotide sequence at the 5'-terminus of virion and replicative intermediate RNAs of poliovirus. *Proc Natl Acad Sci U S A* 1977, **74**(3)**:** 961-965.

82. Sun Y, Wang Y, Shan C, Chen C, Xu P, Song M, *et al.* Enterovirus 71 VPg uridylation uses a two-molecular mechanism of 3D polymerase. *J Virol* 2012, **86**(24)**:** 13662-13671.

83. Huber SA, Gauntt CJ, Sakkinen P. Enteroviruses and myocarditis: viral pathogenesis through replication, cytokine induction, and immunopathogenicity. *Adv Virus Res* 1998, **51:** 35-80.

84. Tapparel C, Siegrist F, Petty TJ, Kaiser L. Picornavirus and enterovirus diversity with associated human diseases. *Infect Genet Evol* 2013, **14:** 282-293.

85. Gradi A, Svitkin YV, Imataka H, Sonenberg N. Proteolysis of human eukaryotic translation initiation factor eIF4GII, but not eIF4GI, coincides with the shutoff of host protein synthesis after poliovirus infection. *Proc Natl Acad Sci U S A* 1998, **95**(19)**:** 11089-11094.

86. Wong J, Zhang J, Yanagawa B, Luo Z, Yang X, Chang J, *et al.* Cleavage of serum response factor mediated by enteroviral protease 2A contributes to impaired cardiac function. *Cell Res* 2012, **22**(2)**:** 360-371.

87. Badorff C, Lee GH, Lamphear BJ, Martone ME, Campbell KP, Rhoads RE, *et al.* Enteroviral protease 2A cleaves dystrophin: evidence of cytoskeletal disruption in an acquired cardiomyopathy. *Nat Med* 1999, **5**(3)**:** 320-326.

88. Feng Q, Langereis MA, Lork M, Nguyen M, Hato SV, Lanke K, *et al.* Enterovirus 2Apro targets MDA5 and MAVS in infected cells. *J Virol* 2014, **88**(6)**:** 3369-3378.

89. Mukherjee A, Morosky SA, Delorme-Axford E, Dybdahl-Sissoko N, Oberste MS, Wang T, *et al.* The coxsackievirus B 3C protease cleaves MAVS and TRIF to attenuate host type I interferon and apoptotic signaling. *PLoS pathogens* 2011, **7**(3)**:** e1001311.

90. Blom N, Hansen J, Blaas D, Brunak S. Cleavage site analysis in picornaviral polyproteins: discovering cellular targets by neural networks. *Protein Sci* 1996, **5**(11)**:** 2203-2216.

91. Jagdeo JM, Dufour A, Fung G, Luo H, Kleifeld O, Overall CM, *et al.* Heterogeneous Nuclear Ribonucleoprotein M Facilitates Enterovirus Infection. *J Virol* 2015, **89**(14)**:** 7064-7078.

92. Wang B, Xi X, Lei X, Zhang X, Cui S, Wang J, *et al.* Enterovirus 71 protease 2Apro targets MAVS to inhibit anti-viral type I interferon responses. *PLoS pathogens* 2013, **9**(3)**:** e1003231.

93. Drahos J, Racaniello VR. Cleavage of IPS-1 in cells infected with human rhinovirus. *J Virol* 2009, **83**(22)**:** 11581-11587.

94. Barral PM, Sarkar D, Fisher PB, Racaniello VR. RIG-I is cleaved during picornavirus infection. *Virology* 2009, **391**(2)**:** 171-176.

95. Wang H, Lei X, Xiao X, Yang C, Lu W, Huang Z, *et al.* Reciprocal Regulation between Enterovirus 71 and the NLRP3 Inflammasome. *Cell Rep* 2015, **12**(1)**:** 42-48.

96. Lei X, Sun Z, Liu X, Jin Q, He B, Wang J. Cleavage of the adaptor protein TRIF by enterovirus 71 3C inhibits antiviral responses mediated by Toll-like receptor 3. *J Virol* 2011, **85**(17)**:** 8811-8818.

97. Dougherty JD, White JP, Lloyd RE. Poliovirus-mediated disruption of cytoplasmic processing bodies. *J Virol* 2011, **85**(1)**:** 64-75.

98. Shiroki K, Isoyama T, Kuge S, Ishii T, Ohmi S, Hata S, *et al.* Intracellular redistribution of truncated La protein produced by poliovirus 3Cpro-mediated cleavage. *J Virol* 1999, **73**(3)**:** 2193-2200.

99. Shi J, Wong J, Piesik P, Fung G, Zhang J, Jagdeo J, *et al.* Cleavage of sequestosome 1/p62 by an enteroviral protease results in disrupted selective autophagy and impaired NFKB signaling. *Autophagy* 2013, **9**(10)**:** 1591-1603.

100. Shi J, Fung G, Piesik P, Zhang J, Luo H. Dominant-negative function of the C-terminal fragments of NBR1 and SQSTM1 generated during enteroviral infection. *Cell Death Differ* 2014, **21**(9)**:** 1432-1441.

101. Harris KG, Morosky SA, Drummond CG, Patel M, Kim C, Stolz DB, *et al.* RIP3 Regulates Autophagy and Promotes Coxsackievirus B3 Infection of Intestinal Epithelial Cells. *Cell host & microbe* 2015, **18**(2)**:** 221-232.

102. Wang C, Wong J, Fung G, Shi J, Deng H, Zhang J, *et al.* Dysferlin deficiency confers increased susceptibility to coxsackievirus-induced cardiomyopathy. *Cell Microbiol* 2015, **17**(10)**:** 1423-1430.

103. Seipelt J, Liebig HD, Sommergruber W, Gerner C, Kuechler E. 2A proteinase of human rhinovirus cleaves cytokeratin 8 in infected HeLa cells. *J Biol Chem* 2000, **275**(26)**:** 20084-20089.

104. Joachims M, Harris KS, Etchison D. Poliovirus protease 3C mediates cleavage of microtubule-associated protein 4. *Virology* 1995, **211**(2)**:** 451-461.

105. Yalamanchili P, Weidman K, Dasgupta A. Cleavage of transcriptional activator Oct-1 by poliovirus encoded protease 3Cpro. *Virology* 1997, **239**(1)**:** 176-185.

106. Yalamanchili P, Banerjee R, Dasgupta A. Poliovirus-encoded protease 2APro cleaves the TATA-binding protein but does not inhibit host cell RNA polymerase II transcription in vitro. *J Virol* 1997, **71**(9)**:** 6881-6886.

107. Yalamanchili P, Datta U, Dasgupta A. Inhibition of host cell transcription by poliovirus: cleavage of transcription factor CREB by poliovirus-encoded protease 3Cpro. *J Virol* 1997, **71**(2)**:** 1220-1226.

108. Wong J, Si X, Angeles A, Zhang J, Shi J, Fung G, *et al.* Cytoplasmic redistribution and cleavage of AUF1 during coxsackievirus infection enhance the stability of its viral genome. *FASEB J* 2013, **27**(7)**:** 2777-2787.

109. Back SH, Kim YK, Kim WJ, Cho S, Oh HR, Kim JE, *et al.* Translation of polioviral mRNA is inhibited by cleavage of polypyrimidine tract-binding proteins executed by polioviral 3C(pro). *J Virol* 2002, **76**(5)**:** 2529-2542.

110. Almstead LL, Sarnow P. Inhibition of U snRNP assembly by a virus-encoded proteinase. *Genes Dev* 2007, **21**(9)**:** 1086-1097.

111. Fung G, Shi J, Deng H, Hou J, Wang C, Hong A, *et al.* Cytoplasmic translocation, aggregation, and cleavage of TDP-43 by enteroviral proteases modulate viral pathogenesis. *Cell Death Differ* 2015.

112. Lamphear BJ, Yan R, Yang F, Waters D, Liebig HD, Klump H, *et al.* Mapping the cleavage site in protein synthesis initiation factor eIF-4 gamma of the 2A proteases from human Coxsackievirus and rhinovirus. *J Biol Chem* 1993, **268**(26)**:** 19200-19203.

113. Liebig HD, Ziegler E, Yan R, Hartmuth K, Klump H, Kowalski H, *et al.* Purification of two picornaviral 2A proteinases: interaction with eIF-4 gamma and influence on in vitro translation. *Biochemistry* 1993, **32**(29)**:** 7581-7588.

114. Joachims M, Van Breugel PC, Lloyd RE. Cleavage of poly(A)-binding protein by enterovirus proteases concurrent with inhibition of translation in vitro. *J Virol* 1999, **73**(1)**:** 718-727.

115. Hanson PJ, Ye X, Qiu Y, Zhang HM, Hemida MG, Wang F, *et al.* Cleavage of DAP5 by coxsackievirus B3 2A protease facilitates viral replication and enhances apoptosis by altering translation of IRES-containing genes. *Cell Death Differ* 2015.

116. Perera R, Daijogo S, Walter BL, Nguyen JH, Semler BL. Cellular protein modification by poliovirus: the two faces of poly(rC)-binding protein. *J Virol* 2007, **81**(17)**:** 8919-8932.

117. Neznanov N, Chumakov KM, Neznanova L, Almasan A, Banerjee AK, Gudkov AV. Proteolytic cleavage of the p65-RelA subunit of NF-kappaB during poliovirus infection. *J Biol Chem* 2005, **280**(25)**:** 24153-24158.

118. Zaragoza C, Saura M, Padalko EY, Lopez-Rivera E, Lizarbe TR, Lamas S, *et al.* Viral protease cleavage of inhibitor of kappaBalpha triggers host cell apoptosis. *Proc Natl Acad Sci U S A* 2006, **103**(50)**:** 19051-19056.

119. Deng H, Fung G, Shi J, Xu S, Wang C, Yin M, *et al.* Enhanced enteroviral infectivity via viral protease-mediated cleavage of Grb2-associated binder 1. *FASEB J* 2015.

120. Watters K, Palmenberg AC. Differential processing of nuclear pore complex proteins by rhinovirus 2A proteases from different species and serotypes. *J Virol* 2011, **85**(20)**:** 10874-10883.

121. Fung G, Ng CS, Zhang J, Shi J, Wong J, Piesik P, *et al.* Production of a dominant-negative fragment due to G3BP1 cleavage contributes to the disruption of mitochondria-associated protective stress granules during CVB3 infection. *PLos ONE* 2013, **8**(11)**:** e79546.

122. Ng CS, Jogi M, Yoo JS, Onomoto K, Koike S, Iwasaki T, *et al.* Encephalomyocarditis virus disrupts stress granules, the critical platform for triggering antiviral innate immune responses. *J Virol* 2013, **87**(17)**:** 9511-9522.

123. Kedersha N, Chen S, Gilks N, Li W, Miller IJ, Stahl J, *et al.* Evidence that ternary complex (eIF2-GTP-tRNA(i)(Met))-deficient preinitiation complexes are core constituents of mammalian stress granules. *Mol Biol Cell* 2002, **13**(1)**:** 195-210.

124. Anderson P, Kedersha N. Stressful initiations. *Journal of cell science* 2002, **115**(Pt 16)**:** 3227-3234.

125. Nover L, Scharf KD, Neumann D. Cytoplasmic heat shock granules are formed from precursor particles and are associated with a specific set of mRNAs. *Mol Cell Biol* 1989, **9**(3)**:** 1298-1308.

126. Collier NC, Schlesinger MJ. The dynamic state of heat shock proteins in chicken embryo fibroblasts. *J Cell Biol* 1986, **103**(4)**:** 1495-1507.

127. Jain S, Wheeler JR, Walters RW, Agrawal A, Barsic A, Parker R. ATPase-Modulated Stress Granules Contain a Diverse Proteome and Substructure. *Cell* 2016, **164**(3)**:** 487-498.

128. Parker R, Sheth U. P bodies and the control of mRNA translation and degradation. *Mol Cell* 2007, **25**(5)**:** 635-646.

129. Eulalio A, Behm-Ansmant I, Izaurralde E. P bodies: at the crossroads of post-transcriptional pathways. *Nature reviews Molecular cell biology* 2007, **8**(1)**:** 9-22.

130. Kedersha N, Anderson P. Mammalian stress granules and processing bodies. *Methods Enzymol* 2007, **431:** 61-81.

131. Kedersha NL, Gupta M, Li W, Miller I, Anderson P. RNA-binding proteins TIA-1 and TIAR link the phosphorylation of eIF-2 alpha to the assembly of mammalian stress granules. *J Cell Biol* 1999, **147**(7)**:** 1431-1442.

132. Kedersha N, Stoecklin G, Ayodele M, Yacono P, Lykke-Andersen J, Fritzler MJ, *et al.* Stress granules and processing bodies are dynamically linked sites of mRNP remodeling. *J Cell Biol* 2005, **169**(6)**:** 871-884.

133. Ingelfinger D, Arndt-Jovin DJ, Luhrmann R, Achsel T. The human LSm1-7 proteins colocalize with the mRNA-degrading enzymes Dcp1/2 and Xrnl in distinct cytoplasmic foci. *Rna* 2002, **8**(12)**:** 1489-1501.

134. Gallois-Montbrun S, Kramer B, Swanson CM, Byers H, Lynham S, Ward M, *et al.* Antiviral protein APOBEC3G localizes to ribonucleoprotein complexes found in P bodies and stress granules. *J Virol* 2007, **81**(5)**:** 2165-2178.

135. Wichroski MJ, Robb GB, Rana TM. Human retroviral host restriction factors APOBEC3G and APOBEC3F localize to mRNA processing bodies. *PLoS Pathog* 2006, **2**(5)**:** e41.

136. Katoh H, Okamoto T, Fukuhara T, Kambara H, Morita E, Mori Y, *et al.* Japanese encephalitis virus core protein inhibits stress granule formation through an interaction with Caprin-1 and facilitates viral propagation. *J Virol* 2013, **87**(1)**:** 489-502.

137. Solomon S, Xu Y, Wang B, David MD, Schubert P, Kennedy D, *et al.* Distinct structural features of caprin-1 mediate its interaction with G3BP-1 and its induction of phosphorylation of eukaryotic translation initiation factor 2alpha, entry to cytoplasmic stress granules, and selective interaction with a subset of mRNAs. *Mol Cell Biol* 2007, **27**(6)**:** 2324-2342.

138. Nie Y, Wang YY. Innate immune responses to DNA viruses. *Protein & cell* 2013, **4**(1)**:** 1-7.

139. Deigendesch N, Koch-Nolte F, Rothenburg S. ZBP1 subcellular localization and association with stress granules is controlled by its Z-DNA binding domains. *Nucleic Acids Res* 2006, **34**(18)**:** 5007-5020.

140. Tourriere H, Chebli K, Zekri L, Courselaud B, Blanchard JM, Bertrand E, *et al.* The RasGAP-associated endoribonuclease G3BP assembles stress granules. *J Cell Biol* 2003, **160**(6)**:** 823-831.

141. Kimball SR, Horetsky RL, Ron D, Jefferson LS, Harding HP. Mammalian stress granules represent sites of accumulation of stalled translation initiation complexes. *American journal of physiology Cell physiology* 2003, **284**(2)**:** C273-284.

142. Gallouzi IE, Brennan CM, Stenberg MG, Swanson MS, Eversole A, Maizels N, *et al.* HuR binding to cytoplasmic mRNA is perturbed by heat shock. *Proc Natl Acad Sci U S A* 2000, **97**(7)**:** 3073-3078.

143. Yang WH, Yu JH, Gulick T, Bloch KD, Bloch DB. RNA-associated protein 55 (RAP55) localizes to mRNA processing bodies and stress granules. *Rna* 2006, **12**(4)**:** 547-554.

144. Wilczynska A, Aigueperse C, Kress M, Dautry F, Weil D. The translational regulator CPEB1 provides a link between dcp1 bodies and stress granules. *Journal of cell science* 2005, **118**(Pt 5)**:** 981-992.

145. Kasim V, Wu S, Taira K, Miyagishi M. Determination of the role of DDX3 a factor involved in mammalian RNAi pathway using an shRNA-expression library. *PLos ONE* 2013, **8**(3)**:** e59445.

146. Lai MC, Lee YH, Tarn WY. The DEAD-box RNA helicase DDX3 associates with export messenger ribonucleoproteins as well as tip-associated protein and participates in translational control. *Mol Biol Cell* 2008, **19**(9)**:** 3847-3858.

147. Weissbach R, Scadden AD. Tudor-SN and ADAR1 are components of cytoplasmic stress granules. *Rna* 2012, **18**(3)**:** 462-471.

148. Andrei MA, Ingelfinger D, Heintzmann R, Achsel T, Rivera-Pomar R, Luhrmann R. A role for eIF4E and eIF4E-transporter in targeting mRNPs to mammalian processing bodies. *Rna* 2005, **11**(5)**:** 717-727.

149. Yoo JS, Takahasi K, Ng CS, Ouda R, Onomoto K, Yoneyama M, *et al.* DHX36 enhances RIG-I signaling by facilitating PKR-mediated antiviral stress granule formation. *PLoS pathogens* 2014, **10**(3)**:** e1004012.

150. Chalupnikova K, Lattmann S, Selak N, Iwamoto F, Fujiki Y, Nagamine Y. Recruitment of the RNA helicase RHAU to stress granules via a unique RNA-binding domain. *J Biol Chem* 2008, **283**(50)**:** 35186-35198.

151. Hua Y, Zhou J. Survival motor neuron protein facilitates assembly of stress granules. *FEBS Lett* 2004, **572**(1-3)**:** 69-74.

152. Hua Y, Zhou J. Rpp20 interacts with SMN and is re-distributed into SMN granules in response to stress. *Biochem Biophys Res Commun* 2004, **314**(1)**:** 268-276.

153. Leung AK, Calabrese JM, Sharp PA. Quantitative analysis of Argonaute protein reveals microRNA-dependent localization to stress granules. *Proc Natl Acad Sci U S A* 2006, **103**(48)**:** 18125-18130.

154. Sen GL, Blau HM. Argonaute 2/RISC resides in sites of mammalian mRNA decay known as cytoplasmic bodies. *Nat Cell Biol* 2005, **7**(6)**:** 633-636.

155. Thomas MG, Martinez Tosar LJ, Loschi M, Pasquini JM, Correale J, Kindler S, *et al.* Staufen recruitment into stress granules does not affect early mRNA transport in oligodendrocytes. *Mol Biol Cell* 2005, **16**(1)**:** 405-420.

156. Dewey CM, Cenik B, Sephton CF, Dries DR, Mayer P, 3rd, Good SK, *et al.* TDP-43 is directed to stress granules by sorbitol, a novel physiological osmotic and oxidative stressor. *Mol Cell Biol* 2011, **31**(5)**:** 1098-1108.

157. Wehner KA, Schutz S, Sarnow P. OGFOD1, a novel modulator of eukaryotic translation initiation factor 2alpha phosphorylation and the cellular response to stress. *Mol Cell Biol* 2010, **30**(8)**:** 2006-2016.

158. Morris AR, Mukherjee N, Keene JD. Ribonomic analysis of human Pum1 reveals cis-trans conservation across species despite evolution of diverse mRNA target sets. *Mol Cell Biol* 2008, **28**(12)**:** 4093-4103.

159. Kwon S, Zhang Y, Matthias P. The deacetylase HDAC6 is a novel critical component of stress granules involved in the stress response. *Genes Dev* 2007, **21**(24)**:** 3381-3394.

160. Vessey JP, Vaccani A, Xie Y, Dahm R, Karra D, Kiebler MA, *et al.* Dendritic localization of the translational repressor Pumilio 2 and its contribution to dendritic stress granules. *J Neurosci* 2006, **26**(24)**:** 6496-6508.

161. Gilks N, Kedersha N, Ayodele M, Shen L, Stoecklin G, Dember LM, *et al.* Stress granule assembly is mediated by prion-like aggregation of TIA-1. *Mol Biol Cell* 2004, **15**(12)**:** 5383-5398.

162. Koromilas AE. Roles of the translation initiation factor eIF2alpha serine 51 phosphorylation in cancer formation and treatment. *Biochim Biophys Acta* 2015, **1849**(7)**:** 871-880.

163. Buchan JR, Parker R. Eukaryotic stress granules: the ins and outs of translation. *Mol Cell* 2009, **36**(6)**:** 932-941.

164. Garcia MA, Meurs EF, Esteban M. The dsRNA protein kinase PKR: virus and cell control. *Biochimie* 2007, **89**(6-7)**:** 799-811.

165. Chen JJ. Regulation of protein synthesis by the heme-regulated eIF2alpha kinase: relevance to anemias. *Blood* 2007, **109**(7)**:** 2693-2699.

166. Berlanga JJ, Ventoso I, Harding HP, Deng J, Ron D, Sonenberg N, *et al.* Antiviral effect of the mammalian translation initiation factor 2alpha kinase GCN2 against RNA viruses. *EMBO J* 2006, **25**(8)**:** 1730-1740.

167. McEwen E, Kedersha N, Song B, Scheuner D, Gilks N, Han A, *et al.* Heme-regulated inhibitor kinase-mediated phosphorylation of eukaryotic translation initiation factor 2 inhibits translation, induces stress granule formation, and mediates survival upon arsenite exposure. *J Biol Chem* 2005, **280**(17)**:** 16925-16933.

168. Koumenis C, Naczki C, Koritzinsky M, Rastani S, Diehl A, Sonenberg N, *et al.* Regulation of protein synthesis by hypoxia via activation of the endoplasmic reticulum kinase PERK and phosphorylation of the translation initiation factor eIF2alpha. *Mol Cell Biol* 2002, **22**(21)**:** 7405-7416.

169. Dong J, Qiu H, Garcia-Barrio M, Anderson J, Hinnebusch AG. Uncharged tRNA activates GCN2 by displacing the protein kinase moiety from a bipartite tRNA-binding domain. *Mol Cell* 2000, **6**(2)**:** 269-279.

170. Williams BR. PKR; a sentinel kinase for cellular stress. *Oncogene* 1999, **18**(45)**:** 6112-6120.

171. Harding HP, Zhang Y, Ron D. Protein translation and folding are coupled by an endoplasmic-reticulum-resident kinase. *Nature* 1999, **397**(6716)**:** 271-274.

172. Shi Y, Vattem KM, Sood R, An J, Liang J, Stramm L, *et al.* Identification and characterization of pancreatic eukaryotic initiation factor 2 alpha-subunit kinase, PEK, involved in translational control. *Mol Cell Biol* 1998, **18**(12)**:** 7499-7509.

173. White JP, Cardenas AM, Marissen WE, Lloyd RE. Inhibition of cytoplasmic mRNA stress granule formation by a viral proteinase. *Cell host & microbe* 2007, **2**(5)**:** 295-305.

174. Cai X, Chen J, Xu H, Liu S, Jiang QX, Halfmann R, *et al.* Prion-like polymerization underlies signal transduction in antiviral immune defense and inflammasome activation. *Cell* 2014, **156**(6)**:** 1207-1222.

175. Anderson P, Kedersha N. RNA granules: post-transcriptional and epigenetic modulators of gene expression. *Nature reviews Molecular cell biology* 2009, **10**(6)**:** 430-436.

176. Mokas S, Mills JR, Garreau C, Fournier MJ, Robert F, Arya P, *et al.* Uncoupling stress granule assembly and translation initiation inhibition. *Mol Biol Cell* 2009, **20**(11)**:** 2673-2683.

177. Eisinger-Mathason TS, Andrade J, Groehler AL, Clark DE, Muratore-Schroeder TL, Pasic L, *et al.* Codependent functions of RSK2 and the apoptosis-promoting factor TIA-1 in stress granule assembly and cell survival. *Mol Cell* 2008, **31**(5)**:** 722-736.

178. Li YR, King OD, Shorter J, Gitler AD. Stress granules as crucibles of ALS pathogenesis. *J Cell Biol* 2013, **201**(3)**:** 361-372.

179. Anderson P, Kedersha N, Ivanov P. Stress granules, P-bodies and cancer. *Biochim Biophys Acta* 2015, **1849**(7)**:** 861-870.

180. Reineke LC, Lloyd RE. The stress granule protein G3BP1 recruits protein kinase R to promote multiple innate immune antiviral responses. *J Virol* 2015, **89**(5)**:** 2575-2589.

181. Onomoto K, Yoneyama M, Fung G, Kato H, Fujita T. Antiviral innate immunity and stress granule responses. *Trends Immunol* 2014, **35**(9)**:** 420-428.

182. Onomoto K, Jogi M, Yoo JS, Narita R, Morimoto S, Takemura A, *et al.* Critical role of an antiviral stress granule containing RIG-I and PKR in viral detection and innate immunity. *PLoS One* 2012, **7**(8)**:** e43031.

183. Onoguchi K, Onomoto K, Takamatsu S, Jogi M, Takemura A, Morimoto S, *et al.* Virus-infection or 5'ppp-RNA activates antiviral signal through redistribution of IPS-1 mediated by MFN1. *PLoS Pathog* 2010, **6**(7)**:** e1001012.

184. Ng CS, Jogi M, Yoo JS, Onomoto K, Koike S, Iwasaki T, *et al.* EMCV Disrupts Stress Granules, the Critical Platform for Triggering Antiviral Innate Immune Responses. *J Virol* 2013.

185. Reineke LC, Lloyd RE. Diversion of stress granules and P-bodies during viral infection. *Virology* 2013, **436**(2)**:** 255-267.

186. Takeuchi K, Komatsu T, Kitagawa Y, Sada K, Gotoh B. Sendai virus C protein plays a role in restricting PKR activation by limiting the generation of intracellular double-stranded RNA. *J Virol* 2008, **82**(20)**:** 10102-10110.

187. Iseni F, Garcin D, Nishio M, Kedersha N, Anderson P, Kolakofsky D. Sendai virus trailer RNA binds TIAR, a cellular protein involved in virus-induced apoptosis. *EMBO J* 2002, **21**(19)**:** 5141-5150.

188. Okonski KM, Samuel CE. Stress granule formation induced by measles virus is protein kinase PKR dependent and impaired by RNA adenosine deaminase ADAR1. *J Virol* 2013, **87**(2)**:** 756-766.

189. Khaperskyy DA, Hatchette TF, McCormick C. Influenza A virus inhibits cytoplasmic stress granule formation. *FASEB J* 2012, **26**(4)**:** 1629-1639.

190. Lu Y, Wambach M, Katze MG, Krug RM. Binding of the influenza virus NS1 protein to double-stranded RNA inhibits the activation of the protein kinase that phosphorylates the elF-2 translation initiation factor. *Virology* 1995, **214**(1)**:** 222-228.

191. Baird NL, York J, Nunberg JH. Arenavirus infection induces discrete cytosolic structures for RNA replication. *J Virol* 2012, **86**(20)**:** 11301-11310.

192. Piotrowska J, Hansen SJ, Park N, Jamka K, Sarnow P, Gustin KE. Stable formation of compositionally unique stress granules in virus-infected cells. *J Virol* 2010, **84**(7)**:** 3654-3665.

193. Qin Q, Hastings C, Miller CL. Mammalian orthoreovirus particles induce and are recruited into stress granules at early times postinfection. *J Virol* 2009, **83**(21)**:** 11090-11101.

194. Smith JA, Schmechel SC, Raghavan A, Abelson M, Reilly C, Katze MG, *et al.* Reovirus induces and benefits from an integrated cellular stress response. *J Virol* 2006, **80**(4)**:** 2019-2033.

195. Emara MM, Brinton MA. Interaction of TIA-1/TIAR with West Nile and dengue virus products in infected cells interferes with stress granule formation and processing body assembly. *Proc Natl Acad Sci U S A* 2007, **104**(21)**:** 9041-9046.

196. Li W, Li Y, Kedersha N, Anderson P, Emara M, Swiderek KM, *et al.* Cell proteins TIA-1 and TIAR interact with the 3' stem-loop of the West Nile virus complementary minus-strand RNA and facilitate virus replication. *J Virol* 2002, **76**(23)**:** 11989-12000.

197. Buratti E, Baralle FE. Characterization and functional implications of the RNA binding properties of nuclear factor TDP-43, a novel splicing regulator of CFTR exon 9. *J Biol Chem* 2001, **276**(39)**:** 36337-36343.

198. Buratti E, Brindisi A, Giombi M, Tisminetzky S, Ayala YM, Baralle FE. TDP-43 binds heterogeneous nuclear ribonucleoprotein A/B through its C-terminal tail: an important region for the inhibition of cystic fibrosis transmembrane conductance regulator exon 9 splicing. *J Biol Chem* 2005, **280**(45)**:** 37572-37584.

199. Dewey CM, Cenik B, Sephton CF, Johnson BA, Herz J, Yu G. TDP-43 aggregation in neurodegeneration: are stress granules the key? *Brain Res* 2012, **1462:** 16-25.

200. Bentmann E, Haass C, Dormann D. Stress granules in neurodegeneration--lessons learnt from TAR DNA binding protein of 43 kDa and fused in sarcoma. *FEBS J* 2013, **280**(18)**:** 4348-4370.

201. Zheng Q, Li J, Wang X. Interplay between the ubiquitin-proteasome system and autophagy in proteinopathies. *International journal of physiology, pathophysiology and pharmacology* 2009, **1**(2)**:** 127-142.

202. Buchan JR, Kolaitis RM, Taylor JP, Parker R. Eukaryotic stress granules are cleared by autophagy and Cdc48/VCP function. *Cell* 2013, **153**(7)**:** 1461-1474.

203. Le Fourn V, Gaplovska-Kysela K, Guhl B, Santimaria R, Zuber C, Roth J. Basal autophagy is involved in the degradation of the ERAD component EDEM1. *Cellular and molecular life sciences : CMLS* 2009, **66**(8)**:** 1434-1445.

204. Narendra D, Tanaka A, Suen DF, Youle RJ. Parkin is recruited selectively to impaired mitochondria and promotes their autophagy. *J Cell Biol* 2008, **183**(5)**:** 795-803.

205. Hara T, Nakamura K, Matsui M, Yamamoto A, Nakahara Y, Suzuki-Migishima R, *et al.* Suppression of basal autophagy in neural cells causes neurodegenerative disease in mice. *Nature* 2006, **441**(7095)**:** 885-889.

206. Gomes LC, Di Benedetto G, Scorrano L. During autophagy mitochondria elongate, are spared from degradation and sustain cell viability. *Nat Cell Biol* 2011, **13**(5)**:** 589-598.

207. Maiuri MC, Zalckvar E, Kimchi A, Kroemer G. Self-eating and self-killing: crosstalk between autophagy and apoptosis. *Nature reviews Molecular cell biology* 2007, **8**(9)**:** 741-752.

208. Thorburn J, Moore F, Rao A, Barclay WW, Thomas LR, Grant KW, *et al.* Selective inactivation of a Fas-associated death domain protein (FADD)-dependent apoptosis and autophagy pathway in immortal epithelial cells. *Mol Biol Cell* 2005, **16**(3)**:** 1189-1199.

209. Shen S, Niso-Santano M, Adjemian S, Takehara T, Malik SA, Minoux H, *et al.* Cytoplasmic STAT3 represses autophagy by inhibiting PKR activity. *Mol Cell* 2012, **48**(5)**:** 667-680.

210. Jung CH, Ro SH, Cao J, Otto NM, Kim DH. mTOR regulation of autophagy. *FEBS Lett* 2010, **584**(7)**:** 1287-1295.

211. Orvedahl A, MacPherson S, Sumpter R, Jr., Talloczy Z, Zou Z, Levine B. Autophagy protects against Sindbis virus infection of the central nervous system. *Cell Host Microbe* 2010, **7**(2)**:** 115-127.

212. Gutierrez MG, Master SS, Singh SB, Taylor GA, Colombo MI, Deretic V. Autophagy is a defense mechanism inhibiting BCG and Mycobacterium tuberculosis survival in infected macrophages. *Cell* 2004, **119**(6)**:** 753-766.

213. Maiuri MC, Galluzzi L, Morselli E, Kepp O, Malik SA, Kroemer G. Autophagy regulation by p53. *Curr Opin Cell Biol* 2010, **22**(2)**:** 181-185.

214. Rouschop KM, van den Beucken T, Dubois L, Niessen H, Bussink J, Savelkouls K, *et al.* The unfolded protein response protects human tumor cells during hypoxia through regulation of the autophagy genes MAP1LC3B and ATG5. *J Clin Invest* 2010, **120**(1)**:** 127-141.

215. Ichimura Y, Waguri S, Sou YS, Kageyama S, Hasegawa J, Ishimura R, *et al.* Phosphorylation of p62 activates the Keap1-Nrf2 pathway during selective autophagy. *Mol Cell* 2013, **51**(5)**:** 618-631.

216. Seguin SJ, Morelli FF, Vinet J, Amore D, De Biasi S, Poletti A, *et al.* Inhibition of autophagy, lysosome and VCP function impairs stress granule assembly. *Cell Death Differ* 2014, **21**(12)**:** 1838-1851.

217. Wolozin B. Regulated protein aggregation: stress granules and neurodegeneration. *Mol Neurodegener* 2012, **7:** 56.

218. Willis MS, Patterson C. Proteotoxicity and cardiac dysfunction--Alzheimer's disease of the heart? *N Engl J Med* 2013, **368**(5)**:** 455-464.

219. Ding B, Abe J, Wei H, Huang Q, Walsh RA, Molina CA, *et al.* Functional role of phosphodiesterase 3 in cardiomyocyte apoptosis: implication in heart failure. *Circulation* 2005, **111**(19)**:** 2469-2476.

220. Wong J, Zhang J, Si X, Gao G, Mao I, McManus BM, *et al.* Autophagosome supports coxsackievirus B3 replication in host cells. *J Virol* 2008, **82**(18)**:** 9143-9153.

221. Feuer R, Ruller CM, An N, Tabor-Godwin JM, Rhoades RE, Maciejewski S, *et al.* Viral persistence and chronic immunopathology in the adult central nervous system following Coxsackievirus infection during the neonatal period. *J Virol* 2009, **83**(18)**:** 9356-9369.

222. Zheng YZ, Berg KB, Foster LJ. Mitochondria do not contain lipid rafts, and lipid rafts do not contain mitochondrial proteins. *J Lipid Res* 2009, **50**(5)**:** 988-998.

223. Chau DH, Yuan J, Zhang H, Cheung P, Lim T, Liu Z, *et al.* Coxsackievirus B3 proteases 2A and 3C induce apoptotic cell death through mitochondrial injury and cleavage of eIF4GI but not DAP5/p97/NAT1. *Apoptosis : an international journal on programmed cell death* 2007, **12**(3)**:** 513-524.

224. Kerekatte V, Keiper BD, Badorff C, Cai A, Knowlton KU, Rhoads RE. Cleavage of Poly(A)-binding protein by coxsackievirus 2A protease in vitro and in vivo: another mechanism for host protein synthesis shutoff? *J Virol* 1999, **73**(1)**:** 709-717.

225. de Breyne S, Bonderoff JM, Chumakov KM, Lloyd RE, Hellen CU. Cleavage of eukaryotic initiation factor eIF5B by enterovirus 3C proteases. *Virology* 2008, **378**(1)**:** 118-122.

226. Morrow CD, Gibbons GF, Dasgupta A. The host protein required for in vitro replication of poliovirus is a protein kinase that phosphorylates eukaryotic initiation factor-2. *Cell* 1985, **40**(4)**:** 913-921.

227. Anderson P, Kedersha N. Stress granules: the Tao of RNA triage. *Trends Biochem Sci* 2008, **33**(3)**:** 141-150.

228. Gallouzi IE, Parker F, Chebli K, Maurier F, Labourier E, Barlat I, *et al.* A novel phosphorylation-dependent RNase activity of GAP-SH3 binding protein: a potential link between signal transduction and RNA stability. *Mol Cell Biol* 1998, **18**(7)**:** 3956-3965.

229. White JP, Lloyd RE. Regulation of stress granules in virus systems. *Trends Microbiol* 2012, **20**(4)**:** 175-183.

230. Linero FN, Thomas MG, Boccaccio GL, Scolaro LA. Junin virus infection impairs stress-granule formation in Vero cells treated with arsenite via inhibition of eIF2alpha phosphorylation. *J Gen Virol* 2011, **92**(Pt 12)**:** 2889-2899.

231. Lindquist ME, Lifland AW, Utley TJ, Santangelo PJ, Crowe JE, Jr. Respiratory syncytial virus induces host RNA stress granules to facilitate viral replication. *J Virol* 2010, **84**(23)**:** 12274-12284.

232. Ariumi Y, Kuroki M, Kushima Y, Osugi K, Hijikata M, Maki M, *et al.* Hepatitis C virus hijacks P-body and stress granule components around lipid droplets. *J Virol* 2011, **85**(14)**:** 6882-6892.

233. Lloyd RE. How do viruses interact with stress-associated RNA granules? *PLoS Pathog* 2012, **8**(6)**:** e1002741.

234. Ohn T, Kedersha N, Hickman T, Tisdale S, Anderson P. A functional RNAi screen links O-GlcNAc modification of ribosomal proteins to stress granule and processing body assembly. *Nat Cell Biol* 2008, **10**(10)**:** 1224-1231.

235. Coller BA, Chapman NM, Beck MA, Pallansch MA, Gauntt CJ, Tracy SM. Echovirus 22 is an atypical enterovirus. *J Virol* 1990, **64**(6)**:** 2692-2701.

236. Carthy CM, Granville DJ, Watson KA, Anderson DR, Wilson JE, Yang D, *et al.* Caspase activation and specific cleavage of substrates after coxsackievirus B3-induced cytopathic effect in HeLa cells. *J Virol* 1998, **72**(9)**:** 7669-7675.

237. Luo H, Yanagawa B, Zhang J, Luo Z, Zhang M, Esfandiarei M, *et al.* Coxsackievirus B3 replication is reduced by inhibition of the extracellular signal-regulated kinase (ERK) signaling pathway. *J Virol* 2002, **76**(7)**:** 3365-3373.

238. Navarro S, Marinelli P, Diaz-Caballero M, Ventura S. The prion-like RNA-processing protein HNRPDL forms inherently toxic amyloid-like inclusion bodies in bacteria. *Microb Cell Fact* 2015, **14:** 102.

239. Fang YS, Tsai KJ, Chang YJ, Kao P, Woods R, Kuo PH, *et al.* Full-length TDP-43 forms toxic amyloid oligomers that are present in frontotemporal lobar dementia-TDP patients. *Nat Commun* 2014, **5:** 4824.

240. Igaz LM, Kwong LK, Chen-Plotkin A, Winton MJ, Unger TL, Xu Y, *et al.* Expression of TDP-43 C-terminal Fragments in Vitro Recapitulates Pathological Features of TDP-43 Proteinopathies. *J Biol Chem* 2009, **284**(13)**:** 8516-8524.

241. Gao G, Zhang J, Si X, Wong J, Cheung C, McManus B, *et al.* Proteasome inhibition attenuates coxsackievirus-induced myocardial damage in mice. *Am J Physiol Heart Circ Physiol* 2008, **295**(1)**:** H401-408.

242. Luo H, Wong J, Wong B. Protein degradation systems in viral myocarditis leading to dilated cardiomyopathy. *Cardiovasc Res* 2010, **85**(2)**:** 347-356.

243. Gustin KE. Inhibition of nucleo-cytoplasmic trafficking by RNA viruses: targeting the nuclear pore complex. *Virus Res* 2003, **95**(1-2)**:** 35-44.

244. Cathcart AL, Rozovics JM, Semler BL. Cellular mRNA decay protein AUF1 negatively regulates enterovirus and human rhinovirus infections. *J Virol* 2013, **87**(19)**:** 10423-10434.

245. Rozovics JM, Chase AJ, Cathcart AL, Chou W, Gershon PD, Palusa S, *et al.* Picornavirus modification of a host mRNA decay protein. *MBio* 2012, **3**(6)**:** e00431-00412.

246. Gustin KE, Sarnow P. Effects of poliovirus infection on nucleo-cytoplasmic trafficking and nuclear pore complex composition. *EMBO J* 2001, **20**(1-2)**:** 240-249.

247. Jagdeo JM, Dufour A, Fung G, Luo H, Overall CM, Jan E. Heterogeneous nuclear ribonucleoprotein M facilitates enterovirus infection. *J Virol* 2015.

248. Pesiridis GS, Lee VM, Trojanowski JQ. Mutations in TDP-43 link glycine-rich domain functions to amyotrophic lateral sclerosis. *Hum Mol Genet* 2009, **18**(R2)**:** R156-162.

249. Gitcho MA, Baloh RH, Chakraverty S, Mayo K, Norton JB, Levitch D, *et al.* TDP-43 A315T mutation in familial motor neuron disease. *Ann Neurol* 2008, **63**(4)**:** 535-538.

250. Kabashi E, Valdmanis PN, Dion P, Spiegelman D, McConkey BJ, Vande Velde C, *et al.* TARDBP mutations in individuals with sporadic and familial amyotrophic lateral sclerosis. *Nat Genet* 2008, **40**(5)**:** 572-574.

251. Sreedharan J, Blair IP, Tripathi VB, Hu X, Vance C, Rogelj B, *et al.* TDP-43 mutations in familial and sporadic amyotrophic lateral sclerosis. *Science* 2008, **319**(5870)**:** 1668-1672.

252. Van Deerlin VM, Leverenz JB, Bekris LM, Bird TD, Yuan W, Elman LB, *et al.* TARDBP mutations in amyotrophic lateral sclerosis with TDP-43 neuropathology: a genetic and histopathological analysis. *Lancet Neurol* 2008, **7**(5)**:** 409-416.

253. Nishimoto Y, Ito D, Yagi T, Nihei Y, Tsunoda Y, Suzuki N. Characterization of alternative isoforms and inclusion body of the TAR DNA-binding protein-43. *J Biol Chem* 2010, **285**(1)**:** 608-619.

254. Zhang YJ, Xu YF, Cook C, Gendron TF, Roettges P, Link CD, *et al.* Aberrant cleavage of TDP-43 enhances aggregation and cellular toxicity. *Proc Natl Acad Sci U S A* 2009, **106**(18)**:** 7607-7612.

255. Zhang YJ, Xu YF, Dickey CA, Buratti E, Baralle F, Bailey R, *et al.* Progranulin mediates caspase-dependent cleavage of TAR DNA binding protein-43. *J Neurosci* 2007, **27**(39)**:** 10530-10534.

256. Carthy CM, Yanagawa B, Luo H, Granville DJ, Yang D, Cheung P, *et al.* Bcl-2 and Bcl-xL overexpression inhibits cytochrome c release, activation of multiple caspases, and virus release following coxsackievirus B3 infection. *Virology* 2003, **313**(1)**:** 147-157.

257. Cunningham KA, Chapman NM, Carson SD. Caspase-3 activation and ERK phosphorylation during CVB3 infection of cells: influence of the coxsackievirus and adenovirus receptor and engineered variants. *Virus Res* 2003, **92**(2)**:** 179-186.

258. Yuan JP, Zhao W, Wang HT, Wu KY, Li T, Guo XK, *et al.* Coxsackievirus B3-induced apoptosis and caspase-3. *Cell Res* 2003, **13**(3)**:** 203-209.

259. Lee EB, Lee VM, Trojanowski JQ. Gains or losses: molecular mechanisms of TDP43-mediated neurodegeneration. *Nat Rev Neurosci* 2012, **13**(1)**:** 38-50.

260. Liu-Yesucevitz L, Bilgutay A, Zhang YJ, Vanderweyde T, Citro A, Mehta T, *et al.* Tar DNA binding protein-43 (TDP-43) associates with stress granules: analysis of cultured cells and pathological brain tissue. *PLoS One* 2010, **5**(10)**:** e13250.

261. Parker SJ, Meyerowitz J, James JL, Liddell JR, Crouch PJ, Kanninen KM, *et al.* Endogenous TDP-43 localized to stress granules can subsequently form protein aggregates. *Neurochem Int* 2012, **60**(4)**:** 415-424.

262. Neumann M, Sampathu DM, Kwong LK, Truax AC, Micsenyi MC, Chou TT, *et al.* Ubiquitinated TDP-43 in frontotemporal lobar degeneration and amyotrophic lateral sclerosis. *Science* 2006, **314**(5796)**:** 130-133.

263. Arai T, Hasegawa M, Akiyama H, Ikeda K, Nonaka T, Mori H, *et al.* TDP-43 is a component of ubiquitin-positive tau-negative inclusions in frontotemporal lobar degeneration and amyotrophic lateral sclerosis. *Biochem Biophys Res Commun* 2006, **351**(3)**:** 602-611.

264. Zhang YJ, Gendron TF, Xu YF, Ko LW, Yen SH, Petrucelli L. Phosphorylation regulates proteasomal-mediated degradation and solubility of TAR DNA binding protein-43 C-terminal fragments. *Mol Neurodegener* 2010, **5:** 33.

265. Buratti E, Dork T, Zuccato E, Pagani F, Romano M, Baralle FE. Nuclear factor TDP-43 and SR proteins promote in vitro and in vivo CFTR exon 9 skipping. *EMBO J* 2001, **20**(7)**:** 1774-1784.

266. Mercado PA, Ayala YM, Romano M, Buratti E, Baralle FE. Depletion of TDP 43 overrides the need for exonic and intronic splicing enhancers in the human apoA-II gene. *Nucleic Acids Res* 2005, **33**(18)**:** 6000-6010.

267. Bose JK, Wang IF, Hung L, Tarn WY, Shen CK. TDP-43 overexpression enhances exon 7 inclusion during the survival of motor neuron pre-mRNA splicing. *J Biol Chem* 2008, **283**(43)**:** 28852-28859.

268. Belov GA, Lidsky PV, Mikitas OV, Egger D, Lukyanov KA, Bienz K, *et al.* Bidirectional increase in permeability of nuclear envelope upon poliovirus infection and accompanying alterations of nuclear pores. *J Virol* 2004, **78**(18)**:** 10166-10177.

269. Park N, Katikaneni P, Skern T, Gustin KE. Differential targeting of nuclear pore complex proteins in poliovirus-infected cells. *J Virol* 2008, **82**(4)**:** 1647-1655.

270. Winton MJ, Igaz LM, Wong MM, Kwong LK, Trojanowski JQ, Lee VM. Disturbance of nuclear and cytoplasmic TAR DNA-binding protein (TDP-43) induces disease-like redistribution, sequestration, and aggregate formation. *J Biol Chem* 2008, **283**(19)**:** 13302-13309.

271. Bhattacharyya S, Yu H, Mim C, Matouschek A. Regulated protein turnover: snapshots of the proteasome in action. *Nature reviews Molecular cell biology* 2014, **15**(2)**:** 122-133.

272. Brunner JE, Nguyen JH, Roehl HH, Ho TV, Swiderek KM, Semler BL. Functional interaction of heterogeneous nuclear ribonucleoprotein C with poliovirus RNA synthesis initiation complexes. *J Virol* 2005, **79**(6)**:** 3254-3266.

273. Ertel KJ, Brunner JE, Semler BL. Mechanistic consequences of hnRNP C binding to both RNA termini of poliovirus negative-strand RNA intermediates. *J Virol* 2010, **84**(9)**:** 4229-4242.

274. Lin JY, Li ML, Brewer G. mRNA decay factor AUF1 binds the internal ribosomal entry site of enterovirus 71 and inhibits virus replication. *PLoS One* 2014, **9**(7)**:** e103827.

275. Lin JY, Li ML, Huang PN, Chien KY, Horng JT, Shih SR. Heterogeneous nuclear ribonuclear protein K interacts with the enterovirus 71 5' untranslated region and participates in virus replication. *J Gen Virol* 2008, **89**(Pt 10)**:** 2540-2549.

276. Monsellier E, Ramazzotti M, de Laureto PP, Tartaglia GG, Taddei N, Fontana A, *et al.* The distribution of residues in a polypeptide sequence is a determinant of aggregation optimized by evolution. *Biophys J* 2007, **93**(12)**:** 4382-4391.

277. Tanida I, Minematsu-Ikeguchi N, Ueno T, Kominami E. Lysosomal turnover, but not a cellular level, of endogenous LC3 is a marker for autophagy. *Autophagy* 2005, **1**(2)**:** 84-91.

278. Yoshimori T, Yamamoto A, Moriyama Y, Futai M, Tashiro Y. Bafilomycin A1, a specific inhibitor of vacuolar-type H(+)-ATPase, inhibits acidification and protein degradation in lysosomes of cultured cells. *J Biol Chem* 1991, **266**(26)**:** 17707-17712.

279. Reineke LC, Dougherty JD, Pierre P, Lloyd RE. Large G3BP-induced granules trigger eIF2alpha phosphorylation. *Mol Biol Cell* 2012, **23**(18)**:** 3499-3510.

280. Mizushima N, Yoshimori T, Levine B. Methods in mammalian autophagy research. *Cell* 2010, **140**(3)**:** 313-326.

281. Reineke LC, Kedersha N, Langereis MA, van Kuppeveld FJ, Lloyd RE. Stress granules regulate double-stranded RNA-dependent protein kinase activation through a complex containing G3BP1 and Caprin1. *MBio* 2015, **6**(2)**:** e02486.

282. Dutzmann J, Daniel JM, Bauersachs J, Hilfiker-Kleiner D, Sedding DG. Emerging translational approaches to target STAT3 signalling and its impact on vascular disease. *Cardiovasc Res* 2015, **106**(3)**:** 365-374.

283. Nguyen PM, Putoczki TL, Ernst M. STAT3-Activating Cytokines: A Therapeutic Opportunity for Inflammatory Bowel Disease? *J Interferon Cytokine Res* 2015, **35**(5)**:** 340-350.

284. Ben Haim L, Ceyzeriat K, Carrillo-de Sauvage MA, Aubry F, Auregan G, Guillermier M, *et al.* The JAK/STAT3 pathway is a common inducer of astrocyte reactivity in Alzheimer's and Huntington's diseases. *J Neurosci* 2015, **35**(6)**:** 2817-2829.

285. Yu H, Lee H, Herrmann A, Buettner R, Jove R. Revisiting STAT3 signalling in cancer: new and unexpected biological functions. *Nat Rev Cancer* 2014, **14**(11)**:** 736-746.

286. Kuchipudi SV. The Complex Role of STAT3 in Viral Infections. *J Immunol Res* 2015, **2015:** 272359.

287. Mammucari C, Milan G, Romanello V, Masiero E, Rudolf R, Del Piccolo P, *et al.* FoxO3 controls autophagy in skeletal muscle in vivo. *Cell metabolism* 2007, **6**(6)**:** 458-471.

288. Szczepanek K, Chen Q, Larner AC, Lesnefsky EJ. Cytoprotection by the modulation of mitochondrial electron transport chain: the emerging role of mitochondrial STAT3. *Mitochondrion* 2012, **12**(2)**:** 180-189.

289. Tasdemir E, Maiuri MC, Galluzzi L, Vitale I, Djavaheri-Mergny M, D'Amelio M, *et al.* Regulation of autophagy by cytoplasmic p53. *Nat Cell Biol* 2008, **10**(6)**:** 676-687.

290. Livesey KM, Kang R, Vernon P, Buchser W, Loughran P, Watkins SC, *et al.* p53/HMGB1 complexes regulate autophagy and apoptosis. *Cancer Res* 2012, **72**(8)**:** 1996-2005.

291. Morselli E, Shen S, Ruckenstuhl C, Bauer MA, Marino G, Galluzzi L, *et al.* p53 inhibits autophagy by interacting with the human ortholog of yeast Atg17, RB1CC1/FIP200. *Cell Cycle* 2011, **10**(16)**:** 2763-2769.

292. Pilati C, Amessou M, Bihl MP, Balabaud C, Nhieu JT, Paradis V, *et al.* Somatic mutations activating STAT3 in human inflammatory hepatocellular adenomas. *J Exp Med* 2011, **208**(7)**:** 1359-1366.

293. Cenit MC, Alcina A, Marquez A, Mendoza JL, Diaz-Rubio M, de las Heras V, *et al.* STAT3 locus in inflammatory bowel disease and multiple sclerosis susceptibility. *Genes Immun* 2010, **11**(3)**:** 264-268.

294. Morselli E, Galluzzi L, Kepp O, Marino G, Michaud M, Vitale I, *et al.* Oncosuppressive functions of autophagy. *Antioxid Redox Signal* 2011, **14**(11)**:** 2251-2269.

295. Fung G, Luo H, Qiu Y, Yang D, McManus B. Myocarditis. *Circ Res* 2016, **118**(3)**:** 496-514.

296. Kraemer BC, Schuck T, Wheeler JM, Robinson LC, Trojanowski JQ, Lee VM, *et al.* Loss of murine TDP-43 disrupts motor function and plays an essential role in embryogenesis. *Acta Neuropathol* 2010, **119**(4)**:** 409-419.

297. Yang C, Wang H, Qiao T, Yang B, Aliaga L, Qiu L, *et al.* Partial loss of TDP-43 function causes phenotypes of amyotrophic lateral sclerosis. *Proc Natl Acad Sci U S A* 2014, **111**(12)**:** E1121-1129.